mRNA VACCINE ENCODING NEOANTIGEN FOR CANCER IMMUNOTHERAPY USING

MOUSE MELANOMA AS A MODEL

Miss Chutamath Sittplangkoon

จุฬาลงกรณ์มหาวิทยาลัย
CHULALONGKORN UNIVERSITY

A Dissertation Submitted in Partial Fulfillment of the Requirements

for the Degree of Doctor of Philosophy in Biotechnology

Common Course

FACULTY OF SCIENCE

Chulalongkorn University

Academic Year 2021

วัคซีนชนิดเอ็มอาร์เอ็นเอประมวลรหัสนีโอแอนติเจนสำหรับภูมิคุ้มกันบำบัดมะเร็งโดยใช้มะเร็งผิวหนัง
ของหนูเมาส์เป็นแบบจำลอง

น.ส.จุฑามาศ สิทธิ์พลางกูร

Thesis Title	mRNA VACCINE ENCODING NEOANTIGEN FOR CANCER IMMUNOTHERAPY USING MOUSE MELANOMA AS A MODEL
By	Miss Chutamath Sittplangkoon
Field of Study	Biotechnology
Thesis Advisor	Professor TANAPAT PALAGA, Ph.D.

Accepted by the FACULTY OF SCIENCE, Chulalongkorn University in Partial Fulfillment of the Requirement for the Doctor of Philosophy

.... Dean of the FACULTY OF SCIENCE

(Professor POLKIT SANGVANICH, Ph.D.)

DISSERTATION COMMITTEE

.... Chairman

(Associate Professor CHULEE YOMPAKDEE, Ph.D.)

.... Thesis Advisor

(Professor TANAPAT PALAGA, Ph.D.)

.... Examiner

(Dr. CHOMPOONIK KANCHANABANCA, Ph.D.)

.... Examiner

(Assistant Professor EAKACHAI PROMPETCHARA, Ph.D.)

.... Examiner

(Professor NATTIYA HIRANKARN, M.D., Ph.D.)

.... External Examiner

(Associate Professor Thawornchai Limjindaporn, M.D., Ph.D.)

จุฑามาศ สิทธิ์พลางกูร : วัคซีนชนิดเอ็มอาร์เอ็นเอประมวลรหัสนีโอแอนติเจนสำหรับภูมิคุ้มกันบำบัดมะเร็งโดยใช้มะเร็งผิวหนังของหนูเมาส์เป็นแบบจำลอง. (mRNA VACCINE ENCODING NEOANTIGEN FOR CANCER IMMUNOTHERAPY USING MOUSE MELANOMA AS A MODEL) อ.ที่ปรึกษาหลัก : ศ. ดร.ธนาภัทร ปาลกะ

มะเร็งเป็นสาเหตุการเสียชีวิตอันดับต้นๆ ของโลก โดยมีความจำเป็นเร่งด่วนในการหาวิธีการป้องกันและการรักษาที่มีประสิทธิภาพมากขึ้น วัคซีนชนิดเอ็มอาร์เอ็นเอมีประสิทธิภาพเหนือกว่าวัคซีนรูปแบบอื่นในแง่ของความปลอดภัย ความสะดวกในการขยายขนาดการผลิต และประสิทธิภาพในการกระตุ้นการตอบสนองของภูมิคุ้มกันทั้งในระดับเซลล์และสารน้ำ ความก้าวหน้าในเทคโนโลยีเอ็มอาร์เอ็นเอทำให้มีการปรับปรุงความเสถียรและประสิทธิภาพของเอ็มอาร์เอ็นเอ รวมถึงการดัดแปลงนิวคลีโอไซด์ อย่างไรก็ตามมีรายงานเกี่ยวกับ N1-methylpseudouridine (m1Ψ) ในการเพิ่มการแสดงออกของโปรตีนและลดการสร้างภูมิคุ้มกันโดยกำเนิด เนื่องจากทำให้ความสามารถในการจับกับตัวรับในภูมิคุ้มกันโดยกำเนิด pattern recognition receptor และการหลั่งอินเตอร์เฟียรอนชนิดที่หนึ่งลดลง ดังนั้น การศึกษานี้จึงมีวัตถุประสงค์เพื่อประเมินการสร้างภูมิคุ้มกัน และการควบคุมการเจริญของมะเร็ง ภายหลังการฉีดเข้ากล้ามเนื้อด้วยวัคซีนเอ็มอาร์เอ็นเอที่มีระดับ m1Ψ ที่แตกต่างกัน ในแบบจำลองมะเร็งผิวหนังเมลาโนมา B16 นอกจากนี้โอแอนติเจนที่ไม่เด่น Pbk และ Actn4 เกิดจากการกลายพันธุ์ของเซลล์ร่างกาย ในมะเร็ง B16F10 ถูกเลือกและเชื่อมต่อเข้าด้วยกันเป็นแอนติเจนเป้าหมายในวัคซีนชนิดเอ็มอาร์เอ็นเอ ประการแรกพบว่าประสิทธิภาพการแปรรหัสเป็นโปรตีนขึ้นอยู่กับระดับการดัดแปลงนิวคลีโอไซด์ และสัมพันธ์แบบผกผันกับการเหนี่ยวนำการหลั่งอินเตอร์เฟียรอนชนิดที่หนึ่ง รวมถึงการเจริญเต็มที่ของ antigen-presenting cell การสร้างภูมิคุ้มกันของอนุภาคลิพิดนาโนพาร์ติเคิล (LNP) ที่มีการบรรจุเอ็มอาร์เอ็นเอที่เข้ารหัสให้ ovalbumin (OVA) และไม่มีการดัดแปลงนิวคลีโอไซด์จะเหนี่ยวนำให้เกิดการตอบสนองของ Th1 และ Th2 ในขณะที่เอ็มอาร์เอ็นเอที่ดัดแปลงนิวคลีโอไซด์จะเหนี่ยวนำให้เกิดการตอบสนองของ Th1 เป็นหลัก และเอ็มอาร์เอ็นเอที่ที่ดัดแปลงและไม่ดัดแปลงนิวคลีโอไซด์สามารถกระตุ้น cytotoxic effector T cell ที่จำเพาะต่อ OVA ได้ ประการที่สองเอ็มอาร์เอ็นเอ OVA ที่ไม่ดัดแปลงนิวคลีโอไซด์แสดงประสิทธิภาพในการต้านการเจริญของมะเร็ง และยับยั้งการแพร่กระจายไปยังปอด และยังแสดงให้เห็นการเพิ่มขึ้นอย่างมีนัยสำคัญของปริมาณ mature cDC1 ในก้อนมะเร็ง นอกจากนี้เอ็มอาร์เอ็นเอทั้งที่ดัดแปลงและไม่ดัดแปลงนิวคลีโอไซด์แสดงการเพิ่มจำนวนอย่างมีนัยสำคัญของของ CD8 effector T cell ที่จำเพาะต่อ OVA และพบว่าเอ็มอาร์เอ็นเอที่ดัดแปลงนิวคลีโอไซด์มีการเพิ่มขึ้นอย่างมีนัยสำคัญของการแสดงออก PD-1 บน CD8$^+$ T cell ประการที่สามศึกษาบทบาทของสัญญาณอินเตอร์เฟียรอนชนิดที่หนึ่งในการควบคุมการเจริญของมะเร็ง โดยฉีดวัคซีนเอ็มอาร์เอ็นเอพร้อมทั้งปิดกั้นตัวรับที่จำเพาะของอินเตอร์เฟียรอนชนิดที่หนึ่ง พบว่าการมีของสัญญาณอินเตอร์เฟียรอนชนิดที่หนึ่งสามารถควบคุมการเจริญของมะเร็ง และเพิ่มการผลิตอินเตอร์เฟียรอนแกมมาจากทีเซลล์ที่จำเพาะต่อ OVA และมีการลดการแสดงออก PD-1 บน T cell และ M2-like macrophage ในก้อนมะเร็ง สุดท้ายอนุภาคลิพิดนาโนพาร์ติเคิลที่บรรจุเอ็มอาร์เอ็นเอที่เข้ารหัสให้นีโอแอนติเจน Pbk และ Actn4 โดยเฉพาะที่ไม่ดัดแปลงนิวคลีโอไซด์แสดงความสามารถเหนี่ยวนำการตอบสนองภูมิคุ้มกัน และควบคุมการเจริญของมะเร็ง B16F10 ได้ จากผลการทดลองทั้งหมดข้างต้นแสดงให้เห็นว่า การนำส่งวัคซีนเอ็มอาร์เอ็นเอที่ไม่ดัดแปลงนิวคลีโอไซด์เข้ากล้ามเนื้อ มีผลในการรักษามะเร็งที่สูงขึ้น ในลักษณะที่ขึ้นกับสัญญาณอินเตอร์เฟียรอนชนิดที่หนึ่ง ในปัจจุบันอนุภาคลิพิดนาโนพาร์ติเคิลมักถูกใช้เป็นตัวนำส่งนิวคลีโอติก เนื่องจากสามารถบรรจุองค์ประกอบวัคซีนได้มาก และมีความยืดหยุ่นในการออกแบบ อีกทั้งช่วยในการเข้าสู่เซลล์ได้อย่างรวดเร็วและปลดปล่อยเอ็มอาร์เอ็นเอสู่ไซโทพลาสซึม ในการศึกษานี้เรากำหนดสูตรอนุภาคลิพิดนาโนพาร์ติเคิลที่แตกต่างกันสองสูตร และผสมกับพลาสมิดดีเอ็นเอ ที่อัตราส่วน N/P ที่หลากหลาย (1:1, 1:3, 1:5, 1:7, 1:9, 3:1, 5:1, 7:1, 9:1) อนุภาคลิพิดนาโนพาร์ติเคิลสูตรแรกประกอบด้วย DOTAP ลิพิดที่มีประจุบวก และ DOPE ที่อัตราส่วนโมล 1:1 LNP สูตรที่สองประกอบด้วย DOTAP, DOPE และพอลิเอทิลีนไกลคอลที่ยึดเกาะด้วยลิพิดที่อัตราส่วนโมล 50:49.25:0.75 องค์ประกอบอนุภาคลิพิดนาโนพาร์ติเคิล และอัตราส่วน N/P มีผลต่อขนาดอนุภาคและประจุ ทั้งสองสูตรแสดงผลที่ไม่เป็นพิษต่อเซลล์ RAW264.7 และช่วยในการนำส่งแอนติเจนเข้าสู่เซลล์และการแปลรหัสเป็นโปรตีนในเซลล์ RAW264.7

จุฬาลงกรณ์มหาวิทยาลัย
CHULALONGKORN UNIVERSITY

| สาขาวิชา | เทคโนโลยีชีวภาพ | ลายมือชื่อนิสิต .... |
| ปีการศึกษา | 2564 | ลายมือชื่อ อ.ที่ปรึกษาหลัก .... |

5972808923 : MAJOR BIOTECHNOLOGY

Chutamath Sittplangkoon : mRNA VACCINE ENCODING NEOANTIGEN FOR CANCER IMMUNOTHERAPY USING MOUSE MELANOMA AS A MODEL . Advisor: Prof. TANAPAT PALAGA, Ph.D.

Cancer is the leading cause of death globally with an urgent need to find more effective approaches for prevention and treatment. mRNA vaccine is a promising vaccine platform over conventional vaccines in terms of safety, ease of large-scale production and effectiveness in inducing both cellular and humoral immune responses. Breakthrough in mRNA technology allowed novel strategies to improve mRNA stability and efficacy including nucleoside modifications. Modification of mRNA with N1-methylpseudouridine (m1Ψ) was reported to enhance protein expression and decrease innate immunogenicity due to low binding affinity to pattern recognition receptors, and low type I interferon (IFN-I) secretion. Therefore, this study aimed to evaluate the immunogenicity and anti-tumor responses of different degrees of m1Ψ replacement in mRNA vaccine following intramuscular administration in B16 melnamoma mouse model. Moreover, non-dominant neoantigens, fusion of Pbk and Actn4 somatic mutations of B16F10 tumor were selected for investigation as neoantigens in mRNA vaccine. First, the translation efficiency of mRNA vaccines depended on the degree of nucleoside modification and inversely correlated with induction of IFN-I secretion and antigen-presenting cell maturation. Immunization of ovalbumin encoding mRNA formulated in lipid nanoparticles (LNPs) (OVA-LNP) with unmodified nucleosides stimulated both Th1 and Th2 responses, whereas modified mRNA induced mainly Th1 response. Both conditions however equally activated OVA-specific cytotoxic effector T cells. Second, unmodified mRNA OVA-LNP showed potent antitumor efficacy and lung metastasis inhibition, accompanied by a significant increase in the influx of mature migratory cDC1 to the tumor. In addition, while both unmodified and modified mRNA showed a significant expansion of OVA-specific splenic CD8 effector T cells, modified mRNA showed a significant increase in PD-1$^+$ CD8$^+$ T cells. Third, the role of IFN-I signaling in anti-tumor response induced by mRNA vaccine administration was investigated by IFN-I receptor blockade. Intact IFN-I signaling resulted in a significant tumor growth suppression and increase in OVA specific IFN-γ-producing T cells with decreased PD-1 expression and less tumor-infiltrating M2-like macrophages. Lastly, LNPs containing neoantigens (Pbk-Actn4) encoding mRNA was immunogenic especially in unmodified mRNA. This neoantigen mRNA-LNP effectively controlled B16F10 tumor growth. Taken together, this study showed that intramuscular administration of unmodified nucleoside mRNA vaccine exhibits higher therapeutic antitumor effects in type I IFN-dependent manner. Presently, lipid nanoparticles (LNPs) are often used as nucleic acid carriers due to greater payload and design flexibility. It facilitates rapid uptake and mRNA escapes to the cytoplasm. In this study, we formulated two different formulas of LNPs and complexed with plasmid DNA (pDNA) at varied N/P ratio (1:1, 1:3, 1:5, 1:7, 1:9, 3:1, 5:1, 7:1, 9:1). The first formula LNP consisted of cationic lipid, 1,2-dioleoyl-3-trimethylammonium-propane (DOTAP) and helper lipid, 1,2-dioleoyl-sn-glycero-3-phosphoethanolamine (DOPE) at 1:1 mole ratio. The second formula LNP consisted of DOTAP, DOPE and Lipid-anchored polyethyleneglycol at 50:49.25:0.75 mole ratio. The LNP composition and the N/P ratio had an effect on particle size and charge. Both formulas showed non-toxic effects on RAW264.7 cell line and facilitated antigen transfection and protein translation in RAW264.7 cell line.

Field of Study:	Biotechnology	Student's Signature ....
Academic Year:	2021	Advisor's Signature ....

ACKNOWLEDGEMENTS

Chutamath Sittplangkoon

TABLE OF CONTENTS

LIST OF FIGURES

LIST OF TABLES

LIST OF ABBREVIATIONS

a.a.	Amino acid
Actn4	Actinin alpha 4
APCs	Antigen-presenting cells
BMs	Bone marrow cells
BMDCs	Bone marrow-derived dendritic cells
BMDMs	Bone marrow-derived macrophages
CAR	Chimeric antigen receptor
CCL	Chemokine (C-C motif) ligand
CCR	CC-chemokine receptor
cDC1	Conventional type 1 DC
cDC2	Conventional type 2 DC
CDP	Common DC progenitor
CFSE	Carboxyfluorescein diacetate succinimidyl ester
CSF1	Colony-stimulating factor 1
CTL	Cytotoxic T lymphocyte
CTLA-4	Cytotoxic T-lymphocyte-associated protein 4
CXCL	C-X-C motif chemokine ligand
DCs	Dendritic cells
DMEM	Dulbecco's Modified Eagle Medium
dLNs	Draining lymph nodes
dsRNA	Double-stranded RNA
DOPE	Dioleoylphosphatidylethanolamine
DOTAP	1,2-dioleoyl-3-trimethylammonium-propane
eIF	Eukaryotic initiation factor
ELISA	Enzyme-linked immunosorbent assay
ELISpot	Enzyme-linked immune absorbent spot
FBS	Fetal bovine serum

Flt3L	FMS-like tyrosine kinase 3 ligand
GAS	IFN-**γ**-activated site
GM-CSF	Granulocyte-macrophage colony-stimulating factor
HBV	Hepatitis B virus
HEK293T	Human embryonic kidney cell line
Hour	Hr
Hours	Hrs
HPLC	High-performance liquid chromatography
HPV	Human papillomaviruses
HSC	Hematopoietic stem cell
IFIT	Interferon-induced protein with tetratricoid repeat
IFN	Interferon
IFN-I	Type I interferon
IFNAR1	Interferon-alpha/beta receptor alpha chain
IL	Interleukin
ICS	Intracellular cytokine staining
i.d.	Intradermal
i.m.	Intramuscular
i.n.	Intranodal
i.p.	Intraperitoneal
ISGF3	IFN-stimulated gene factor-3
i.t.	Intratumoral
i.v.	Intravenous
iNOS	Inducible nitric oxide synthase
IRF	Interferon regulatory factor
IVT	*In vitro* transcription
JAK	Janus kinase
LNPs	Lipid nanoparticles
LPX	Lipoplexes
Luc	Luciferase
L929	Murine fibroblast cell line

m1Ψ	N1-Methylpseudouridine
MDA5	Melanoma differentiation-associated antigen 5
MHC class I	Major histocompatibility complex class I
MHC class II	Major histocompatibility complex class II
mAb	Monoclonal antibody
MAGE-A3	Melanoma-associated antigen A3
Neo	Neoantigen
NK	Natural killer cells
NY-ESO-1	New York oesophageal squamous cell carcinoma 1
OAS	Oligoadenylate synthase
ORF	Open reading frame
OVA	Ovalbumin
Pbk	PDZ-binding kinase
PBS	Phosphate buffer saline
PD-1	Programmed cell death protein 1
pDC	Plasmacytoid dendritic cell
PD-L1	Programmed death-ligand 1
pDNA	Plasmid DNA
PEG	Polyethyleneglycol
PKR	Protein kinase receptor
PRRs	Pattern recognition receptors
RAW264.7	Murine macrophage cell line
RPMI	Roswell Park Memorial Institute
s.c.	Subcutaneous
ssRNA	Single stranded RNA
STAT	Signal transducer and activator of transcription
TAAs	Tumor-associated antigens
TCR	T cell receptor
Th	T helper cell
TLR	Toll-like receptor
TMB	3, 3', 5, 5'- tetramethylbenzidine

TME	Tumor microenvironment
TNF	Tumor necrosis factor
TOPK	T-lymphokine-activated killer cell-originated protein kinase
TPTE	Transmembrane phosphatase with tensin homology
UTP	Uridine 5'-triphosphate
UTRs	Untranslated regions
v/v	Volume by volume
µg	Microgram
ng	Nanogram
g	Gram
µl	Microliter
ml	Milliliter
L	Liter
µm	Micrometer
nm	Nanometer
µM	Micromolar
M	Molar
°C	Degree Celsius
%	Percentage
/	Per
:	Ratio
α	Alpha
β	Beta
γ	Gamma
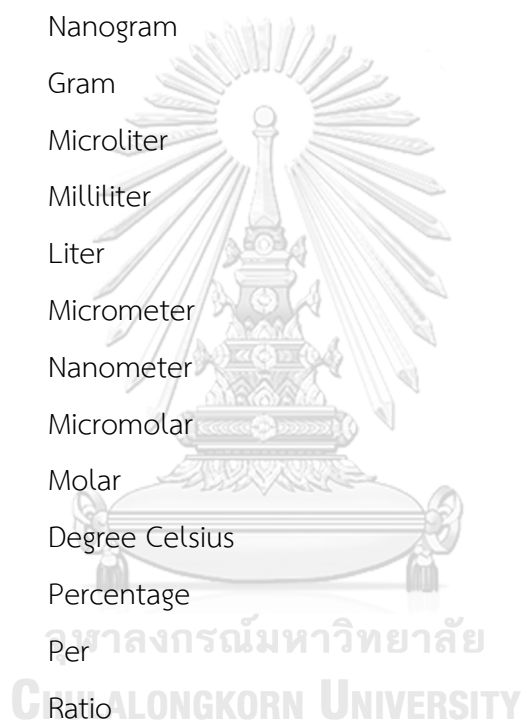
CHAPTER I

BACKGROUND

Cancer is one of the global health problems with urgent needs for more effective solution (1). The first defense system of host immunity against tumor cells is initiated by innate immune cells including natural killer (NK) cells, neutrophils, and macrophages (2). Subsequently obtaining tumor antigen-specific adaptive immunity requires three signaling cascades. Antigen-presenting cells (APCs) such as dendritic cells (DCs) capture tumor associated antigens from dying tumor cells or antigens released from tumor cell which trigger APC maturation, and antigen processing and presentation on major histocompatibility complex class I (MHC class I) and II (MHC class II) molecules for recognition by T cell receptors (TCRs) (signal 1). Full T cell activation further requires co-stimulatory signaling from surface molecules including B7 on APCs and CD28 on T cells (signal 2) and APC-derived cytokines including interleukin-12 (IL-12) and type I interferon (IFN-I) (signal 3) (3). However, in the absence of costimulatory signals causes T cell tolerance (4, 5). In addition, in tumor microenvironment (TME) there is often an upregulation of immune inhibitory molecules such as programmed cell death protein 1 (PD-1) and cytotoxic T-lymphocyte-associated protein 4 (CTLA-4) on T cells or programmed death-ligand 1 (PD-L1) on APCs and cancer cells which competitively interact with co-stimulatory molecules/receptors and contribute to T-cell exhaustion and tumor immune escape (6).

Although the standard cancer care has improved in the recent decades, many such cares have insufficient efficacy and severe side effects. Cancer immunotherapy utilizes the patient's own immune system to mount antitumor immune functions of the suppressed immune functions (7) . The current approaches for cancer

immunotherapy can be summarized into 4 categories i.e. monoclonal antibody (mAb) treatment, immune checkpoint blocker treatment, cancer vaccine treatment and cell-based therapies (8). The mAb can be naked or conjugated with drugs or toxins that are specifically delivered to cancer cells (9). Immune checkpoint blockade overcomes the immunosuppressive checkpoints exploited by the cancer cells and trigger the antitumor response T cells (10). The use of cancer vaccines aims to stimulate the immune cells to recognize the antigens that are present on the tumor (11). Adoptive T-cell therapy is a cell-based immunotherapy that requires reinfusion of *ex vivo* activated autologous T cells into patients (12). In recent years, immunotherapy combined with nanotechnology has gained more attentions because it allows a directed target therapy with decreasing unwanted side effects (13). Traditionally, tumor-associated antigens (TAAs) are the main targets for cancer vaccine. However, using TAAs is not always effective for cancer treatment because extensive variability of TAAs in each patients can cause immune evasion. In addition, central and peripheral tolerance could be initiated due to presence of TAAs in some normal tissues which waning vaccine efficacy (14). Advances in omics technologies such as the next generation sequencing and proteomics enable scientists to identify potential neoantigens that are the result of somatic mutations, that can be unique to individual patients (15). Generally, neoantigens are expressed by the tumor cells, but are absent in the normal cells. Criteria of selection for mutated genes as neoantigens, include high expression levels in tumor cells and MHC class I and class II-binding affinity for antigen presentation (16).

mRNA vaccine emerges as new anticancer vaccine. It provides several advantages over the peptide cancer vaccines which is currently in clinical trials and use. Peptide vaccines can effectively treat only patients with complete fit of human leukocyte antigen/ MHC type with those peptides and the adjuvants are needed. While endogenously expressed mRNA vaccine, antigen can be processed and

presented by APCs and does not have such limitation. Furthermore, mRNA itself provides potent adjuvant activity by direct activation of pattern recognition receptors (PRRs) in innate immune cells. Moreover, once the mRNA reaches the cytoplasm, translation process can occur immediately with no risk of insertional mutagenesis (17, 18). On the manufacturing side, mRNA vaccine can be easily produced with relatively low cost by an enzymatic process.

The application of mRNA vaccines for cancer immunotherapy can be categorized into 2 groups. The first type is mRNA vaccine encoding TAAs or personalized neoantigens derived from exome sequencing. This vaccine is directly immunized into patients which effectively induce antigen specific humoral and cellular immunity. The second type is mRNAs for cellular therapies by transfecting mRNA encoding TAAs into patient-derived DCs *in vitro* and infuse back into the patient for activation of TAAs-specific T cells or transfecting mRNA encoding chimeric antigen receptors into patient-derived T cells, which mediates recognition of specific tumor antigens by T cells (19).

FixVac vaccine from BioNTech company is an example of successful mRNA vaccine for advanced melanoma in phase I trial. Patients received at least eight intravenously administered of lipid nanoparticles (LNPs) loaded mRNA (mRNA doses ranging from 7.2 to 400 µg) encoding four TAAs, including New York oesophageal squamous cell carcinoma 1 (NY-ESO-1), melanoma-associated antigen A3 (MAGE-A3), tyrosinase, and transmembrane phosphatase with tensin homology (TPTE). These TAAs show limited expression in normal tissue, high immunogenicity and widespread presence in melanoma (20). It was optimized to target immature DCs in lymphoid organs and could potententially initiate antigen presentation of TAAs on both MHC class I and class II molecules on DCs and subsequently induced effector T cell responses against TAAs. The authors reported that tumor progrssion could be controlled by FixVac vaccinations in patients who had failed from prior received anti-

PD-1 therapy but the tumor later grew back. Interestingly, FixVac significantly induced PD-1$^+$ effector memory T cells and after second round treatment with anti-PD-1 therapy, morethan 35% of tumor regression rate was seen (21). This result suggest the advantages of combination therapy of potent therapeutic mRNA vaccine and immune checkpoint blockade.

The delivery system of mRNA vaccine is another key technology for an effective mRNA vaccine. Ideal delivery system should be able to effectively deliver mRNA to lymphoid tissues and protect mRNA from degradation by ubiquitous RNase. In addition, the mRNA should be specifically taken up by the APCs. Physical delivery methods including gene gun and electroporation, have shown efficient delivery of mRNA in only mouse models but so far not in large animals and humans because of increasing cell death rate and difficulty in target cell access (22, 23). The use of lipid or polymer-based nanoparticles as potent delivery vehicles are more reliable and suitable.

The cationic peptide protamine can protect mRNA from ubiquitous RNase but the tight connection between protamine and mRNA could limit the protein expression (24). Currently, LNPs are the most frequently used vehicles for mRNA delivery. LNPs are generally compost of an aqueous core surrounded by a lipid bilayer shell that is made of a combination of different lipids (25, 26). Most LNP formulations rely on cationic lipids to efficiently complex the negatively charged RNA (27). The main concerning aspects of effective LNP delivery system include the composition of lipid, size and charge. Small-sized (200-400 nm) particles of 1,2-dioleoyl-3-trimethylammonium-propane (DOTAP) complexed with mRNA can specifically target DCs (28). The toxicity of cationic lipid can be decreased by co-structure with the neutral lipid. Furthermore, dioleoylphosphatidylethanolamine (DOPE) neutral lipid is useful for transfection efficiency *in vivo*, which can facilitate membrane fusion and aid the destabilization of the plasmalemma or endosome (29).

DOTAP-lipoplexes (LPX) showed low toxicity in MCF-7, HeLa and HEK-293 cell lines after 48 hrs incubation (30). In addition, the surface of LNPs can be decorated to express specific molecules such as DCs targeting mannose receptor that enhances the uptake by DCs (31). Adjusting the net charge of lipid to mRNA could also target precisely and effectively to the lymphoid organs. RNA complexed with LPX formulation with a charge ratio of 1.3:2 effectively targeted RNA to the spleen, which is an organ with the highest density of APCs (32). Another critical component of the LNPs is the pH-sensitive ionizable lipids which maintain more biocompatible neutral charge at physiological pH with less interaction to anionic membrane of blood cells. However, once mRNA-LNPs reached inside an endosome, at low pH, the ionizable lipids are protonated and leading to promote membrane destabilization and facilitate endosomal escape of the nanoparticles and release mRNA to the cytosol (33). Currently, the use of mRNA encoding mono-epitope induces either CD4$^+$ or CD8$^+$ immune responses (16) but effective vaccines induce both arms of immune response.

In this study, mRNAs were prepared using ovalbumin as a model antigen and mutation-induced neoantigens- PDZ-binding kinase (Pbk) and actinin alpha 4 (Actn4) of B16F10 melanoma cells (16) for therapeutic evaluation against B16 melanoma model. Furthermore, DsRed2 red fluorescent protein encoding mRNA was prepared by varying net charge of lipid formulations containing DOTAP cationic lipid, DOPE neutral lipid and polyethyleneglycol. The translation efficiency of LNPs were investigated *in vitro*. The results obtained from this study may provide insight and prototype of the effectiveness of mRNA vaccine against cancer.

Objectives
1. To develop mRNA vaccine encoding the fusion of two neoepitopes
2. To develop novel delivery system using lipid nanoparticles (LNPs)

CHAPTER II

LITERATURE REVIEWS

2.1 Cancer and anti-cancer immunity

Cancer is the top three causes of death globally with the increasing incidence which is followed by heart disease and stroke (1, 34). There are various causes of cancer, such as genetic factors, unhealthy food habits, stress, radiation exposure, toxins consumption, chronic infection and inflammation (35, 36) which leading to uncontrolled growth of cells in any organs and tissues and forming of a cancer mass (37-39). In tumor microenvironment (TME), immunosuppression, and tumor evasion strategies by cancer cells result in the inability of the immune cells to detect and eliminate the cancer cells (40-42). Immune checkpoint inhibitors such as programmed cell death protein 1 (PD-1) keep T cell responses in check which helps in autoimmunity prevention. However, these inhibitory signaling is taken advantage by the cancer cells to induce T cell exhaustion. Ligation of PD-1 with its ligands programmed death-ligand 1 or 2 (PD-L1 or PD-L2) induces tyrosine phosphorylation of the PD-1 cytoplasmic domain and subsequent recruitment of cytosolic tyrosine phosphatase SHP-2 which preferentially dephosphorylates CD28 (43-45) and prevents CD28-mediated activation of phosphatidylinositol 3-kinase to produce cytotoxic mediators required for killing by effector T cell (46).

Anti-cancer immunity requires consecutive steps for effective killing of cancer cells as shown in Figure 2.1. The release of cancer cell derived antigens or neoantigens created from changes in genetic modification of cancer cells are taken up by antigen-presenting cells (APCs) for processing (step 1). Antigen-peptides are loaded on MHC class I and II molecules (step 2). The priming and activation of cancer-specific effector T cells is mediated (step 3). The activation of T cells appears to govern by three signals, including T cell receptor (TCR) engagement (signal 1)

which is from the interaction between APCs presented peptide-MHC complexes and antigen-specific T cells. Co-stimulation from costimulatory molecules (signal 2) is required to prevent anergic responses. Proinflammatory cytokines such as type I interferon (IFN-I) (signal 3) directly helps in T cell differentiation to effector cells and survival of activated T cells from natural killer (NK) cell attack by upregulating the MHC class I expression for inhibitory NK cell receptors and downregulating T cell ligands for the activating NK cell receptor natural cytotoxicity triggering receptor 1 (47). Finally, the activated effector T cells travel to tumor and infiltrate into the tumor site (step 4) and specifically interact to cancer cells through TCR and cancer antigen bound to MHC class I molecules, and kill their target cancer cells (step 5). However, the presence of an immunosuppressive regulator within the TME could limit protective immunity. Combination with treatments that selectively target negative regulators to T cell responses in each step of the cycle could overcome mechanisms of immune suppression (48).
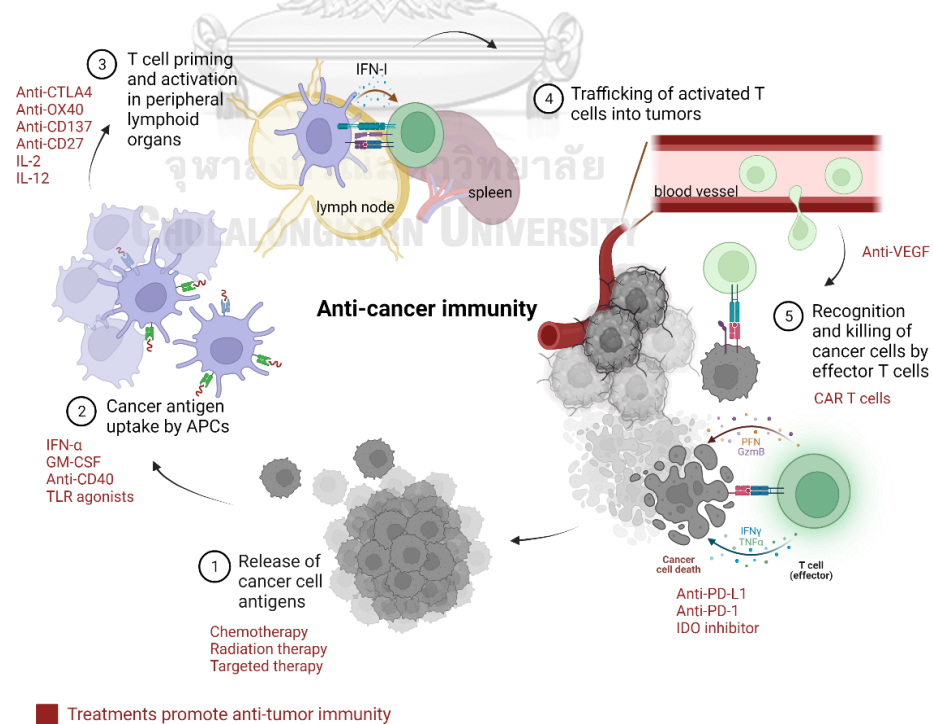
Figure 2.1 The anti-cancer immunity cycle

The generation of anti-cancer immunity requires consecutive steps. This cycle can be divided into five major steps, initiating with the release of antigens from the cancer cell and ending with the killing of cancer cells. Treatment agents mediating anti-tumor immunity are indicated in red. (Modified from Chen, DS. and Mellman, I., 2013 (48))

2.2 Antigen-presenting cells (APCs)

The major target cell population of vaccine are professional APCs especially macrophages and dendritic cells (DCs) which function as bridge between innate and adaptive immune responses (49). Activation of innate immune response is usually initiated by detecting exogeneous motifs called pathogen-associated molecular patterns via the pattern recognition receptors (PRRs) and these receptors are particularly highly expressed in APCs (50).

2.2.1 Macrophages

Tissue-resident macrophages are mainly derived from embryonic progenitors which enrich tissue remodeling and wound healing gene sets. Macrophage development are regulated by macrophage colony-stimulating factor 1 receptor (M-CSFR) which are the receptor for M-CSF and interleukin-34 (IL-34), which are important cytokines in differentiation and survival of macrophages (51). By contrast, tumor-associated macrophages predominantly derive from circulating monocytes (52) as shown in Figure 2.2 and upregulate gene sets involved in immune suppression and antigen presentation (53). Cellular activity and function of macrophages are regulated by developmental origin, tissue environment cues such as fibrosis, hypoxia, nutrient accessibility, and lymphocyte-derived factors (49, 54). In addition, epigenetic mechanism also affects phenotype plasticity of macrophage (55). In TME, tissue hypoxia induces monocyte recruitment factor secretion from malignant cells and stroma such as colony-stimulating factor 1 (CSF1), CC-chemokine ligand 2 (CCL2),

CCL5, CXC-chemokine ligand 12 (CXCL12) and vascular endothelial growth factor (56). The functional roles of macrophage in cancer are delineated by macrophage-expressed molecules. M1 macrophages present anti-tumorigenic properties express high levels of tumor necrosis factor (TNF), inducible nitric oxide synthase (iNOS) or MHC class II molecules. IFN-γ produced by CD8^{+} cytotoxic T lymphocytes (CTLs), T helper 1 (Th1) cells and NK cells could shape the phenotype of macrophages towards antigen presentation, pro-inflammatory cytokine production and tumor cell killing (57). Likewise, activation through CD40 on macrophages upregulates expression of MHC class II, iNOS and TNF which promote anti-tumor immunity (58). While M2 macrophages present pro-tumorigenic properties express high levels of arginase 1, IL-10, CD163, CD204 or CD206 (59). The mannose receptor, CD206, which is highly expressed by M2 macrophages, suppress CD45 phosphatase activity leading to impair of cytotoxicity of CD8^{+} T cells (60).
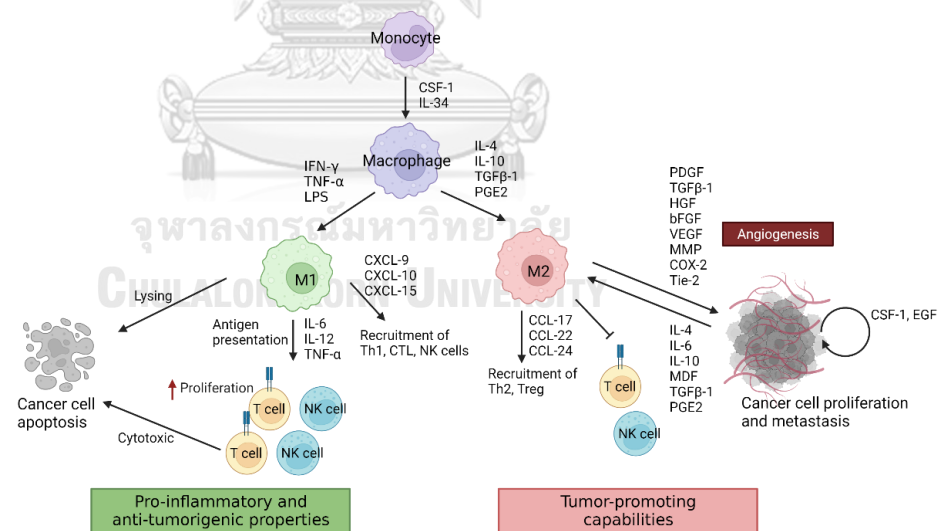
Figure 2.2 Schematic diagram for the origins and functions of macrophages in tumor response

Tumor-associated macrophages (TAMs) are derived from circulating monocytes. CSF-1 and IL-34 play crucial role in macrophages origination. TAMs are phenotypically polarization to proinflammatory M1 macrophage due to the efect of IFN-γ, TNF-α

and LPS and tumor-promoting M2 macrophage due to the effect of IL-4, IL-10, TGFβ-1 and PGE2. M1 macrophage directly kills tumor cells by lysis after phagocytosis, enhances tumor antigen-presentation or indirectly promote the proliferation of CD8^{+} T cells and NK cells due to the effect of IL-6, IL-12 and TNF-α. While, growth factors and enzymes secreted by M2 macrophage promote angiogenesis and immunosuppression by recruitment of regulatory T cell (Treg). As a feed-back loop, cytokines and factors secreted by tumor cells enhance the effect of M2. (Modified from Liu, J., *et al*., 2021 (61) and Lakshmi, N. B., *et al*., 2013 (62))

2.2.2 Dendritic cells (DCs)

DCs are derived from hematopoietic stem cell (HSC)-derived precursor named as common DC precursor (CDP) in bone marrow (63) as shown in Figure 2.3. DC lineage development from HSC is influenced by cytokines including granulocyte-macrophage colony-stimulating factor (GM-CSF) and IFN-I under the direction of FMS-like tyrosine kinase 3 ligand (Flt3L) and Flt3L receptor (Flt3) signaling (64, 65). The uptake of antigens causes DC maturation which loses ability of antigen uptake and acquire capacity in antigen presentation and T cell activation correlated with upregulation of cell surface MHC class II, costimulatory molecules such as CD40, CD80, CD86, and adhesion molecule CD54 (26, 66-68). Moreover, activated DCs can be induced by exposure to danger signals such as heat shock proteins (69), necrotic cells (70) or contact with CD40 ligand-expressing T cells (71). In addition, IFN-I produced by DCs also act in an autocrine manner through type I IFN-receptor (IFNAR) to activate DCs shown upregulation of costimulatory molecules on cell surface which enable to stimulate T cells (72, 73). DC surface markers are characterized by CD11c^{+} and MHC class II^{hi} cells (74) and are divided into three subtypes including two classical DCs; conventional type 1 DC (cDC1) and cDC2 and plasmacytoid DCs (pDCs) (63). Moreover, the differentiation of cDC subtypes is modulated by distinct sets of transcription factors (75, 76). cDC1 is defined as CD8α^{+} CD103^{+} XCR1^{+} (65), while cDC2

is defined as CD11b$^+$ CD172a$^+$ (65). IFNAR triggering in cDC1 was critical for spontaneous CD8$^+$ T cell responses against B16 melanoma (77). cDC1 performs in antigen cross-presentation to prime CD8$^+$ T cells and also helps in early priming of CD4$^+$ T cells and delivery of cell-associated antigens to the T cell zone of draining lymph nodes (dLNs), where antigens can be captured by cDC2 and further present to CD4$^+$ T cells (78). This finding suggests that cDC1 acts as the primary APCs for early presentation to naïve CD4$^+$ T cells, while at advanced stage of CD4$^+$ T cell proliferation is regulated by cDC2. In addition, the absence of CD40 signaling on cDC1 causes the reduction of antigen specific CD8$^+$ T cells expansion (79). Murine pDC is defined as CD11c$^+$ CD11b$^-$ B220$^+$ PDCA1$^+$ SiglecH$^+$ (65). Triggering of endosomal toll-like receptor 7 (TLR-7) by single stranded RNA (ssRNA) can activate pDCs to secrete IFN-I and become mature (80). Mature pDCs subsequently downregulate IFN-I secretion and upregulate expression of MHC class II and costimulatory molecules (81). Fate of T helper cells can be determined by the type of DC subsets. CD8α^+ DC subset induces Th1 cell differentiation (82), whereas the development of Th2 cells requires mediator like CD301b$^+$ DC subset (83).
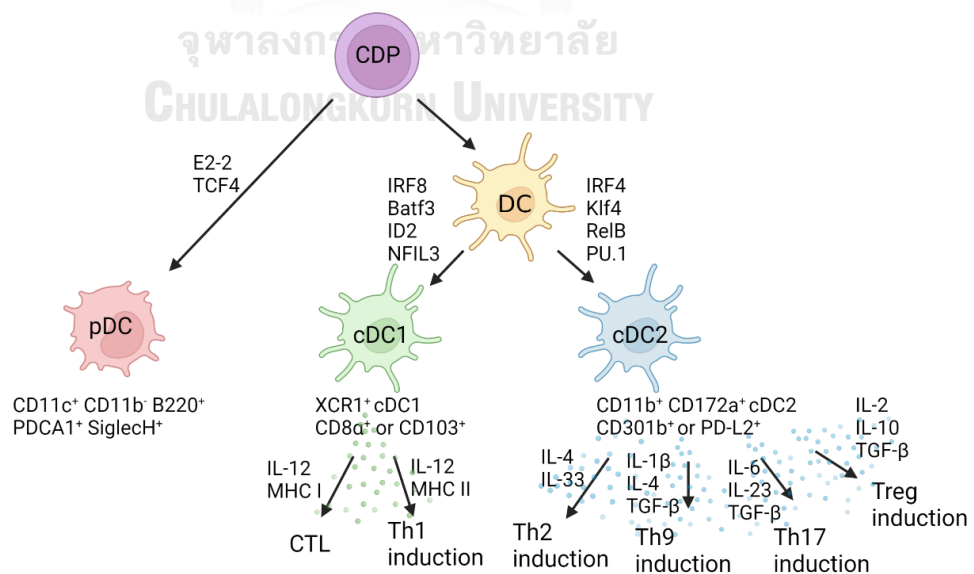
Figure 2.3 Schematic diagram for the origin of DCs and the involvement of cDC1 and cDC2 subsets in the T cell differentiation

Population of DCs are divided into three subsets including pDC, cDC1 and cDC2 which are all derived from CDP modulated by distinct sets of transcription factors. cDC1 is involved in the differentiation of CTL and Th1 cells with IL-12 cytokine. While, cDC2 facilitates the T cell development into Th2, Th9, Th17, and Treg cells with cDC2 cytokines. CDP, common dendritic cell progenitor; pDC, plasmacytoid dendritic cell; cDC1, conventional type 1 dendritic cell; cDC2, conventional type 2 dendritic cell (Modified from Kumar, S., *et al.*, 2018 (84))

2.3 Type I interferons (IFN-I)

The activity of IFN-I was discovered by Isaacs and Lindenmann in 1957 from the growth inhibition of live influenza virus by the secreted factor from heat-inactivated influenza virus (85). IFN can be categorized into 3 families including type I (IFN-α and IFN-β), type II (IFN-γ), and type III (IFN-λ1, 2, 3 and 4) (86). IFN-I signaling has been reported to be associated with either helps or resistance to cancer therapies (87-89). The expression of IFN-I requires activation of PRRs as shown in Figure 2.4 followed by interaction with adaptor proteins; TRIF or MyD88 which subsequently activate serine/threonine kinases that phosphorylate interferon regulatory factor 3 (IRF-3), IRF-7, AP-1, and NF-κB triggering their translocation into the nucleus, where they bind to regulatory domains of the IFN-β gene promoter and drive transcription of IFN-I (90). While major producer of IFN-α is pDCs, IFN-β is released by many types of cells (91). IFN-I expression can be induced by viral infection, LPS, bacterial DNA, and double-stranded RNA (dsRNA) (92, 93). IFN-α signals through heterodimeric receptors, comprising a low-affinity IFNAR1 and a high-affinity IFNAR2, whereas IFN-β signals through homodimer receptor IFNAR1 (47). The binding of IFN-α/β to IFNAR leads to the activation of the Janus kinase (JAK) and signal transducer and activator of

transcription (STAT) pathway (94). The activation of JAK kinase results in the recruitment, phosphorylation, and dimerization of STAT proteins. The STAT dimer, which binds IRF9 to form the IFN-stimulated gene factor 3 complex. This complex translocates to the nucleus and binds to IFN-stimulated response elements, initiating transcription of IFN-stimulated genes (92). The combination of different STAT complexes will determine in turn the transcriptional and functional consequences of IFN-I. Interestingly, induction of autophagy-associated death of cancer cells via IFN-γ/STAT1 activation and STAT3 activation inhibition could reestablish the antimetastatic effect in therapeutic condition (95).

IFN-I indirectly influences on T cell priming by APCs. IFN-I induce APC maturation by upregulation of MHC molecules and costimulatory molecules which promote antigen presentation (96) as well as facilitate migration of mature APCs to secondary lymphoid organs by upregulating CC-chemokine receptor 5 (CCR5) and CCR7 expression on mature APCs (97) and adhesion molecule lymphocyte function-associated antigen 1 and inducing T-cell chemoattractant secretion from APCs including CXCL9 and CXCL10 (98, 99). In addition, cross-presentation efficiency is improved in IFN-I expressing DCs which cause delay in endosomal acidification and prolong antigen survival and retention in the early endosomal compartment and redirect of antigens towards MHC class I processing pathways (100). Furthermore, IFN-I also shows direct effects on immune cells by promoting NK cell-mediated cytotoxicity and IFN-γ secretion. Moreover, cytokine production induced by IFN-I facilitates proliferation and survival of memory T cells and NK cells which dependent on IL-15 producing APCs and the differentiation of Th1 cells which dependent on IFN-γ producing DCs and NK cells (101). There is study showed that DC-specific Ifnar$^{-/-}$ mice could not reject highly immunogenic tumor cells due to defects in antigen cross-presentation to CD8$^+$ T cells. This evidence shows that IFN-I can act through DCs to promote T cell immunity (77). However, in persistent exposure of IFN such as

during chronic infection will induce immunosuppressive phenotype of DCs which drives T cell exhaustion by release of IL-10 and expression of PD-L1 (102).
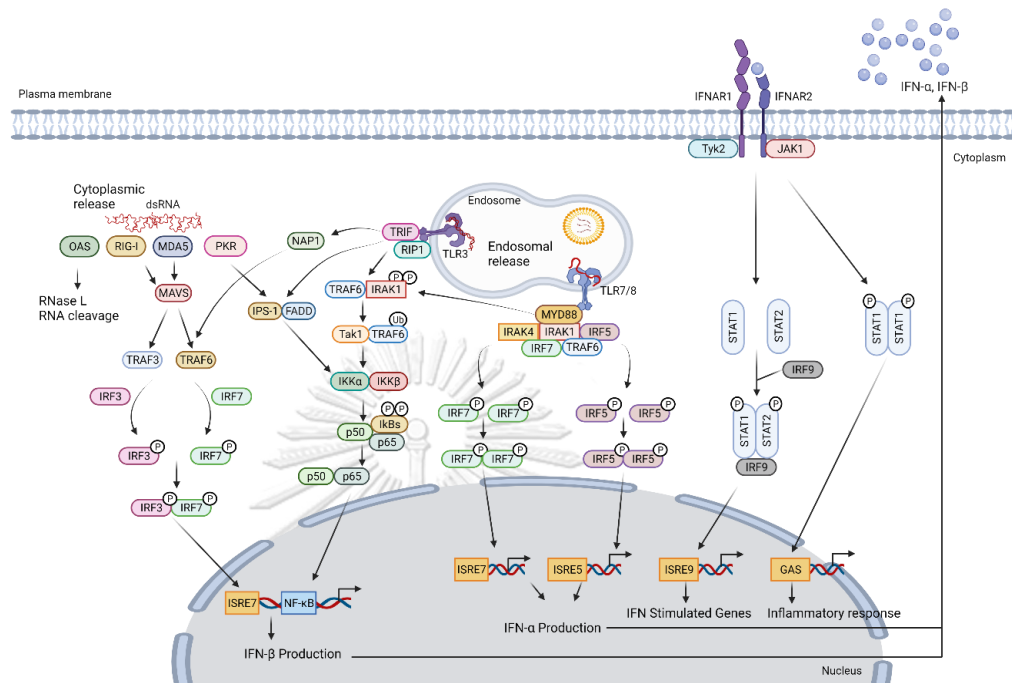
Figure 2.4 Upstream and downstream signalings of type I interferon upon detection of cytosolic and endosomal RNA

Intracellular endosomal TLRs including TLR-3 and TLR-7/8 are known to induce production of IFN-I and activated by dsRNA and ssRNA, respectively. TLR-3 signals via adaptor TRIF and activates IRF3 and NF-**K**B pathways encoded for IFN-β production. TLR-7/8 transmit the signal via the adaptor molecule MyD88 and activates IRF5 and IRF-7 leading to activation of IFN-I pathways and secretion of proinflammatory cytokines. Two RNA helicases, retinoic acid-inducible gene 1 (RIG-1) and melanoma differentiation-associated gene 5 (MDA-5), detect dsRNA in the cytoplasm. Activated RIG-1 and MDA-5 interact with adaptor protein MAVS anchored by its C-terminal domain to a mitochondrion. This interaction triggers signaling through TRAF3 and TRAF6 adaptors and results in activation of IRF3, IRF7 and NF-**K**B pathway. Sensing of dsRNA by 2',5'-oligoadenylate synthase (OAS) results in activation of nuclease RNase L, resulting in the degradation of cytoplasmic RNAs. Protein kinase dsRNA-dependent

serine-threonine kinase (PKR) activates NF-κB pathways encoded for IFN-β production, and which inactivates the alpha subunit of initiation factor eIF2, resulting in rapid inhibition of protein translation. (Modified from Delgado-Vega, AM., *et al.*, 2010 (103))

2.4 Neoantigens

Tumor-specific mutations are ideal targets for cancer immunotherapy as they can potentially be recognized as foreign antigens by the TCR repertoire without self-tolerance. Tumor antigens are categorized into two groups. Tumor-associated antigens (TAAs) are highly expressed by tumor cells, and very slightly expressed by normal cells. In contrast, tumor-specific antigens raised from random somatic mutations are expressed only in tumor cells known as neoantigen. Neoantigens, are now the main targets of mRNA vaccines. Identification of patient-specific immunogenic non-synonymous somatic mutations expressed in the tumor for personalized neoantigen vaccine using whole-exome, RNA, or transcriptome sequencing of a biopsy of tumor tissue are compared with sequences of healthy tissues. Next, the highest immunogenic mutations are screened, and identified using MHC class I epitope prediction algorithms (14) as shown in Figure 2.5.

Recently, nonsynonymous somatic point mutations in B16F10 murine melanoma cells have been reported. The genes that were found mutations often function as tumor suppressor genes, DNA repair and genes which control cell proliferation, adhesion, migration, and apoptosis (104). Unexpectedly, most of somatic mutations are recognized by CD4$^+$ T cells (16). This possibly because of less stringent length and sequence requirement for peptides binding to MHC class II molecules as compared to MHC class I epitopes. The main function of CD4$^+$ T cells is to provide cross-priming of CD8$^+$ cytotoxic T cells which responses by CD40 ligand-mediated activation of DCs (105).

2.4.1 Neoantigen in B16 melanoma model

PDZ-binding kinase (PBK), also known as T-lymphokine-activated killer cell-originated protein kinase (TOPK) is a 322 amino-acid MAPKK-like serine/threonine kinase (mitogen-activated protein kinase kinase-like serine/threonine kinase) which rarely found in normal tissues (106). PBK/ TOPK was suggested to be used as a biomarker (107) and a promising target for cancer therapy because overexpression of PBK/TOPK was found in proliferative cells and during mitosis (108, 109). The threonine-9 of upregulated PBK/TOPK will be phosphorylated after binding to cdk1/cyclin B1 complex. which promotes cytokinesis. In addition, elevated PBK/ TOPK expression in tumor tissue was associated with poor overall survival of patients and short disease-free survival. Apart from being a biomarker, HI-TOPK-032, a specific inhibitor for PBK/TOPK, may provide an anticancer therapy by reducing cell viability and colony formation via a dramatic increase in apoptotic cells *in vitro* and results in a significant decrease of colon cancer growth *in vivo* (110). Immunogenic point mutation of PBK/TOPK in B16F10 melanoma at protein position 145 from valine to aspartic acid (p.V145D) elicited CD8^{+} T cell responses upon mRNA immunization (16).

The actinin alpha 4 (ACTN4) is an actin-binding protein that participates in cytoskeleton organization and enhances RelA/p65-dependant expression of c-*fos*, *MMP-3* and *MMP-1* genes (111). Moreover, high ACTN4 expression also displayed a tumor suppressor activity and associated with LN metastasis. Patients with high copy number of ACTN4 showed weakened responses to the chemotherapy and radiotherapy and lower survival rate. Overexpression of ACTN4 induces invasive phenotypes through epithelial-to-mesenchymal transition by activating Akt signaling pathway. In migratory condition, epithelial cells will lose contacts with neighboring cells, change cytoskeletons organization and shape from globular to spindle-like. Consequently, ACTN4 become a predictive marker for cancer (112). The

phenylalanine to valine point mutation at protein position 835 (p.F835V) elicited CD4$^+$ T cell responses upon mRNA immunization (16).
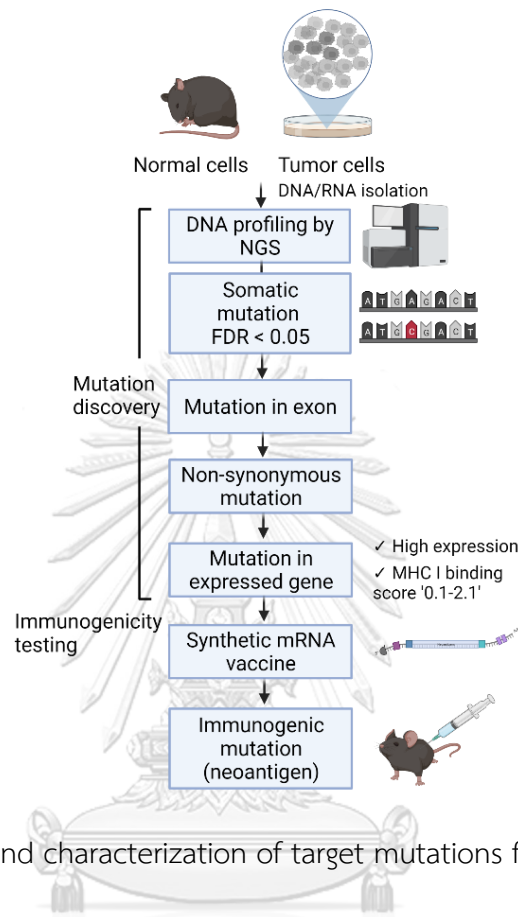
Figure 2.5 Discovery and characterization of target mutations for mRNA vaccine development

DNA and RNA from normal cells and tumor cells are extracted and cDNA libraries are prepared. All libraries are sequenced on an Illumina HiSeq2000. RNA reads are aligned to the reference genome and transcriptome using bowtie. Gene expression is determined by comparison with RefSeq transcript coordinates. DNA reads are aligned to the reference genome. Mutations are identified by algorithms and assigned a false discovery rate (FDR) confidence value. DNA-derived mutations are validated by either Sanger sequencing or the RNA-Seq reads. Finally, selected vaccine targets are from prioritization of mutations based on their expression levels and MHC binding capacity. Good MHC class I binding has 'low score' 0.1–2.1 contrast to poor binding

has 'high score' >3.9. Immunogenicity of mutation encoded mRNA vaccine is tested *in vivo*. (Modified from Castle, JC., *et al*., 2012 (113) and Kreiter, S., *et al*., 2012 (114))

2.5 Cancer immunotherapy

Current cancer clinical treatments include surgically remove of cancerous mass, chemotherapy, radiation therapy, cancer-specific medication, such as hormonal therapy and immunotherapy (115, 116). Cancer immunotherapy aims to educate or restore host's immune system ability to recognize and eradicate cancer cells through the recruitment and activation of cytotoxic effector cells and overcome immunosuppressive microenvironment in tumor. Cancer immunotherapy has gained more attention since FDA approvals of immune checkpoint inhibitors (117) and chimeric antigen receptor (CAR)-T cells (118). CAR-T cell therapy relies on isolating the patient's own T cells from the blood, engineering them *in vitro* to express receptors targeted to a specific tumor antigen then infusing them back to the patient. CAR-T cells can directly identify the tumor antigen without the involvement of the MHC complex and are more efficient at destroying the cancer (119). During this time, the realization that T cell activation requires antigenic stimulation through TCR as first signal, co-stimulation, and cytokine support as second and third signals respectively (120). While the co-inhibitory immune checkpoints naturally constrain T cell reactivity to prevent chronic activation of the immune system and maintain immune homeostasis, cancer cells or tumor-associated APCs exploits these brakes as a means of dampening anti-tumor T cell responses and promoting tumor immune escape. Designing monoclonal antibody for immune checkpoint blockade could unleash the effector activity and clinical impact of anti-tumor T cells (121). Other immunotherapeutic strategies include cytokine treatment such as IL-2 treatment which promotes differentiation of T cells (122), antibody-drug conjugates which target to antigen-specific cancer and at the same time loaded with anti-cancer drug (123),

oncolytic viruses that infect only cancer cells, kill, and make them visible to the immune system (124), adoptive transfer of ex vivo activated T and NK cells (125), and cancer vaccines that inject cancer antigen to stimulate immune responses against the cancer (126). Combination therapy between immunotherapeutic strategies alongside with radiation therapy and chemotherapy causes more effective prevention to immune escape due to visible cancer cell death and danger signal to immune system (127).

2.6 Cancer therapeutic vaccines

Vaccine is one of powerful tools to save lives more than million each year (128). Cancer vaccines are designed to educate immune cells to recognize the tumor-derived antigens which usually have a low immunogenicity and to break the establishment of immunosuppressive tumor environment to induce a potent antigen-specific immune response to eradicate tumor burden. In 1990, Bacillus Calmette-Guérin tuberculosis vaccine is the first FDA approval for cancer immunotherapy and is currently used for early-stage bladder cancer therapy (129). There are currently three FDA approved preventive cancer vaccines in preventing infection by human papillomaviruses (HPV) that can develop HPV-related anal, cervical, head and neck, penile, vulvar, and vaginal cancers including Cervarix® (HPV type 16 and 18), Gardasil® (HPV types 16, 18, 6, and 11), and Gardasil-9® (HPV types 16, 18, 6, 11, 31, 33, 45, 52, and 58) (130), in addition to another FDA-approved preventive vaccine, Hepatitis B vaccine (HEPLISAV-B®) in preventing infection by the hepatitis B virus (HBV) that cause HBV-related liver cancer (131). Most of cancers are curable if they could be detected at an early stage (132). However, there are several reasons why vaccine cancer treatment fails in the clinic such as the immune suppressive tumor microenvironment with expression of checkpoint inhibitors including PD-1, cytotoxic T-lymphocyte-associated protein 4 (CTLA-4), lymphocyte-

activation gene 3, and T-cell immunoglobulin and mucin domain 3 and presence of immune suppressive cells such as regulatory T cells, myeloid-derived suppressor cells, M2 macrophages, regulatory natural killer T cells or cytokines such as transforming growth factor-beta, IL-10, and IL-13 which leading to lack of a robust T cell responses (133). Furthermore, high mutation rate of cancer that cause dysregulated expression of oncogenes and tumor suppressor genes is another restriction in treatment, therefore multivalent formulation of vaccine is suggested (134-136). Successful vaccine development requires understanding of a pathogenic mechanism, a deeply knowledge of the immune mechanisms required for protection which leading to a rational vaccine regimen, and finding a new effective and safe adjuvant and delivery system (137). Breakthrough in targeted therapy directed at specific target in cancer cells (138) and next generation sequencing technology (139, 140) permits scientists to identify a strong immunogenic antigen for vaccines. Taking advantage of that insight, in 2010 the FDA approved therapeutic cancer vaccine, sipuleucel-T was designed for metastatic castration-resistant prostate cancer treatment by stimulating the patient's T-cells to recognize and attack prostate cancer cells that produce abnormally high levels of prostatic acid phosphatase antigen (141).

Conventional vaccine platforms including subunit vaccine, killed and live-attenuated vaccines, and nucleic acid (DNA or RNA)-based vaccine could provide a strong immune response. However, there is still a major drawback in eradication of pathogens which can evade adaptive immune responses (142). Although, subunit vaccines have been proved that elicit the humoral-mediated immunity, they fail to induce cell-mediated immunity which is important to get rid of intracellular pathogens (143). Live-attenuated vaccines have a powerful ability in inducing both humoral and cellular immunity, but safety concerns are considerable (144). Nucleic acid-based vaccine allows multiple tumor mutations or antigens encoded for nucleic

acid, allowing APCs to simultaneously present multiple epitopes on both MHC class I and II associated with the induction of broader humoral and cell-mediated immune responses leading to less MHC restriction in contrast to subunit vaccine and overcome immune evasion due to an effect of tumor heterogeneity (145). However, DNA-based vaccine need to be delivered cross the nuclear membrane and mutagenesis is considerable from integrating of DNA into host chromosomal genome (146). All these vaccine limitations are overcome by mRNA-based vaccine qualification which provide adjuvant effect to stimulate potent induction of both humoral and cell-mediated immune responses (147) without the risk of safety concerns due to non-infectious and non-integrating into host genome, and they are naturally degraded in a short time by host machinery. Furthermore, mRNAs are efficient vectors which can be encoded for any protein antigens by using host cell's translational machinery without MHC restriction (148, 149). mRNA vaccines are cost effective and extremely rapid and scalable production which is less than 2 months after nucleotide sequence available (150). Synthetic RNA pentatope encoding five neoantigens connected by 10mer non-immunogenic glycine/serine linkers were investigated to solve the problem of tumor heterogeneity and antigen escape. Mice with B16 melanoma cancer immunized with RNA pentatope shown 80% survival on day 32 whereas all control mice had died (16).

2.7 mRNA-based cancer vaccines

2.7.1 *In vitro* transcription of mRNA

mRNA vaccine platforms are applicable for both infectious and non-infectious diseases including cancer immunotherapy and protein replacement therapy (151). mRNA can be produced in a cell-free system via *in vitro* transcription (IVT). In 1990, the first success of an *in vivo* delivery of mRNA was reported. Protein translation was detected in animals after intramuscular administration of an IVT mRNA (152).

However, disadvantages of mRNA vaccines including the inherent instability and low level of protein expression as a result of high innate immunogenicity and inefficient delivery system made mRNA unpopular (153). Recently, breakthrough technologies have overcome these defects and bring up the distinctive point of mRNA vaccines (154).

Basically, an IVT mRNA is prepared from linearized plasmid DNA (pDNA) template which is transcribed into mRNA in a mixture of recombinant T7 RNA polymerase and nucleoside triphosphates. pDNA for IVT contains a bacteriophage T7 promoter, an open reading frame (ORF), a poly [d(A/T)] sequence transcribed into poly(A) and multiple restriction sites for linearization of the plasmid to ensure the termination of transcription. Cap is added enzymatically during or post transcription flanked at 5'-end via a 5' triphosphate (155). Cap and poly(A) tail are essential elements for efficient translation and stability of mRNA in the cytosol (50). The translation of mRNA lacking the 5'cap modification can be suppressed by interferon-induced protein with tetratricoid repeats (IFIT) family. IFIT can bind to subunits of eukaryotic initiation factor 3 (eIF3) complex. Normally, eIF3 interacts with eIF2 to form the 43S pre-initiation complex to allow the complex formation with 60s ribosome subunit and initiate the translation (156). Capping step with CleanCap (157) provides high capping efficiency with natural Cap1 (^{m7}GpppN$_{2'Om}$ N) product which has much lower affinity with IFIT. Cap 1 is the product of methylation of the 2' ribose position of the first cap-proximal nucleotide (Cap 0). Cap 1 has been shown to modulate binding or activation of innate immune sensors in contrast to Cap 0 and 5'-triphosphate can bind to retinoic acid inducible gene I and melanoma differentiation-associated antigen 5 (MDA5) which leading to transcription induction of IFN-I and proinflammatory cytokines (156). Moreover, mRNA also requires appropriate sequences at 5' and 3' untranslated regions (UTRs) to avoid destabilizing signals such as the signal from specific cis-acting destabilizing sequences like AU-rich elements

and microRNA binding sites which mostly reside in UTRs (155, 157). The β-globin gene of Xenopus at 5'- and 3'-UTRs were demonstrated to provide greater translational efficiency on heterologous mRNA in the mouse NIH 3T3 fibroblast cell line (158). Codon usage is also considered as a factor affecting the efficiency of translation relating to tRNA concentration (159). Moreover, mRNA stability can be regulated by sequence-engineered mRNA (160). Kozak sequence (5'-GCCRCCAUGG-3'; R is a purine base) is recommended to be part of a start codon which helps in translation efficiency (161). Accordingly, basic elements of synthetic mRNA contain a protein-encoding ORF flanked at 5'-end with a "cap" via a 5' triphosphate, 5'- and 3'-UTRs and a poly(A) tail at the 3'-end.

Following the transcription, the pDNA template is digested by DNase (155). The contaminants within a mixture with desired mRNA transcript including various nucleotides, oligodeoxynucleotides are removed by lithium chloride (LiCl) precipitation (162). In addition, foremost transcriptional by-product of an IVT is dsRNA which activates MDA5, protein kinase receptor (PKR) and oligoadenylate synthase (OAS). The activation of cytoplasmic RNA sensors PKR and OAS inhibit protein translation through phosphorylation of eIF2α and overexpression of ribonuclease L that degrades foreign and cellular RNA (155) . However, dsRNA can be efficiently removed by selective binding of dsRNA to cellulose-packed column filled with 16% ethanol-containing buffer. The removal rate of two-cycle purification is as high as 90%, and the recovery rate of pure IVT mRNA is more than 65%. Ranges of dsRNA which can bind to cellulose are between 30 to 1,000 bp (163). IVT mRNA can also be purified by a high-performance liquid chromatography (HPLC) that separates mRNA according to size, yielding a pure mRNA product (153, 164). The increase of protein expression was observed when transcripts coding for luciferase was purified by HPLC (165).

Purified unmodified IVT mRNA continues to induce high level release of IFN-I through activation of TLR-7. Activation of this receptor results in upregulation of gene transcription coding for IFN-I, proinflammatory cytokines such as IL-6, IL-12, TNF and chemokines (166) but it can be circumvented by incorporation of N1-Methylpseudouridine (m1Ψ) which has a lower affinity to the innate immune receptor and can diminish PKR activation which leading to translation inhibition (167, 168). Interestingly, mice immunized with unmodified mRNA elicited higher levels of CD8 T cell response and IFN-α in serum after 6 hrs of administration compared to nonimmunogenic-m1Ψ containing mRNA. This results perhaps due to benefits of IFN-I release as a result of activation of innate immune receptors and cross-present antigen to mount an adaptive immune response (169) as shown in Figure 2.6.
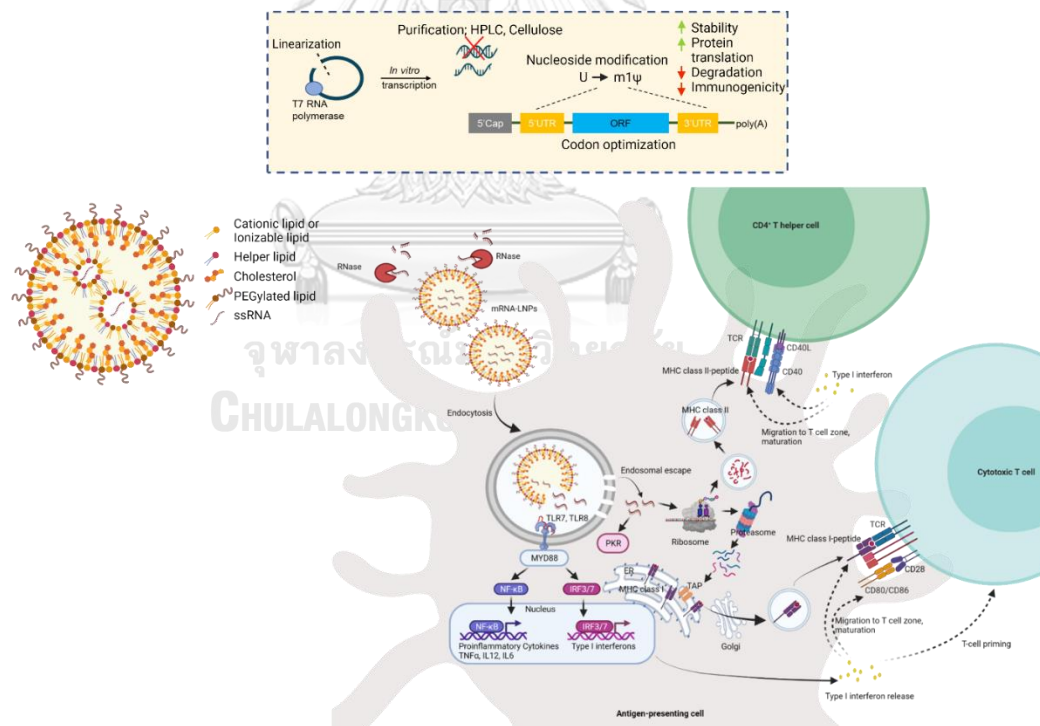
Figure 2.6 Designing of an mRNA vaccine and mechanism of action of mRNA-LNP

mRNA molecules are synthesized *in vitro* with the substitution of uridine with N1-methylpseudouridine (m1Ψ). mRNAs encoding target antigens are encapsulated in lipid nanoparticles (LNPs) which protect mRNA from degradation by RNase. mRNA-

LNPs enter cells by endocytosis. There is an interaction between cationic lipids in the LNP with anionic lipids of the endosome membrane which induces hexagonal HII phase formation, leading to disruption of the endosome membrane and release mRNA into the cytosol. ssRNA can be sensed by endosomal innate immune receptors. TLR7 and 8 can bind to uridine base in the sequence of ssRNA and trigger signaling cascades of NF-kB and IRF7 transcription factor which subsequently triggering of proinflammatory cytokines and IFN-I production. IFN-I helps in upregulation of the costimulatory and MHC molecules. mRNAs are translated in the cytoplasm by ribosome and subsequently processed by the proteasome, and the generated peptide enter the endoplasmic reticulum (ER) where they are loaded onto MHC class I molecules. The peptide-MHC class I complexes are presented to CD8$^+$ T cells. The translated proteins can also be phagocytosed into endosome and fused to lysosome and the proteins are degraded by lysosomal enzyme and peptides can be loaded onto MHC class II molecules. The peptide-MHC class II complexes are presented to CD4$^+$ T cells. Eventually, activated T cells are fully primed to become effector cells by IFN-I (Modified from Xu, S., *et al.*, 2020 (170)).

2.7.2 mRNA cancer vaccines

Ex vivo transfection of DCs with mRNA for adoptive transfer to patients was the first mRNA-based cancer vaccine entering clinical trial (171). Recently, non-viral vectors loaded with IVT mRNA-based vaccines have been extensively investigated in clinical trials. IVT mRNA-based non-cancer vaccines encoding immunostimulants such as IL-12, IL-32, OX40L, CD40L, and CD70 that induce APC maturation and promote antigen-presentation required for potent T-cell mediated immunity are usually co-administered with cancer vaccines or checkpoint inhibitors in order to break the establishment of immunosuppressive tumor microenvironment and induce a potent immune responses. Multiple IVT mRNA-based cancer vaccines encoding a cocktail of

TAAs which preferentially expressed in malignant cells such as NY-ESO-1, MAGE-A3, tyrosinase, TPTE, gp100, and melano-A/MART-1 identified as TAAs for melanoma and MUC-1, surviving, Trophoblast Glycoprotein, NY-ESO-1, MAGE-C1, and MAGE-C2 identified as TAAs for non-small cell lung cancers (NSCLC) are currently tested in clinical trials. With the advance in antigen selection technologies, personalized target neoantigens can be identified for encoding in mRNA cancer vaccines.

Table 2.1 List of active, or completed clinical trials of mRNA vaccines in cancer therapy (modified from Miao, L., et al., 2021 (172))

NCT number	Status/ Phase	Cancer type	mRNA and combination therapy	Formulation/ Route	Study Results
mRNA encoding immunostimulants					
NCT03394937	Recruiting/ I	Melanoma	Trimix mRNA (mRNA encoding CD40L, CD70, acTLR4) + TAA: tyrosinase, gp100, MAGE-A3, MAGE-C2, PRAME	Naked mRNA/ *i.n.*	Vaccine was immunogenic at low dose (600 μg) and high dose (1800 μg).
NCT01676779	Completed/ II	Melanoma	Trimix mRNA + TAA: MAGE-A3, MAGE-C2, tyrosinase,	DC-based/ *i.v.* and *i.d.*	71% disease free in treatment group vs 35% in

			gp100		control arm
NCT01302 496	Comple ted/ II	Melanoma	Trimix mRNA + TAA + CTLA4 inhibitor	DC- based/ *i.v.* and *i.d.*	T-cell stimulation were shown in 12/15 patients. Multifunctional CD8$^+$ T-cell responses were detected.
NCT03739 931	Recruitin g/ I	Solid Tumor or lymphoma	mRNA encoding OX40L, IL-23, IL-36γ + PD-L1 inhibitor	LNP/ *i.t.*	Administration can be associated with tumor shrinkage (52% Tumor reduction. Elevated IFN-γ, TNF-α, and PD-L1 levels were detected.
mRNA encoding tumor-associated antigens (TAAs)					
NCT00923 312	Comple ted/ I/II	NSCLC	MAGE-C1, MAGE-C2, NY-SEO-1, survivin, 5T4	RNActive (Protamin e)/ *i.d.*	Median progression-free and overall survival were 5 and 10.8 months.

NCT00831467	Completed/ I/II	Prostate cancer	PSA, PSCA, PSMA, STEAP1	RNActive/ *i.d.*	Vaccine was well tolerated and immunogenic
NCT00204516	Completed/ I/II	Melanoma	Melan-A, Mage-A1, Mage-A3, survivin, gp100, and tyrosinase	Naked mRNA/ *i.d.*	Not available

mRNA encoding neoantigens (Neo-Ag)

NCT02035956	Completed/ I	Melanoma	Neo-Ag	Naked mRNA/ *i.n.*	60% of neoantigens elicited a T- cell response.
NCT03289962	Recruiting/ I	Melanoma, NSCLC, Bladder Cancer, CRC, Breast Cancer	Neo-Ag + PD-L1 inhibitor	Lipo-MERIT/ *i.v.*	The release of pro-inflammatory cytokines and peripheral T-cell responses were induced.
NCT03815058	Recruiting/ II	Melanoma	Neo-Ag + PD-1 inhibitor	Lipo-MERIT/ *i.v.*	Not available

2.7.3 Delivery systems for mRNA vaccine

Since the advance of delivery technologies helps in success of cytosolic delivery of mRNA (173). Various delivery systems have been invented. RNA-conjugates linked mRNA to molecules which protect mRNA from degradation, but it can cause serum protein binding and aggregation which leading to vascular blockage (174). Viral vectors have an immunogenicity and carcinogenicity concerns and are difficult in production (24, 175, 176). Although non-viral vectors provide less transfection efficiency, they are simpler to synthesize and provide larger capacity to carry larger payloads, contain lower immunogenicity. In addition, due to no previous immune response in patients, multiple time of boost is applicable (177). Presently, lipid nanoparticles (LNPs) are the most commonly used of non-viral vector for delivery of nucleic acids because of ease in scale up manufacture, and protection of mRNA from hydrolysis by ubiquitous ribonucleases, and targeting specific cells (178), as well as help in rapid uptake, and mRNA escape to the cytoplasm (179-182). In addition, encapsulation in LNPs can increase the payloads which combined multiple mRNA encoding antigens and lead to induce strong immune response after a single immunization (183).

Main composition of LNPs includes cationic lipids, phospholipid, cholesterol, and polyethyleneglycol (PEG) (26). 1,2-dioleoyl-3-trimethylammonium-propane (DOTAP) has a permanent positive charge amine head group coupled to a glycerol backbone with two oleoyl chains. The backbone and chains are linked with hydrolysable ester bonds, which causes a biodegradable DOTAP and cytotoxicity reduction (184). DOTAP is completely protonated at pH 7.4 and more energy is required to separate DNA from it after delivery into the cell. For effective gene delivery, it should be combined with a helper lipid such as 1,2-dioleoyl-sn-glycero-3-phosphoethanolamine (DOPE). DOPE promotes an inverted hexagonal H (II) phase, which destabilizes endosomal membranes and facilitates endosomal escape of LNPs

(185). Phospholipids possess polymorphic features which promote a transition from a lamellar to a hexagonal phase in endosome (186). Cholesterol plays a stabilizing element role. A higher cholesterol content provides a lower transition temperature, which helps in the transition from lamellar to hexagonal phases (187). Lipid-anchored PEGs act as a barrier to reduce nonspecific binding of proteins to LNPs and increase the blood circulation time by lowering interactions with the anionic membranes of blood cells and, thus, improve the biocompatibility of LNPs (188). However, PEGylated lipid causes reduction of cellular uptake and interaction with the endosomal membrane (179, 189). The studies reported the toxic effects of cationic lipids despite of high transfection efficiency (190, 191). Afterwards, ionizable lipids were investigated which contained amine groups to provide a neutral or mildly cationic surface charge at physiological pH. At low pH, the ionizable lipid has a positive charge which enable complex with negatively charged nucleic acid. After uptake of mRNA-LNPs via endocytosis, the acidification in the endosome causes an ionization of the amine groups and helps in induction of hexagonal phase structure, which disrupts the membrane of the late endosomes (192, 193). Besides endosomal escape, the surface charge can also influence nanoparticle transportation. Small-sized negatively charged particles are efficiently transported to dLNs and reached the T cell zone (194).

LNP size is another key parameter. The size of particles less than 10 nm mainly enters blood capillaries rather than the lymphatic capillaries (195). Only diameter smaller than 200 nm can go through the lymphatic capillaries and consequently drains to the peripheral lymphatics and specifically 30 nm can reach to the T cell zone (196-198). The cellular transport by DCs is required for LN delivery of large particles (size > 200 nm) (199). APCs dwell at high density in LNs and spleen. mRNA can be injected directly in the LNs (193) or LNPs can be decorated with specific ligand on the surface to target LNs and effectively target to APCs (196). mRNA

complexed with LNPs functionalized with mannose can facilitate mRNA uptake by DCs in lymphoid organ and inhibit tumor growth and metastasis (197). LNPs have successfully used for the delivery of nucleic acid in many clinical trials (200) including COVID-19 mRNA vaccines of the Pfizer-BioNTech (201) and Moderna (202) which approved for emergency use by the United States Food and Drug Administration in December 2020.

2.7.4 Routes of administration for mRNA

Routes of administration are also important for targeting vaccine to lymphoid organs and induce effective immune responses. For both local and systemic immunization of mRNA vaccine, the utmost peak of IFN-α concentration in the circulation was at 6 hrs post immunization (18, 203). Recent reports have attributed contradictory impact of IFN-I in modulating CD8$^+$ T cell immunity, from stimulatory to inhibitory which determined by the timing and intensity of IFN-I induction relative to TCR activation. The kinetics expression of mRNA encoding firefly luciferase in secondary lymphoid organs upon intravenous (*i.v.*) injection showed high peak between 1 and 4 hrs in splenic DCs. Therefore, antigen presentation of DCs to activate splenic TCR signaling happen before IFNAR triggering. IFN-I functions as 'signal 3', in promoting the expansion and differentiation of primed CD8$^+$ T cells into cytolytic effector cells (18). The vital of IFN-α in initiating CD8$^+$ T cell immunity upon systemic immunization of mice with mRNA vaccines was reported. In an absence of IFN signaling prohibited effector cytokine secretion from CD8$^+$ T cells (31). In contrast with local delivery, protein antigen was predominantly expressed in transfected cells at the site of injection and took several hours for antigen uptake by Langerhans and migrated to dLNs for antigen presentation and TCR signal triggering. So, IFNAR triggering is likely to happen before TCR triggering, designating an antiproliferative and apoptotic program in CD8$^+$ T cells (204, 205). Recently, the observation of intradermal vaccination with mRNA lipoplexes in an absence of IFN-I signaling, mice

showed an increase of antigen specific CD8$^+$ T cell response and elicited a B16OVA melanoma growth control. This study indicates a detrimental effect of IFN-I in local delivery system (18). Intramuscular injection (*i.m.*) is preferred route of administration due to its simpler for implementation. Since few immune cells harbored in skeletal muscle, a local inflammation such as treatment with adjuvants which caused transient inflammation at the injection site is required to promote immune cell recruitment and activation for induction of an efficient immune responses (206-208). Moreover, adjuvant can predict the particular type of immune response being generated in order to provide the right arms to fight against the rivals (209, 210). The ideal of cancer vaccine adjuvant must drive a robust Th1-polarized and cell-mediated immunity response. mRNA vaccines possess a self-adjuvanticity by triggering release of immunostimulatory molecules (204) which interact with innate immune sensors on APCs which provide signaling cascades, resulting in mature APCs (104, 211). Thus, the difference of composition of mRNA vaccines, the quality of the mRNA, and the route of administration effect on innate immunogenicity and type of immune cell responses and impact the kinetics of antigen presentation which augment cytotoxic T cell responses.

2.8 Murine melanoma model

Malignant melanoma is the most dangerous skin cancer which developed from uncontrolled cellular growth of pigment-producing cells known as melanocytes mainly due to DNA damage from ultraviolet radiation exposure (212). Normally, once melanoma cancer spreading from original site to distant organs and tissues, it becomes incurable and causes deaths. The low immunogenicity and immunosuppression of cancer are associated with a low survival rate in metastatic melanoma patients (213). The incidence of death for patients who diagnosed with melanoma in the world in 2018 was 287,723 people accounting for 1.6% of all new

cancer cases and 60,712 people died accounting for 0.6% of all cancer deaths (214). The American Cancer Society reports incidences of melanoma in the United States in 2021 are about 106,110 new melanoma cases and about 7,180 people are expected to die of melanoma (215). The main current treatment, surgical excision is efficient only at early stage of melanoma. At late and metastatic stages, combination therapeutics to target specific mutated genes is needed, such as *BRAF* which frequently has the base substitution in advanced melanoma (216). Nevertheless, the limitation in duration of responses due to development of acquired resistance emerged after BRAF inhibitor treatment (217, 218).

B16 melanoma of C57BL/6 mice is an established tumor model for human melanoma. In subcutaneous model, palpable tumor will form within 10 days after implantation (1×10^5 cells) and tumor size will reach 1,000 mm^3 by day 21 (219). Recently, combination treatment of PD-L1 small interfering RNA and mRNA vaccine encoding tyrosinase related protein-2 exhibited effective treatment in a B16F10 melanoma mouse model associated with downregulation of PD-L1 in APCs and induction of cytotoxic T cell and humoral immune responses (220, 221). Moreover, tumor growth was significantly eradicated upon multiple boost of ovalbumin encoding mRNA on day 3, 7, 10, and 17 after tumor inoculation in contrast to mice in the control group died within 40 days (222).

CHAPTER III

MATERIALS AND METHODS

3.1 Animals

All C57BL/6 mice were purchased from Charles River Laboratories (Wilmington, MA, USA) or Nomura Siam International (Bangkok, Thailand). Age-matched (6–12 weeks) female mice were used in all experiments. Mice were maintained in a specific pathogen-free facility, and all protocols involving laboratory animals were approved by the institutional animal care and use committee (IACUC) at the University of Pennsylvania and Chulalongkorn University (Protocol Review No. 803941; 1723013; 1873005; 003/2565). The results are reported in accordance with the ARRIVE Guidelines (223).

3.2 Cell cultures

3.2.1 RAW264.7 cell line

RAW264.7, a murine macrophage cell line (ATCC TIB-71) was cultured in DMEM complete media containing DMEM supplemented with 10% (v/v) FBS, 10 mM HEPES, 1 mM sodium pyruvate and 1x Penicillin/Streptomycin G at 37°C with 5% CO_2.

3.2.2 Generation of bone marrow-derived macrophages (BMDMs)

3.2.2.1 L929-conditioned medium preparation

L929 cell, a murine fibroblast cell line (ATCC CCL-1) was seeded at 5×10^5 cells in tissue culture-treated plate (Corning, NY, USA) and cultured in 8 ml of DMEM complete media containing DMEM supplemented with 10% (v/v) FBS, 10 mM HEPES, 1 mM sodium pyruvate and 1x Penicillin/Streptomycin G at 37°C with 5% CO_2. After 95% confluence of the cells, the culture supernatant was collected and filtered through 0.22 μm filter (MF-Millipore, Germany).

3.2.2.2   BMDMs differentiation

Bone marrow cells (BMs) were flushed from humerus, femur and tibia of 6-8 weeks old C57BL/6 mice. BMDMs were prepared according to the protocol previously described (224). Briefly, BMs were cultured in non-treated cell culture petri dish (Hycon Plastics) with 8 ml of DMEM complete media containing DMEM supplemented with 10% (v/v) FBS, 10 mM HEPES, 1 mM sodium pyruvate and 1x Penicillin/Streptomycin G, supplemented with 5% (v/v) horse serum, and 20% (v/v) L929-conditioned media. On day 4, three ml of fresh media supplemented with 20% L929-conditioned media and 5% horse serum was added to the culture. Cells were harvested on day 7 using ice-cold phosphate buffer saline (PBS). Macrophage phenotype was confirmed by flow cytometry by staining using mouse anti-F4/80 and CD11b antibodies (BioLegend, USA). The derived BMDMs were seeded at 5×10^4 cells/well in 200 µl of DMEM complete media in 96-well plate before transfection.

3.2.3   Generation of bone marrow-derived dendritic cells (BMDCs)

BMDCs were prepared according to the protocol previously described (225). Briefly, BMs were cultured in 96-well tissue culture treated plate at 1×10^4 cells/well in 100 µl of BMDC media containing RPMI-1640 supplemented with 10% (v/v) FBS, 10 mM HEPES, 1 mM sodium pyruvate, 1x Penicillin/Streptomycin G, 1x GlutaMAX™ (Gibco, USA), 1x MEM Non-Essential Amino Acid (Gibco, USA), 55 µM β-mercaptoethanol (Gibco, USA). On day 0, recombinant mouse GM-CSF (20 ng/ml) (Peprotech, USA) was added to the media. On day 3, 6, and 8, fresh BMDC media containing recombinant mouse GM-CSF (20 ng/mL) were added. On day 10, the culture supernatant was discarded and the same volume of fresh BMDC media containing recombinant mouse GM-CSF (20 ng/mL) and recombinant mouse IL-4 (10 ng/mL) (Peprotech, USA) were added. On day 11, ¾ the volume of culture supernatant was discarded and the same volume of fresh BMDC media containing recombinant mouse GM-CSF (20 ng/mL) and recombinant mouse IL-4 (5 ng/mL) was

added. The derived BMDCs were cultured in BMDC media without cytokines and used for transfection on day 12. DC phenotype was confirmed by flow cytometry by staining with mouse anti-CD11c, MHC class II, CD40, CD86 antibodies (BioLegend, USA).

3.2.4 Tumor cell lines

B16F10-Luc2 melanoma cell line was obtained from the American Type Culture Collection (ATCC CRL-6475-LUC2™). This cell line was generated by lentiviral transduction of luciferase under the control of the EF-1 alpha promoter. Cells were maintained in DMEM media supplemented with 10% FBS and 10 µg/ml Blasticidin (InvivoGen, USA). The culture was maintained in CO_2 incubator at 37°C, 5% CO_2.

The ovalbumin (OVA)-expressing B16F0-OVA cell line was kindly provided by Dr. Edith Lord (Univ. Rochester, Rochester, NY). Cells were maintained in RPMI-1640 supplemented with 10% FBS, 10 mM HEPES, 1 mM sodium pyruvate, 1x GlutaMAX™, 1x MEM Non-Essential Amino Acid, 55 µM β-mercaptoethanol, 1x Penicillin/Streptomycin G and G418 (400 µg/ml) (InvivoGen, USA). The culture was maintained in CO_2 incubator at 37°C, 5% CO_2.

3.3 RNA constructs and *in vitro* transcription

Plasmid templates for *in vitro* transcription of antigen-encoding RNAs were based on the previously published pUC-ccTEV-A101 vector (181). pUC-ccTEV-ovalbumin-A101 (OVA), pUC-ccTEV-neoantigens-A101 (Neo), pUC-ccTEV-luciferase-A101 (Luc2) and pUC-ccTEV-mCherry-A101 vectors were synthesized by GenScript (Piscataway, NJ, USA). The Neo construct contained the sequence encoding two point-mutated 27-meric peptides (Pbk and Actn4) linked by a sequence encoding a 10 amino-acid long glycine-serine linker. The mRNAs were produced from plasmids encoding codon-optimized antigens. Plasmids were linearized with restriction enzyme including AflII and NotI (New England BioLabs, USA). In the transcription procedure, the MEGAscript

T7 Transcription Kit (Ambion, USA) was used. Percent of N1-methylpseudouridine-5′-triphosphate (m1Ψ) (TriLink) and UTP nucleotides were varied by mole (0, 5, 10, 20, 30, 40, 50, 60, 70, 80, 90 and 100% m1Ψ). RNAs were capped using CleanCap AG (3'OMe) (TriLink, USA). The mRNA was purified by cellulose purification, as described (163). All RNAs were analyzed for the integrity by native agarose gel electrophoresis and dot blot analysis. mRNAs were stored frozen at −80°C until use.

3.4 Cellular transfection with mRNA

BMDMs were harvested after 7-days of differentiation as described above with cold PBS and seeded $5×10^4$ cells/well in 200 µl of DMEM complete media in a 96-well plate. BMDCs were used for transfection after 12 days of differentiation. BMDCs and BMDMs were incubated with mRNA encoding mCherry or luciferase complexed with lipid nanoparticles (LNPs) (Acuitas Therapeutics, Canada) or TransIT transfection reagent (Mirus Bio, USA) (0.1 µg mRNA). This complex was added to cells. Reporter proteins in mRNA-transfected cultured cells were detected and quantified at 48 hrs after transfection. mCherry positive cells were quantified by LSR Fortessa flow cytometer (BD Biosciences, USA) and analyzed with FlowJo 10.6.0 software (Tree Star, USA). For firefly luciferase expression, cells were lysed in firefly-specific lysis reagent (Promega, USA). Aliquots were assayed for enzyme activity using the firefly luciferase assay system (Promega, USA) and a MiniLumat LB 9506 luminometer (Berthold/EG&G; Wallac, USA).

3.5 *In vivo* cellular uptake and protein expression

Mice were injected intramuscularly (*i.m.*) with 5 µg of mCherry encoding mRNA-LNP per mouse. Draining lymph node (inguinal) and spleen were excised 48 hrs after injection. Single-cell suspensions were prepared by crushing the tissues between frosted microscope slides (Sail brand, China). Cells were filtered through a 70-µm cell

strainer (BD Falcon, USA), washed twice, and stained with LIVE/DEAD Fixable Aqua Dead Cell Stain Kit (Life technologies, USA) for 10 minutes at room temperature. Then, cells were washed once in FACS buffer containing 2% (v/v) FBS in PBS and cells were blocked with purified anti-mouse CD16/CD32 (0.5 µg) (BD Biosciences, USA) for 20 minutes at 4°C. Monoclonal antibodies for extracellular staining shown in Table 3.1 were stained for 30 minutes at 4°C. Cells were washed and fixed in PBS containing 1% paraformaldehyde (Sigma-Aldrich, USA) then acquired on an LSR Fortessa flow cytometer and analyzed with FlowJo 10.6.0 software.

Table 3.1 List of antibodies used for detection of *in vivo* cellular uptake and expression

Antigen/ Clone/ Fluorophore	Manufacturer	Catalog number	Amount used per 2×10^6 cells in 100 µl
CD11c, clone N418, APC	BioLegend, USA	117310	0.2 µg
MHCII, clone M5/114.15.2, AF700	BioLegend, USA	107622	0.2 µg
XCR1, clone ZET, BV650	BioLegend, USA	148220	0.2 µg
CD103, clone 2E7, APC/Cy7	BioLegend, USA	121432	0.2 µg
CD11b, clone M1/70, BV421	BioLegend, USA	101236	0.2 µg
F4/80, clone BM8, PE/Cy7	BioLegend, USA	123114	0.2 µg
CD172a, clone P84, FITC	BioLegend, USA	144006	0.5 µg
CD301b, clone URA-1, PE	BioLegend, USA	146804	0.2 µg
CD40, clone 3/23, PE/Cy5	BioLegend, USA	124618	0.2 µg
CD86, clone GL-1, PE	BioLegend, USA	105008	0.2 µg
B220, clone RA3-6B2, BV711	BioLegend, USA	103255	0.2 µg
NK1.1, clone PK136, BV711	BioLegend, USA	108745	0.2 µg
CD3, clone 17A2, BV711	BioLegend, USA	100241	0.2 µg

TER119, clone TER119, BV711	BioLegend, USA	740686	0.2 µg
CD19, clone 6D5, BV711	BioLegend, USA	115555	0.2 µg

3.6 *Ex vivo* tissue imaging study

Mice were injected intradermally (*i.d.*) or *i.m.* with 5 µg of luciferase encoding mRNA complexed with LNPs (Luc mRNA-LNP). Four hrs later, lymphoid tissues and organs including inguinal lymph nodes, spleens, livers, lungs, hearts, kidneys were harvested for *ex vivo* tissue imaging to assess signal biodistribution. The images were evaluated by using the IVIS spectrum imaging system (Caliper Life Sciences, USA) and analyzed with the IVIS Living Image 4.0 software (Caliper Life Sciences).

3.7 Bioluminescence imaging

Uptake and translation of mRNA encoding luciferase were evaluated by *in vivo* bioluminescence imaging using the IVIS spectrum imaging system. The expression of luciferase was measured at 4 hrs after *i.d.* or *i.m.* injection of 5 µg Luc mRNA-LNP and every 24 hrs on day 1-14 post-injection. Mice were anesthetized in a chamber with 3% isoflurane and administered D-luciferin (PerkinElmer) at a dose of 150 mg/kg intraperitoneally (*i.p.*) and placed on the imaging platform while being maintained on 2% isoflurane via a nose cone. Mice were imaged at 5 minutes post administration of D-luciferin using an exposure time of 1 second or longer to ensure that the signals were above the noise levels and below the saturation limit. The photon fluxes (photons/second) were measured in the region of interest which was defined by using the IVIS Living Image 4.0 software.

3.8 Melanoma tumor model

3.8.1   Immunogenicity study

Eight weeks old C57BL/6 female mice were randomly divided into 11 groups (n = 5 per group) as shown in Table 3.2. Vaccination was performed by *i.m.* injection of 10 µg mRNA-LNP in 35 µl PBS (Gibco, USA). Mice were immunized with LNPs loaded mRNA encoding ovalbumin (OVA mRNA-LNP) or neoantigen (Neo mRNA-LNP) on day 0 and boosted on day 4 with the same dose and formulation. Luciferase or mCherry encoded mRNA-LNP was used as a control. Mice were sacrificed 7 days after the booster dose to collect blood and spleens (Figure 3.1).

Table 3.2 Vaccine formulas (per dose) for testing immunogenicity of OVA and neoantigen model vaccines

Group No.	Construct	Percentage of m1Ψ in mRNA
1	pUC-ccTEV-ovalbumin-A101	0
2		40
3		70
4		100
5	pUC-ccTEV-luciferase-A101	100
6	PBS (negative control for ovalbumin vaccine)	-
7	pUC-ccTEV-neoantigen-A101	0
8		100
9	pUC-ccTEV-mCherry-A101	0
10		100
11	PBS (negative control for neoantigen vaccine)	-
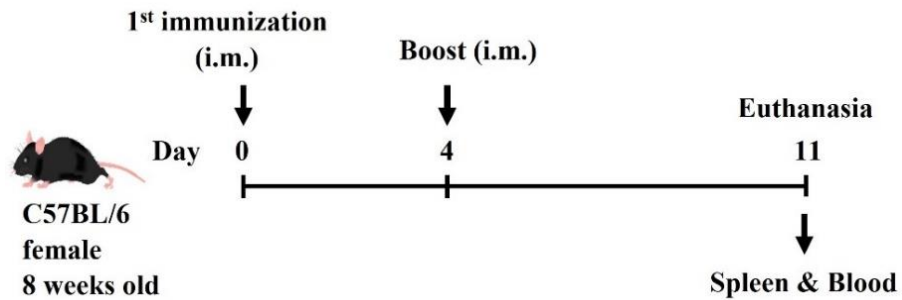
Figure 3.1 Schematic immunization regimen for immunogenicity test

3.8.2 Restimulation of splenocytes with synthetic peptides

For an *in vitro* re-stimulation of splenocytes, a pool of six synthetic peptides (Jerini Peptide Technologies, Germany) of 11-27 amino acids (a.a.) in length of B16F10 neoantigens (Pbk and Actn4), with eight overlapping residues were used. The purity of the peptides was > 95% with HPLC purification. Peptides were derived from the mutated sequences of Pbk (PAAVILRDALH, VILRDALHMAR and DSGSPFPAAVILRDALHMARGLKYLHQ) and Actn4 (FQAFIDVMSRE, FIDVMSRETTD and NHSGLVTFQAFIDVMSRETTDTDTADQ). Peptides were used at the final concentration of 2.5 µg/ml per peptide. A synthetic peptide of 8 a.a. in length from the sequence of ovalbumin (H2-K^b-restricted OVA$_{257-264}$ SIINFEKL) (Invivogen, USA) was used at a concentration of 2.5 µg/ml.

3.8.3 Therapeutic efficacy test

3.8.3.1 Localized melanoma

Eight weeks old C57BL/6 female mice were randomly divided into 10 groups (*n* = 6-10 per group) as shown in Table 3.3.

3.8.3.1.1 OVA model

Anesthetized mice were injected subcutaneously (*s.c.*) into the flank with 2×10^5 cells of B16F0-OVA tumor cell lines in 200 µl of sterile Hanks' balanced salt solution (HBSS) (Gibco, USA) on day 0. Two doses of 10 µg of

ovalbumin or luciferase (irrelevant antigen) encoded mRNA-LNP were administerd *i.m.* on day 4 and 8 after tumor inoculation.

3.8.3.1.2 Neoantigen model

Anesthetized mice were injected subcutaneously (*s.c.*) into the flank with 2×10^5 cells of B16F10-Luc2 tumor cell lines in 200 µl of sterile HBSS on day 0. Two doses of 10 µg of neoantigens or mCherry (as irrelevant antigen) encoded mRNA-LNP were administerd *i.m.* on day 4 and 8 after tumor inoculation. Tumor growth was monitored 2–3 times a week, and the survival was recorded for at least 60 days (Figure 3.2). Tumor volumes were monitored by using vernier caliper and calculated using the equation: $V = (4\times3.14\times A \times B^2)/3$, where V = volume ($mm^3$), A = the largest diameter (mm), and B = the smallest diameter (mm) (31). Mice were sacrificed when tumor size reached 20 mm in diameter or 400 mm^2 (226).

Table 3.3 Vaccine formulas (per dose) for therapeutic test of OVA and neoantigen model antigen vaccines

Group No.	Tumor cell line	Construct	Percentage of m1Ψ in mRNA
1	B16F0-OVA	pUC-ccTEV-ovalbumin-A101	0
2			100
3		pUC-ccTEV-luciferase-A101	0
4			100
5		PBS (negative control)	-
6	B16F10-Luc2	pUC-ccTEV-neoantigen-A101	0
7			100
8		pUC-ccTEV-mCherry-A101	0
9			100
10		PBS (negative control)	-
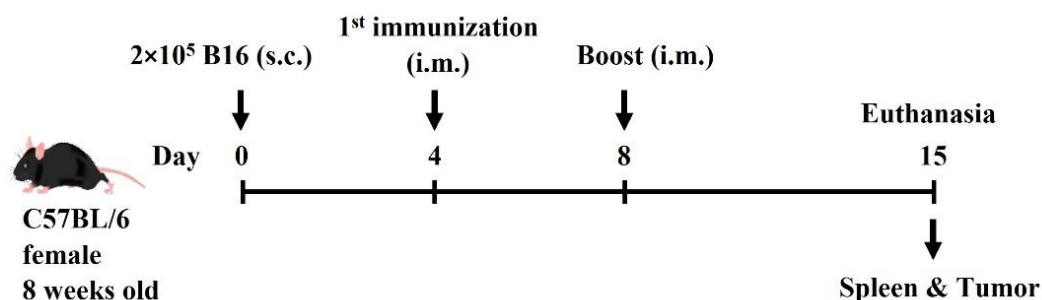
Figure 3.2 Schematic immunization regimen for therapeutic efficacy test

3.8.3.2 Metastatic melanoma

Eight weeks old C57BL/6 female mice were divided into 5 groups (n = 6 per group) as shown in Table 3.4. Mice were injected intravenously (*i.v.*) through lateral tail veins with 2×10^6 cells of B16F0-OVA tumor cells in 200 μl of sterile HBSS. Mice were immunized with 10 μg of mRNA encoding ovalbumin or PR8HA (irrelevant antigen) on day 4 and 8 after tumor inoculation. On day 18, mice were euthanized with isoflurane (Figure 3.3). Lungs were fixed and bleached in Fekete's solution to count the tumor nodules on the lung surface.

Table 3.4 Vaccine formulas (per dose) for study of lung metastasis inhibition of model vaccine

Group No.	Tumor cell line	Construct	Percentage of m1Ψ in mRNA
1	B16F0-OVA	pUC-ccTEV-ovalbumin-A101	0
2			100
3		pUC-ccTEV-PR8HA-A101	0
4			100
5		PBS (negative control)	-
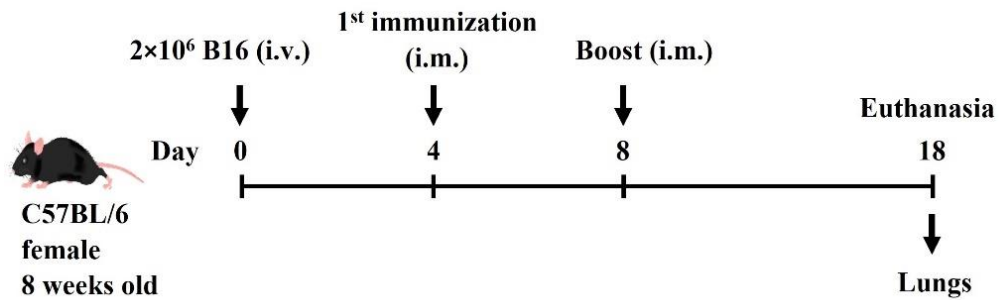
Figure 3.3 Schematic immunization regimen for lung metastasis inhibition study

3.9 Serum and tissue preparation

Peripheral blood was collected from the orbital sinus with capillary tube (Hirsch mann, Germany). The collecting blood was left at room temperature for 30 minutes and serum were collected after centrifugation at 10,000 g, 5 minutes. Serum were stored at -80°C until use.

Spleens and lymph nodes were collected, and single-cell suspensions were prepared in RPMI-1640 containing 10% (v/v) FBS after homoginization by frosted microscope slides and passed through 70-μm cell strainer. Erythrocytes in splenocyte suspension were removed by ACK lysing buffer (Quality Biological, USA).

Murine B16 tumors were harvested and chopped into small pieces (1-2 mm). Cells were washed once with 10% (v/v) FBS in RPMI-1640. After centrifugation at 2,000 rpm for 10 minutes at 4°c, 1 mg/ml collagenase IV (Sigma-Aldrich, USA) and 100 mg/ml DNase I (Sigma-Aldrich, USA) in RPMI-1640 containing 10% (v/v) FBS, 1x Penicillin/Streptomycin G, 55 μM β-mercaptoethanol were added and incubated at 37°C for 20 minutes in 250 rpm shaking incubator to disperse aggregates and facilitate digestion to release stromal cells. Then, cells were passed through 40-μm cell strainer and grinded the small pieces on the strainer with syringe and rinsed with 2% (v/v) FBS in RPMI-1640 to pass all remaining cells through the strainer. Cells were was hed once with 2% (v/v) FBS in RPMI-1640 and centrifuges at 2,000 rpm for 10 minutes at 4°c. Erythrocytes in tumor suspension were removed by ACK lysing buffer. Cell

numbers were counted with Vi-Cell XR cell counter (Beckman Coulter, USA).

3.10 Cell surface staining and intracellular cytokine staining (ICS) of *in vitro* re-stimulated splenocytes

After *in vitro* re-stimulation of 2×10^6 splenocytes with peptide OVA$_{257-264}$ SIINFEKL (2.5 µg/ml) or a pool of six synthetic peptides of Pbk and Actn4 neoantigens (2.5 µg/ml per peptide) with purified anti-mouse CD28 antibody (1 µg/ml) (BioLegend, USA) for 6 hrs in the presence of brefeldin A (20 µg/ml), and GolgiStop^{TM} (40 µg/ml) (BD Pharmingen, USA) for the last 5 hrs, cells were washed in PBS and stained with the LIVE/DEAD Fixable Aqua Dead Cell Stain Kit for 10 minutes at room temperature. Cells were washed once in FACS buffer containing 2% (v/v) FBS in PBS and blocked with purified anti-mouse CD16/CD32 (0.5 µg/sample) for 20 minutes at 4°C. Cells were washed once in FACS buffer and the cell surface markers were stained for 30 minutes at 4°C. Cells were then fixed and permeabilized by Fixation/Permeabilization solution (BD Biosciences, USA) for 20 minutes at 4°C. After two times washing in 1x BD Perm/Wash buffer (BD Biosciences, USA), the fixed/permeabilized cells were stained for detecting intracellular cytokines for 30 minutes at 4°C. Three times of the final wash was performed in 1x BD Perm/Wash buffer and cells were resuspended in FACS buffer. Monoclonal antibodies for surface staining and ICS staining were listed in Table 3.5. Flow cytometric data were acquired on an LSR Fortessa flow cytometer and analyzed with FlowJo 10.6.0 software.

3.11 Cell surface staining of tumor infiltrating immune cells

After single cell suspensions from tumor mass were prepared as stated above, cells were counted, and 2×10^6 cells were stained with the LIVE/DEAD Fixable Aqua Dead Cell Stain Kit or PI (BioLegend, USA) for 10 minutes at room temperature. Cells were washed once in FACS buffer and blocked with purified anti-mouse CD16/CD32

(0.5 µg) for 20 minutes at 4°C. Cells were washed once in FACS buffer and the cell surface markers were stained for 30 minutes at 4°C. The final wash was performed once in FACS buffer and cells were resuspended in FACS buffer. Monoclonal antibodies for cell surface staining were listed in Table 3.5.

Table 3.5 List of antibodies and concentration used for surface and intracellular cytokine staining

Antigen/ Clone/ Fluorophore	Manufacturer	Catalog number	Amount used per 2×10^6 cells in 100 µl
CD3, clone 17A2, biotin	BioLegend, USA	100244	0.25 µg
CD3, clone 17A2, FITC	BioLegend, USA	100204	0.5 µg
CD3, clone 17A2, BV605	BioLegend, USA	100237	0.25 µg
CD4, clone GK1.5, AF488	BioLegend, USA	100423	0.25 µg
CD4, clone GK1.5, PerCP/Cy5.5	BioLegend, USA	100434	0.2 µg
CD8, clone 53-6.7, PE	BioLegend, USA	100708	0.25 µg
CD8, clone 53-6.7, BV785	BioLegend, USA	100750	0.2 µg
CD44, clone IM7, BV650	BioLegend, USA	103049	0.2 µg
CD62L, clone MEL-14, AF700	BioLegend, USA	104426	0.5 µg
PD-1, clone RMP1-30, PE/Cy7	BioLegend, USA	109110	0.25 µg
PD-1, clone 29F.1A12, APC/Cy7	BioLegend, USA	135224	0.2 µg
F4/80, clone BM8, AF488	BioLegend, USA	123120	0.25 µg
CD206, clone C068C2, PE	BioLegend, USA	141706	0.25 µg
IL-5, clone TRFK5, PE	BioLegend, USA	504304	0.2 µg

IL-17A, clone TC11-18H10.1, APC/Cy7	BioLegend, USA	506940	0.2 µg
Granzyme B, clone GB11, Pacific Blue	BioLegend, USA	515408	2.5 µl
IFN-γ, clone XMG1.2, FITC	BioLegend, USA	505806	0.5 µg
IFN-γ, clone XMG1.2, AF700	BioLegend, USA	505824	0.5 µg
IL-2, clone JES6-5H4, APC	BioLegend, USA	503810	0.2 µg
TNF-α, clone MP6-XT22, PE/Cy7	BD Pharmingen, USA	557644	0.2 µg
CD69, clone H1.2F3, APC	BioLegend, USA	104514	0.2 µg
CD11b, clone M1/70, PE	BioLegend, USA	101208	0.25 µg
CD86, clone GL-1, biotin	BioLegend, USA	105004	0.25 µg
CD11c, clone N418, BV711	BioLegend, USA	117349	0.2 µg
CD45R, clone I3/2.3, PC7	Beckman Coulter, USA	A88587	0.25 µg
XCR1, clone ZET, BV650	BioLegend, USA	148220	0.2 µg
CD103, clone 2E7, APC/Cy7	BioLegend, USA	121432	0.2 µg
CD40, clone 3/23, PE/Cy5	BioLegend, USA	124618	0.2 µg

3.12 Measurement of cytokines by ELISA

Culture supernatants from transfected BMDMs and BMDCs were harvested at 48 hrs after transfection with TransIT-complexed mRNA (0.1 µg/well). Serum collected from immunized mice treated as indicated was prepared. Mouse IFN-α (Invitrogen, USA) and IFN-β ELISA (BioLegend, USA) was carried out according to the manufacturer's instructions. Briefly, ELISA plate was pre-coated with an anti-mouse IFN-α or IFN-β coating antibodies. The samples were diluted to 1:10 in PBS and

standard was prepared in 2-fold serial dilutions. All standards and samples were run in duplicate. The wells were washed with wash buffer and assay buffer was added to all wells. Diluted sample or standard was added. Calibrator diluent was added to the blank well. Biotin-conjugate was added to all wells and incubated for 2 hrs at room temperature on microplate shaker. Wells were emptied and washed. Streptavidin-HRP was added to all wells and incubated for 1 hr at room temperature on microplate shaker. Wells were emptied and washed with wash buffer. 3, 3', 5, 5'-tetramethylbenzidine (TMB) substrate solution was added to all wells and incubated for 30 minutes at room temperature. The 2N H_2SO_4 stop solution was added to all wells and the absorption was read at 450 nm using microplate reader (Biochom Anthos, UK).

3.13 Measurement of specific antibody titer in serum by ELISA

Firstly, 10 µg/ml (100 µl/well) of OVA whole protein (InvivoGen, USA) was coated on 96 well MaxiSorp plate (Nunc, Denmark) in coating buffer ($NaHCO_3$ and Na_2CO_3 in PBS, pH 9.5) and the plate was incubated at 4°C for overnight. Next day, plate was washed 4 times (200 µl/well) with 0.05% Tween20 in PBS and blocked (100 µl/well) with 10% FBS in PBS for 1 hr at room temperature. Plates were washed 4 times (200 µl/well). Serial dilutions of serum were prepared (1: 20 dilution) in 10% FBS in PBS and added (100 µl/well). After 2 hrs of incubation, plates were washed 4 times (200 µl/well) and rat anti-mouse IgG1-HRP (Invitrogen, USA) or goat anti-mouse IgG2c-HRP (Cell Signaling Technology, USA) or sheep anti-mouse IgG-HRP (GE Healthcare, UK) (100 µl/well) was added as listed in Table 3.6. Plates were incubated for 30 minutes. After 6 times of washing step, TMB (Sigma Aldrich, USA) (100 µl/well) was added to develop the signal and 1N of H_2SO_4 stop solution (100 µl/well) was added. The absorbance at 450 nm was measured with microplate reader.

Table 3.6 List of antibodies and their dilution used for ELISA

Detected target	Antibody	Manufacturer	Catalog number	dilution
IgG1	Rat anti-mouse IgG1-HRP	Invitrogen, USA	04-6120	1:3,000
IgG2c	Goat anti-mouse IgG2c-HRP	Cell Signaling Technology, USA	56970S	1:3,000
Total IgG	Sheep anti-mouse IgG-HRP	GE Healthcare, UK	LNA931V/AH	1:5,000

3.14 *In vivo* cytotoxicity assay

Assay was performed according to the protocol previously described (227). Briefly, single cell suspension of splenocytes were harvested from naïve mice. After washing, cells were divided into two aliquots with equal numbers. Cells were stained with carboxyfluorescein diacetate succinimidyl ester (CFSE) (Invitrogen, USA). One aliquot was stained with 0.7 µM (CFSE^{low}), another was stained with 7 µM (CFSE^{high}) for 15 minutes at 37°C, 5% CO_2 and washed once in 10% (v/v) FBS in RPMI-1640. CFSE^{high} population was pulsed with 2.5 µg/ml OVA$_{257-264}$ SIINFEKL for 40 minutes at 37°C, 5% CO_2. Cells were washed three times with 10% (v/v) FBS in RPMI-1640. Each immunized mouse received two million cells of CFSE^{low} and CSFE^{high} (four million cells in total). After two weeks of immunization, mice were injected *i.v.* with a peptide-pulsed CFSE^{high} splenocytes (target cells) and non-pulsed CFSE^{low} splenocytes (nontarget cells). After the transfer of CFSE-labeled cells for 18 hrs, mice were sacrificed, and spleens were dissected. The ratio of target cells versus nontarget cells in the spleen was measured by LSR Fortessa flow cytometer and analyzed with

FlowJo 10.6.0 software. The % of specific target cell lysis was calculated by the following formula:

$$100-100\times((CFSE^{high}/CFSE^{low})^{\ immunized\ mice}\ /\ (CFSE^{high}/CFSE^{low})^{\ mock\text{-}mice})$$

3.15   *In vivo* blocking of IFN-I by IFNAR1-specific monoclonal antibody

B16F0-OVA cell lines were injected *s.c.* into mice to allow for tumor formation as described above. At day 4 and day 8, mice were *i.p.* injected with 400 μg/dose of IFNAR1-specific MAR1-5A3 monoclonal antibody (mAb) (BioLegend, USA) (228) or MOPC-21 isotype control mAb (BioLegend, USA) following previous report (229) for 1 hr before mRNA-LNP vaccination (31). Tumor growth and immune infiltrated cells were analyzed at day 42.

3.16   Detection of IFN-γ secreting-splenocytes by ELISpot

ELISpot was performed according to the manufacturer's instructions (BD Biosciences, USA). In brief, membrane on ELISpot plate was pre-wet with 70% ethanol (15 μl/well) for 45 seconds and washed 5-times with PBS (200 μl/well) and diluted BD NA/LE purified anti-mouse IFN-γ capture antibody in 1x PBS (1:200) was added (100 μl/well). The plate was incubated at 4°C for overnight. The next day, the plate was washed once (200 μl/well) with blocking solution containing RPMI-1640 with 10% (v/v) FBS, 1x Penicillin/Streptomycin G, and L-glutamine and blocked (200 μl/well) with blocking solution for 2 hrs at 37°C, 5% CO_2. After dumping blocking solution, splenocytes (2×10^6 cells/100 μl) were seeded into each well. Diluted OVA whole protein (20 μg/ml) or concanavalin A (Sigma-Aldrich, USA) (10 μg/ml) in blocking solution was added (100 μl/well) and the plate was incubated for 48 hrs at 37°C, 5% CO_2. The plate was washed (200 μl/well) 2 times with deionized water and 3 times with 1x PBS containing 0.05% (v/v) Tween-20. Diluted biotinylated anti-mouse IFN-γ detection antibody in 1x PBS with 10% (v/v) FBS (1:250) was added (100

μl/well) and incubated for 2 hrs at room temperature. After 3 times washing step, diluted streptavidin-HRP (1:100) was added (100 μl/well) and incubated for 1 hr at room temperature. After 6 washing steps, AEC substrate solution was added (100 μl/well) and spot development was monitored for 30 minutes and the plate was wahed with deionized water (10 times) to stop reaction and the plate was air-dried at room temperature for overnight in dark. Spots were enumerated by ELISpot plate reader (ImmunoSpot, USA).

3.17   LNP-based delivery system for plasmid DNA (pDNA)

3.17.1 Plasmid construct

Plasmid template was based on pVAX1 vector (Thermo Fisher Scientific). DsRed2, red fluorescent protein was cloned into the pVAX1 vector (Figure 3.4). For validation, plasmid constructs encoding reporter genes were subjected to Sanger sequencing.
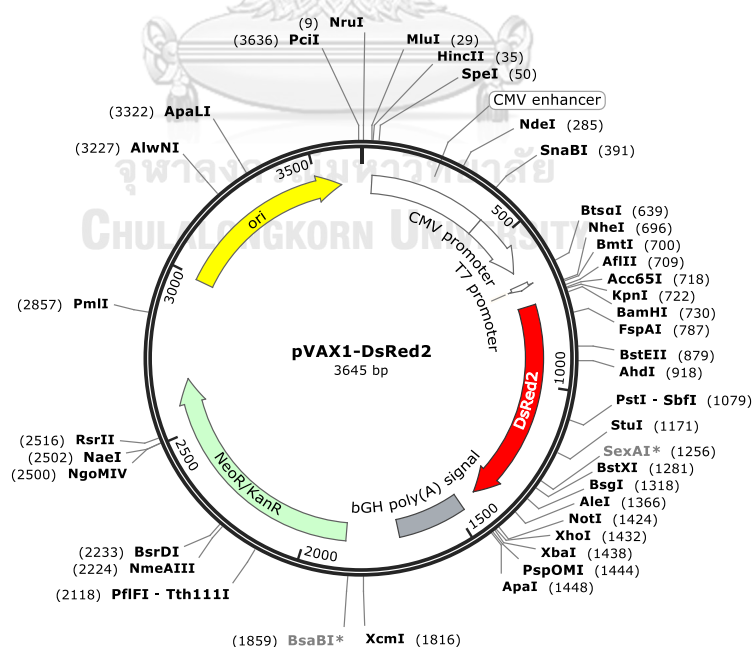
Figure 3.4 pVAX1-DsRed2 plasmid vector

3.17.2 LNP preparation based on commonly used lipids

LNPs with cationic net charge were used to complex with pDNA. LNP

preparation was divided into 2 groups of different formulas. The first formula was comprised of cationic lipid DOTAP and the helper lipid DOPE (both from Avanti Polar Lipids, USA) at a mole ratio of 1:1 (31). The second formula was prepared from DOTAP, DOPE and PEG2000-C18 lipid (Avanti Polar Lipids, USA) at a mole ratio of 50: 49.25: 0.75. LNPs were produced based on the thin film hydration method (230). In brief, individual lipid stock solution was prepared in chloroform at a concentration of 2 mM, and the appropriate amounts of the stock solutions was mixed according to the intended lipid ratio in total volume 100 μl. Sixty μl of 10 mM glucose-methanol was added to the mixture and gently vortex for 10 seconds. To obtain lipid film, solvent was dried using N_2 gas and the lipid film was left in desiccator for overnight and was hydrated with nuclease-free water on the next day. The hydrated thin film was left for 3 hrs at 37°C for equilibration. For size adjustment, the lipid suspension was extruded ten times through a polycarbonate filter with 0.1 μm pore size (Whatman, USA) using a 1 ml extruder (Avanti Polar Lipids, USA) (231). The Z-average diameter, size distribution and zeta potential were measured at 25°C on a dynamic light scattering system using a Zetasizer Nano ZS (Malvern Instruments Ltd, Malvern, UK).

3.17.3 pDNA-LNP complex formation

Electrostatic interaction of pDNA with LNPs was formed by adding an appropriate amount of LNPs dispersion to a constant amount of pDNA (1 μg) in Opti-MEM media (Gibco) to reach the selected N/P ratio (1:1, 1:3, 1:5, 1:7, 1:9, 3:1, 5:1, 7:1, 9:1). The mixture was incubated for 10 minutes at room temperature to allow binding of nucleic acid to cationic LNPs. The N/P ratio represents the charge ratio of cationic lipid to nucleotide base and was calculated from the number of positive charge represented by lipid-specific head groups (one positive charge per head group) and the number of negative charge represented by nucleotides (from the

phosphodiester groups, i.e. one negative charge per phosphodiester) using the following equations (232).

Equation 1;   Molecular weight (MW) of dsDNA = (number of nucleotides × 607.4) + 157.9

Equation 2;   Mole plasmid = 1×10^{-6} g × 1 mole/ MW of pDNA

Equation 3;   Z mole of phosphate = mole plasmid × number of nucleotides

Equation 4;   N/P = number of mole of cationic lipid/ Z mole of phosphate

3.17.4 pDNA-LNP toxicity test

RAW264.7 cell lines were seeded at 1×10^{4} cells/well in 96-well plate for and incubated at 37°C, 5% CO_2 for overnight and treated with pDNA-LNP which contained various concentrations of cationic LNPs (1×10^{-6}, 2.5×10^{-6}, 5×10^{-6} mmol) for 48 hrs. Then, 10 μl of thiazolyl blue tetrazolium bromide (Alfa Aesar, UK) solution (5 mg/ml in PBS) was added to the wells and incubated for 4 hrs at 37°C. Then, DMSO was added and mixed by pipetting to dissolve the insoluble formazan and measured absorbance at 540 nm by microplate reader. The percentage of viable cells was calculated by the following formula.

% cell viability = ((Absorbance of treated cells) – (Absorbance of blank)) / (Absorbance of blank) × 100

3.17.5 Cellular transfection with pDNA-LNP

RAW264.7 cell lines were seeded 2×10^{5} cells/well in 24-well plate and incubated at 37°C, 5% CO_2 for overnight. Medium was removed and cells were washed once with 1 ml Opti-MEM media. pDNA formulated with LNPs were prepared by mixing the 1 μg of pDNA with specified amount of LNPs to create the various N/P ratios (1:1, 1:3, 1:5, 1:7, 1:9, 3:1, 5:1, 7:1, 9:1). To each well, pDNA-LNP complex (250 μl) was added directly to the cells and incubated for 3 hrs before complete medium (250 μl) was added to each well. Cells were incubated further for 21 hrs. Complete medium was removed and fresh complete medium (500 μl) was added to each well.

Cells were incubated further for 24 hrs at 37°C in 5% CO_2 incubator (233). After incubation for 48 hrs, cells were harvested and analyzed by flow cytometry for protein expression.

3.18 Statistical analysis

Statistical analysis were performed with Prism 8.0 (GraphPad Software). Data were analyzed and compared with an unpaired two-tailed Student's t test, one-way or two-way ANOVA with Bonferroni multiple comparisons test. The log-rank test followed by the Mantel-Cox posttest was used for the survival analysis. Statistical significance was defined by a value of probability (p); *, **, *** for $p < 0.05$, 0.01, 0.001, respectively or statistical significance ($p < 0.05$); (a) when compared to the unmodified nucleoside containing mRNA encoding for target antigen, (b) when compared to untreated control or PBS.

CHAPTER IV

RESULTS

4.1 Translation efficiency, APC maturation, immunogenicity, and cytotoxicity induced by different degrees of modified nucleosides in mRNA-LNP

    4.1.1   Translation efficiency is inversely related to IFN-I secretion and APC maturation and the degree of nucleoside modification.

The effect of nucleoside modified mRNA on protein translation, IFN-I production and APC maturation, were initially evaluated *in vitro* using the commercial reagent TransIT to deliver mCherry encoding mRNA with different degrees of m1Ψ substitution (0, 5, 10, 20, 30, 40, 50, 60, 70, 80, 90, and 100%) into BMDCs and BMDMs. *In vitro* transfection of 0.1 µg mRNA with levels of m1Ψ substitution in the range of 70-100% showed significantly higher mRNA uptake and transfection efficiency, compared to the untreated control in both BMDCs and BMDMs at 48 hrs post transfection (Figure 4.1A-B). Only mRNA with 0% of m1Ψ substitution (from now on referred to as unmodified mRNA) showed a strong induction of IFN-I production in both cells (Figure 4.1C-D). Based on this initial result, mRNA with 0, 40, 70, and 100% of m1Ψ substitutions were selected for formulation with proprietary LNP (Acuitas Therapeutics) in further experiments.

Similar to the results obtained by TransIT reagent, mRNA with 100% of m1Ψ substitution formulated with LNP resulted in a significant higher mRNA uptake, transfection and translation efficiencies than other conditions in both BMDCs and BMDMs, with 77% and 39% of mCherry positive cells, respectively (Figure 4.1E). Although modified mRNA with 100% of m1Ψ substitution showed efficient protein translation, this treatment did not significantly induce maturation of BMDCs. In contrast, BMDCs transfected with unmodified mRNA significantly upregulated CD40 and CD86, suggesting a stage of DC maturation (Figure 4.1F).

% mCherry positive cells   =   mRNA uptake + transfection efficiency

MFI of mCherry   =   mRNA translation efficiency
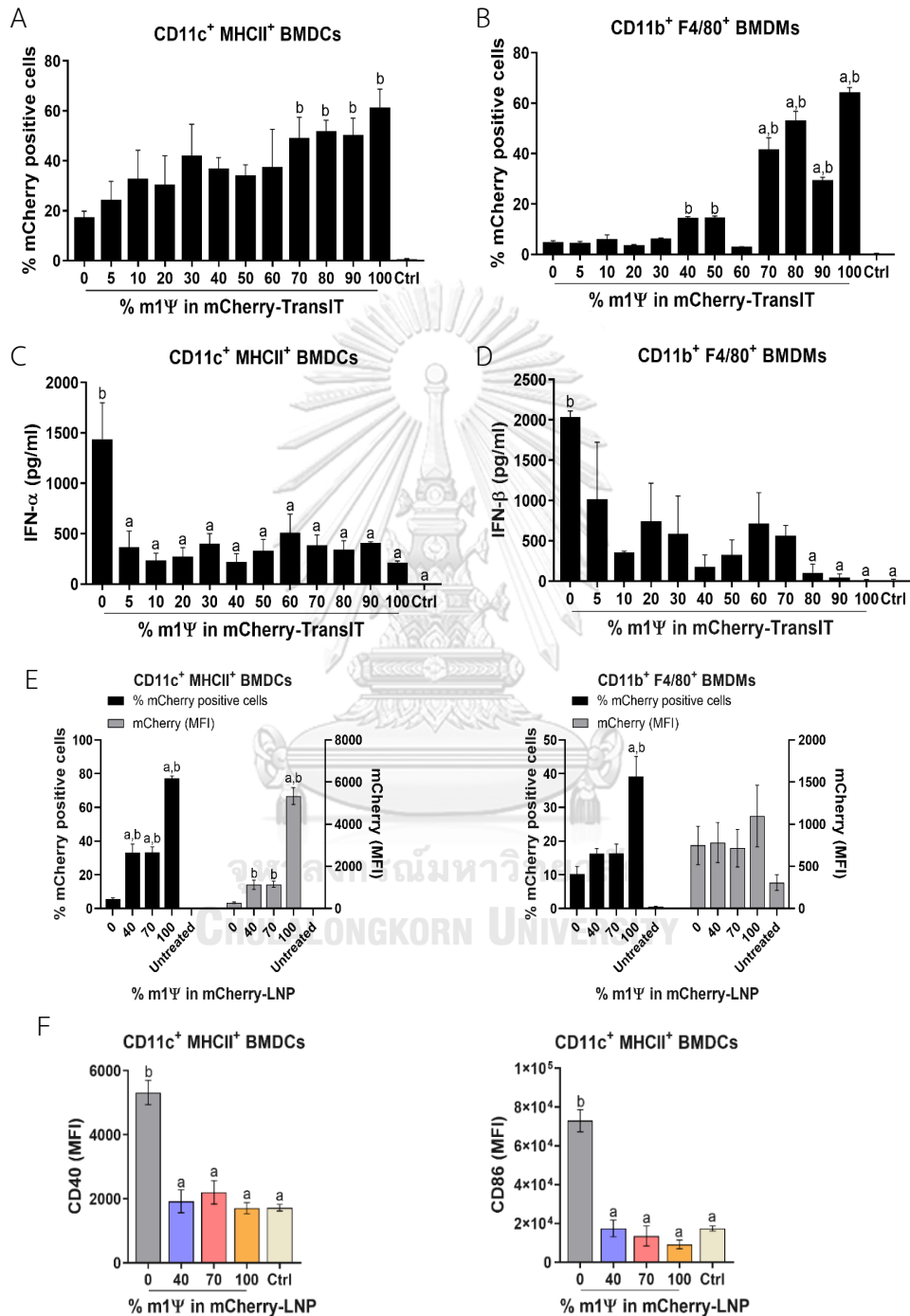
Figure 4.1 TransIT and LNP efficiently delivered mRNA to murine BMDCs and BMDMs *in vitro*.

(A-D) mCherry-encoding mRNA modified with different % of m1Ψ (0.1 μg) were transfected into BMDCs and BMDMs using TransIT reagent. The frequencies of mCherry positive (A) BMDCs and (B) BMDMs were determined by flow cytometry at 48 hrs after transfection. (C) The levels of IFN-α and (D) IFN-β released upon mRNA transfection from BMDCs and BMDMs, respectively were measured by ELISA. (E) mCherry-encoding mRNA modified with different % of m1Ψ (0.1 μg) were delivered into BMDCs and BMDMs using LNP. The frequencies of mCherry positive BMDCs (left) and BMDMs (right) and MFI of mCherry delivered by LNP were determined by flow cytometry. (F) Median fluorescence intensity (MFI) of CD40 (left panel) and CD86 (right panel) on BMDCs upon mRNA-LNP transfection was shown. The control were untranfected cells. The results are presented as the mean ± SEM of at least duplicate samples and experiments were performed at least two times. Statistical significance by one-way ANOVA with Bonferroni multiple comparisons test were indicated when $p < 0.05$ compared to the unmodified target antigen: a, or control: b.

For an *in vivo* delivery of mRNA-LNP, DCs and macrophages in draining lymph nodes (LN) (popliteal and inguinal LNs) and spleens were examined after intramuscular administration (*i.m.*) of mCherry mRNA-LNP (10 μg) for 48 hrs. mRNA-LNP with 100% of m1Ψ substitution was efficiently taken up and translated into proteins by cDC1, cDC2 and macrophages in both LNs and spleens with the highest percentages of mCherry^{+} cells after 48 hrs (Figure 4.2A-B). CD40 upregulation in LN cDC1 was equally observed in all types of mRNA, regardless of m1Ψ substitution that is higher than the untreated control (Figure 4.2C). However, exposure to unmodified mRNA or mRNA with 40% of m1Ψ substitution significantly enhanced CD40 expression in LN cDC2 and splenic cDC1 and cDC2, respectively (Figure 4.2C-D). Taken together, these results indicated that modified mRNA with 100% m1Ψ

substitution significantly improves translation efficiency and decreases innate immunogenicity. Although unmodified mRNAcompromises the translation efficiency, it substantially induces type I IFN production and maturation of APCs.
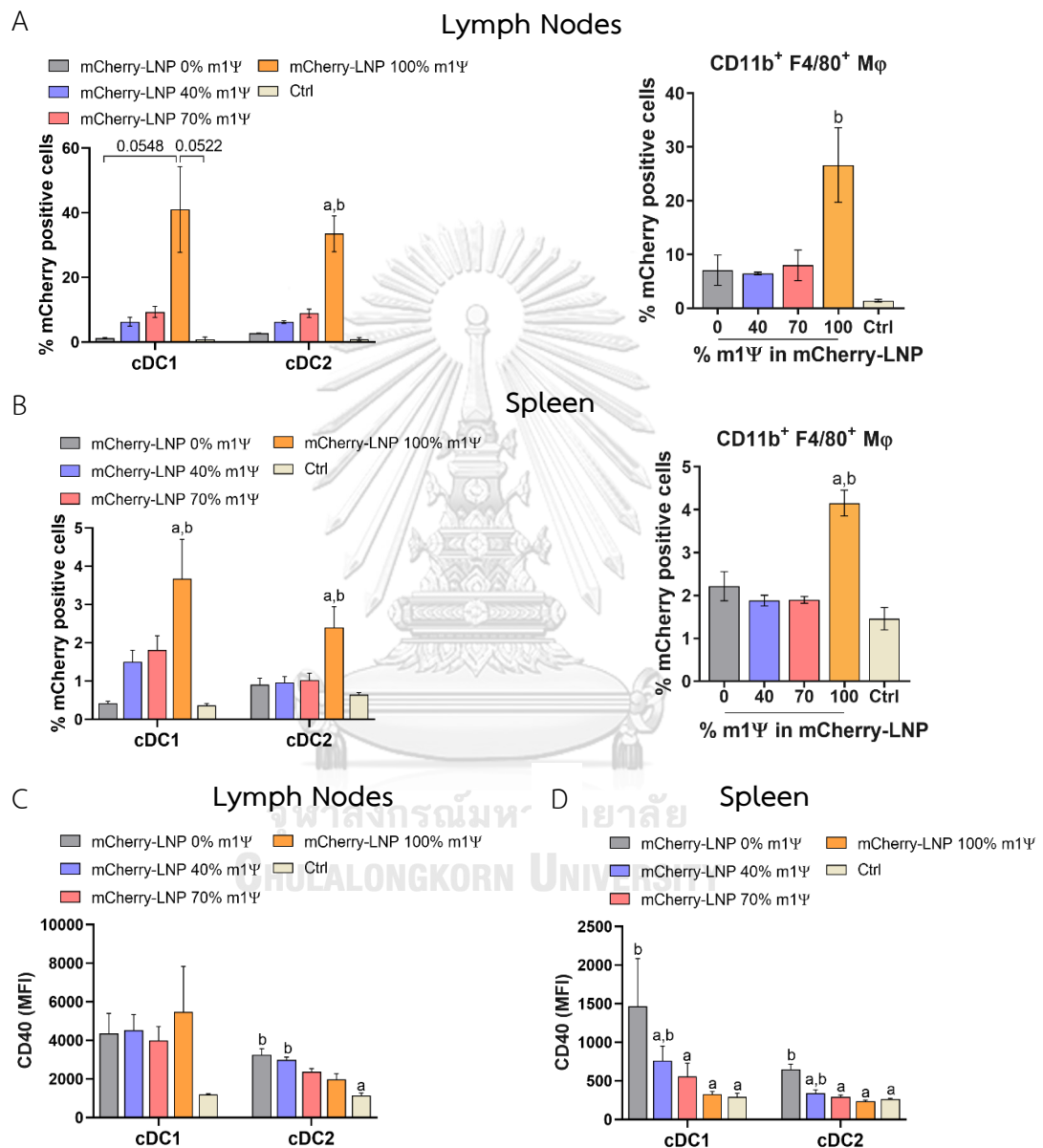
Figure 4.2 mRNA-LNP uptake and reporter protein expression in APCs in LNs and spleens *in vivo*

Mice were intramuscularly injected with 10 μg of mCherry mRNA-LNP with 0, 40, 70, or 100 % of m1Ψ substitution and the control group received PBS. At 48 hrs of mRNA administration, quantification of mCherry-positive cells in (A) LNs and (B) spleen of cDC1 and cDC2 (left), and macrophages (right) were determined. MFI of costimulatory molecule CD40 on cDC1 and cDC2 from (C) LNs and (D) spleen were shown. The results are presented as the mean ± SEM of biologically independent mice (*n* = 6 per group). Statistical significance by one-way ANOVA with Bonferroni multiple comparisons test when *p* < 0.05 compared to the unmodified target antigen: a, or control: b.

4.1.2 Immunization with OVA mRNA-LNP induces robust immune responses and activates OVA-specific cytotoxic effector T cells.

To evaluate whether mRNA prepared with varying degrees of m1Ψ substitution differentially induces antigen-specific T cell responses, mice were intramuscularly immunized with two doses of ovalbumin (OVA-LNP) (10 μg/dose) or PBS with 4 days interval between the two doses as described in Figure 3.1. Luciferase (Luc-LNP) encoding mRNA was used as unrelated antigen control. Immunization with OVA-LNP with unmodified mRNA or with 40% m1Ψ substitution significantly increased serum IFN-α concentration at 6 hrs after the first dose and a booster dose of immunization compared to the mRNA with m1Ψ substitution of 70 and 100% (Figure 4.3A). After the booster dose, the level of IFN-α induced by unmodified mRNA was much lower compared to that from the first dose but remained at detectable level.

Seven days after the booster dose, splenocytes were restimulated with SIINFEKL OVA peptide *in vitro*. For CD4$^+$ T cells, the frequencies of IL-2 and IFN-γ producing cells were significantly induced at a comparable level in all mRNA vaccines tested (Figure 4.3B). The frequencies of TNFα-producing cells were the

highest in the group receiving unmodified mRNA. For double cytokine producers, IL-2/IFN-γ-double producers were similarly induced by all mRNA vaccines, regardless of the substitution while IFN-γ/TNFα-double producers showed the highest percentages in the group receiving OVA-LNP with 0 and 40% substitution of m1Ψ (Figure 4.3B). Interestingly, unmodified OVA-LNP groups showed significant increase in the frequency of IL-5-producing CD4$^+$ T cells (Figure 4.3C).

For CD8$^+$ T cells, the frequencies of IL-2- and IFN-γ producing CD8$^+$ T cells were increased in all groups receiving OVA-LNP, regardless of the level of m1Ψ substitution. On the other hand, percentages of TNFα-producing CD8$^+$ T cells were increased in OVA-LNP with unmodified or m1Ψ substitution of 40%. Furthermore, significantly increased percentages of IL-2/IFN-γ-double producers were detected in the groups receiving OVA-LNP with m1Ψ substitution of 40, 70, and 100% (Figure 4.3D). A significantly higher percentages of granzyme B and IFN-γ/granzyme B-producing CD8$^+$ T cells were observed in the group with OVA-LNP with unmodified or m1Ψ substitution of 40%, compared to those with 70 or 100% m1Ψ substitution (Figure 4.3E).

We next determined the *in vivo* cytotoxic activity of vaccine induced OVA-specific T cells. Mice were intramuscularly immunized with a single dose of 20 µg OVA-LNP with m1Ψ substitution of 0, 40, 70, or 100% or Luc-LNP with m1Ψ substitution of 100% as an unrelated antigen control on day 0. At day 13, mice received CFSE-labeled splenocytes (1:1 ratio) that were pulsed with the OVA$_{257-264}$ (SIINFEKL) peptide or left unpulsed as target cells. At day 14, mice were sacrificed and the percentages of target cells were measured. As shown in Figure 4.3F, OVA$_{257-264}$-specific T cells (CD4$^+$ and/or CD8$^+$ T cells) were significantly enhanced in mice receiving all mRNA types of OVA-LNP compared with those treated with Luc-LNP. Taken together, these results demonstrated that administration of OVA-LNP robustly

activates OVA-specific CD4^{+} and CD8^{+} T cell responses, particularly unmodified mRNA effectively stimulates Th1 response. In addition, this result indicated that mRNA vaccine induces robust antigen specific CTL activation regardless of the degree of substitution.
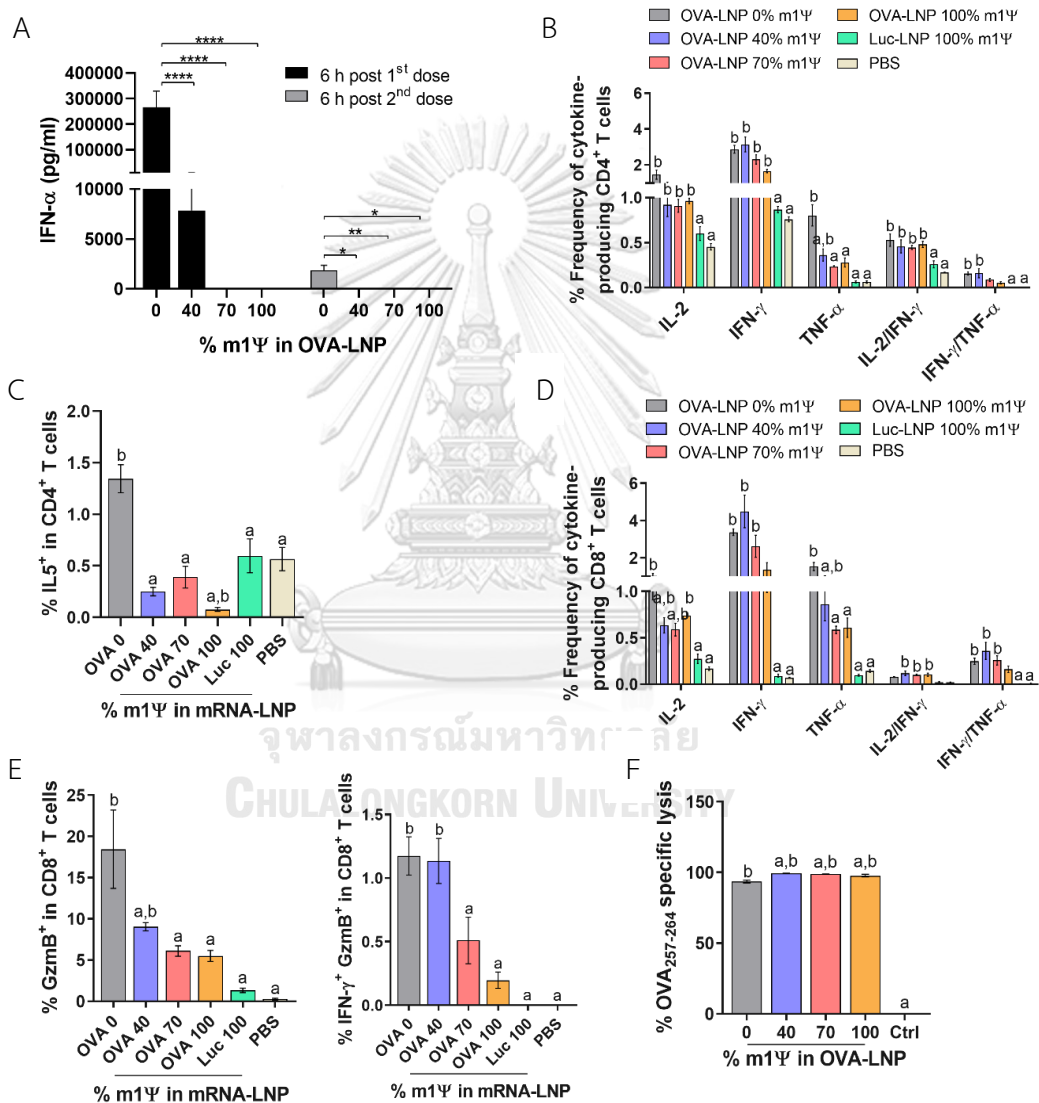
Figure 4.3 Immunization of mRNA-LNP elicits robust antigen-specific T cell responses. (A) IFN-α concentration in the serum 6 hrs after the first (day0) and the second (day4) immunizations of OVA mRNA-LNP were detected by ELISA. (B-C) The frequencies of IL-2, IFN-γ, TNF-α and IL-5 producing CD4^{+} T cells after 6 hr

stimulation with OVA$_{257-264}$ (SIINFEKL) were measured by flow cytometry. (D-E) The frequencies of IL-2, IFN-**γ**, TNF-**α** and GzmB and IFN-**γ**/GzmB-producing CD8$^+$ T cells after 6 hrs stimulation with OVA$_{257-264}$ (SIINFEKL) were measured by flow cytometry. (F) The frequencies of target cell lysis is shown. The results are presented as the mean ± SEM, n = 4-8 biologically independent mice per group. Statistical significance: (*) $p < 0.05$, (**) $p < 0.01$, (***) $p < 0.001$ and (****) $p < 0.0001$ by one-way ANOVA with Bonferroni multiple comparisons test or $p < 0.05$ compared to the unmodified target antigen: a, or control: b.

4.1.3 Neoantigens (Pbk-Actn4) encoding mRNA-LNP is immunogenic.

From now on, we focused the comparison between unmodified and 100% m1**Ψ** substitution and would refered to 100% m1**Ψ** substitution of mRNA as modified mRNA. Following previous reports on mutanomes of B16F10 tumor (16, 113), we selected two somatic mutations of *Pbk* and *Actn4* as neoantigens to test in our study. Based on the study by Kreiter *et al.*, these mutated epitopes of *Pbk* and *Actn4* were recognized and reacted to by CD8$^+$ or CD4$^+$ T cells, repectively, upon RNA monotope vaccinations and showed good MHC class I binding scores ('low score' 0.1 and 0.2, respectively) (16). We hypothesized that by selected CD4 and CD8 epitopes, the neoantigen vaccine should induce Th and CTL more effectively. These selected neoantigens were linked together with 10-mer non-immunogenic glycine/serine linkers and used as a neoantigen vaccine. In this study, unmodified and modified mRNA encoding Pbk-Actn4 neoantigens were evaluated whether antigen-specific CD4$^+$ and CD8$^+$ T cell responses could be induced. Mice were immunized *i.m.* with two doses of 10 μg/dose neoantigens (Neo-LNP) or control mCherry (mCherry-LNP) encoding mRNAs or PBS on day 0 and boosted with the same dose on day 4 as described in Figure 3.1. Seven days after the booster dose, splenocytes were restimulated with overlapping peptide pools of *Pbk* and *Actn4*. Antigen-specific

CD4^{+} and CD8^{+} T cell responses were significantly induced upon immunization with
unmodified Neo-LNP at higher level, compared to that from modified Neo-LNP.
Increased percentages of cells producing IL-2, IFN-γ and TNF-α in the group receiving
unmodified Neo-LNP were also observed (Figure 4.4A-B). In addition, a significant
increase in the frequencies of granzyme B and IFN-γ/granzyme B-producing CD8^{+} T
cell were observed only in the group with unmodified Neo-LNP (Figure 4.4C).
Consistent with the robustly activated T cells, PD-1 expression were significantly
increased on CD4^{+} and CD8^{+} T cells in unmodified Neo-LNP immunized group (Figure
4.4D).
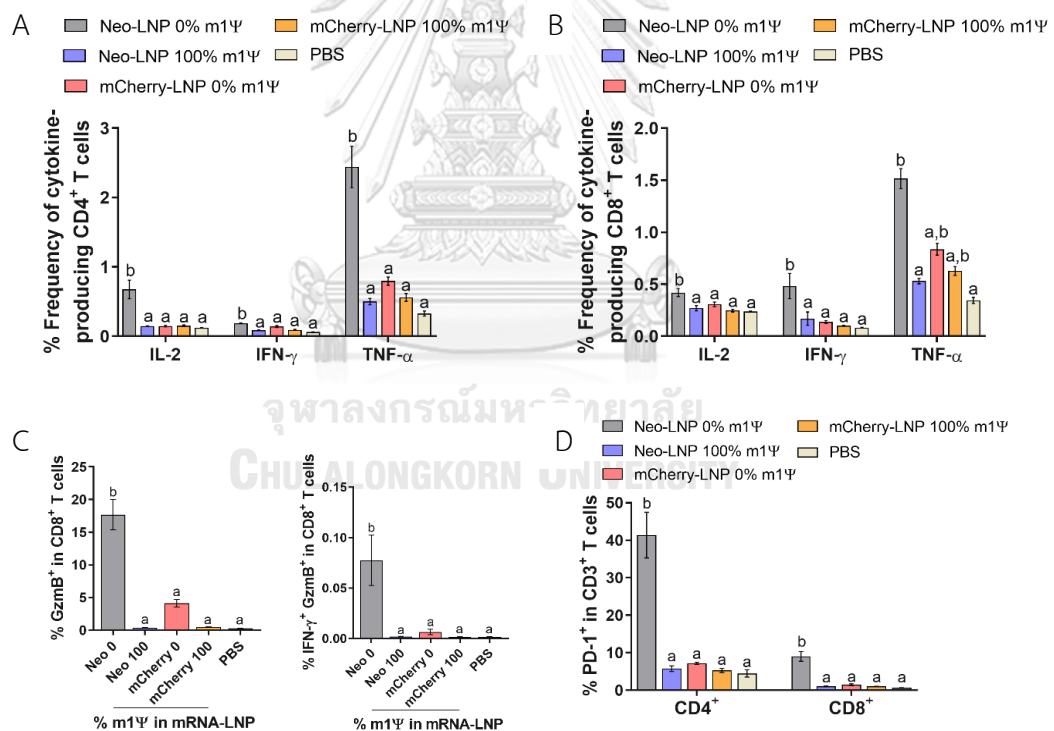
Figure 4.4 Immunization of neoantigens (Pbk-Actn4) encoding mRNA-LNP elicits
robust antigen-specific T cell responses.

(A) CD4^{+} and (B) CD8^{+} T cells on CD3^{+} T cell subsets determined by flow cytometry
after 6 h stimulation with pool of Pbk and Actn4 peptides at 7 days post-boost. (C)
Frequencies of GzmB (left) and IFN-γ/GzmB (right)-producing CD8^{+} T cells on CD3^{+}

CD8$^+$ T cell subsets were determined by flow cytometry. Frequencies of PD-1 exhaustion marker on splenic CD4$^+$ and CD8$^+$ T cells (D) in mice were examined. GzmB, granzyme B. Each column are represented as the mean ± SEM, n = 4 biologically independent mice per group. Statistical significance by one-way ANOVA with Bonferroni multiple comparisons test when p < 0.05 compared to the unmodified target antigen: a, or control: b.

4.2 Anti-tumor immunity and tumor-infiltrating immune profiles induced by modified or unmodified mRNA-LNP *in vivo*

4.2.1 Unmodified mRNA induces antitumor immunity and alters tumor-infiltrating immune cell profiles.

To determine whether the immune responses induced by OVA-LNP is sufficient to control tumor growth, murine B16F0-OVA melanoma expressing OVA was used as a model. Mice were transplanted with B16F0-OVA at day 0 and intramuscularly immunized with two doses (10 µg/dose) of unmodified OVA-LNP or modified OVA-LNP or modified Luc-LNP or PBS on day 4 and 8 as described in Figure 3.2. All mice immunized with unmodified OVA-LNP survived until the end of experimental period of 31 days while all mice in the PBS or Luc-LNP control group were dead (Figure 4.5A). For modified OVA-LNP group, 50% of the mice survived (n = 9). The survival rates reflected the delay and significant decrease in tumor growth in unmodified OVA-LNP group compared with the other groups (Figure 4.5B-C).

To monitor the impact of mRNA vaccine on tumor infiltrated immune cells, seven days after a booster dose, mice were sacrificed and the tumor infiltrated immune cells (T cells and DCs) were characterized. The majority of tumor-infiltrating CD3$^+$ T cell population in unmodified OVA-LNP group were CD3$^+$CD4$^-$CD8$^-$ T cells, while the group receiving modified OVA-LNP had CD8$^+$ T cells as the major T cell population (Figure 4.5D). In addition, the majority of tumor-infiltrating CD3$^+$ T cell

population in unmodified and modified Luc-LNP and PBS immunized groups were also $CD3^+CD4^-CD8^-$ T cells (Figure 4.5D). We next determined the presence of intratumoral migratory cDC1 ($CD11c^+$ $XCR1^+$ $CD103^+$) as they play important role in T cell activation. In a group receiving unmodified OVA-LNP, a significant increase in CD40 level among cDC1 subset was observed whereas modified OVA-LNP did not induce CD40 expression (Figure 4.5E). This result strongly supports that unmodified mRNA induces more efficient antigen presentation that may augment the anti-tumor immunity in the tumor microenvironment.
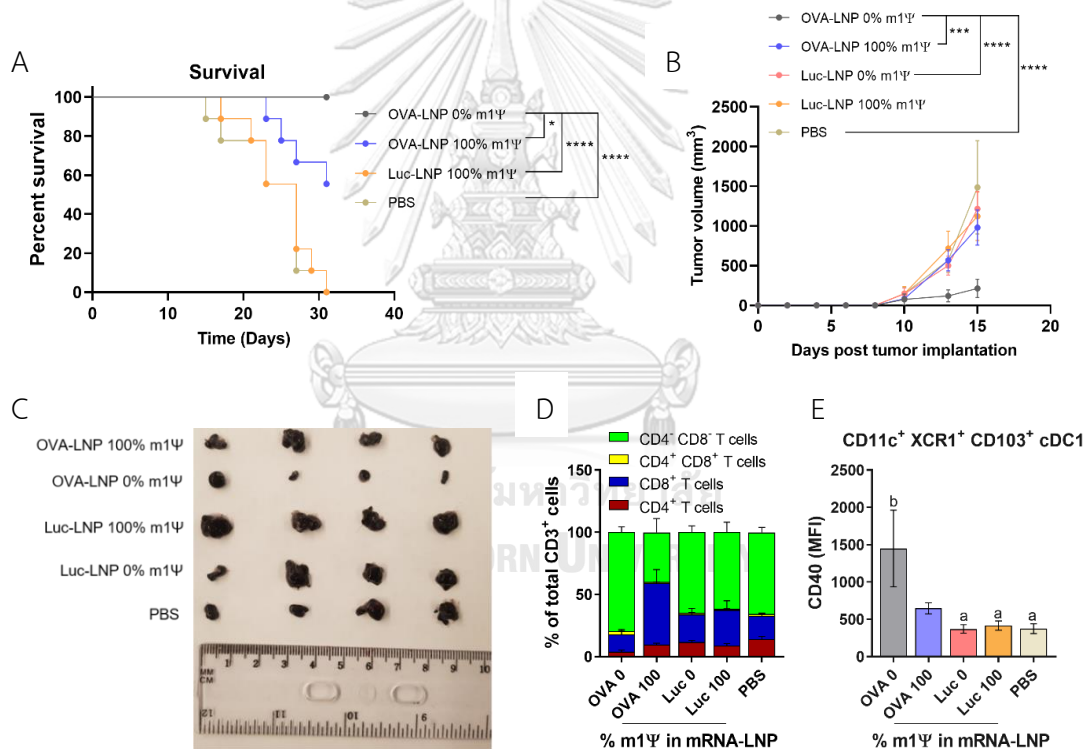
Figure 4.5 Therapeutic efficacy of unmodified OVA-LNP in B16F0-OVA melanoma model

(A) The percentages of survival mice was followed until day 31 after tumor implantation. Mice that reached the maximal allowed tumor size of 20 mm, or 400 mm^2 were euthanized and recorded as having tumor areas of 400 mm^2 (n = 9 per group). (B) Tumor volume was shown during the 15 days after tumor implantation (n

= 10 per group). (C) Representative tumor mass harvested 15 days after the tumor implantation from mice treated with OVA-LNP, Luc-LNP or PBS is shown (n = 7 per group). (D) Compositions of tumor-infiltrating T cells and (E) MFI of costimulatory molecule CD40 on cDC1 are shown (n = 6 per group). The results are presented as the mean ± SEM. Statistical significance: (*) $p < 0.05$, (**) $p < 0.01$, (***) $p < 0.001$ and (****) $p < 0.0001$ by two-way ANOVA with Bonferroni multiple comparisons test or $p < 0.05$ compared to the unmodified target antigen: a, or control: b. Survival curves were compared using log-rank (Mantel–Cox) test.

We next investigated the impact of OVA-LNP vaccination on the phenotypes of immune cell population in the spleens on day 15 after tumor implantation. Consistent with the strong anti-tumor phenotype, mice immunized with unmodified OVA-LNP or modified OVA-LNP showed significant expansion of effector CD8$^+$ T cells (CD8$^+$ CD44$^+$ CD62L$^-$) whereas mice receiving unmodified OVA-LNP increased memory CD8$^+$ T cell population (CD8$^+$ CD44$^+$ CD62L$^+$) more than modified OVA-LNP (Figure 4.6A). Previously, it was reported that chronic antigen exposure downregulated CD62LhighCCR7$^+$ central memory T cell markers and drove differentiation toward effector memory T cells which showed less protective and therapeutic immunity (234, 235). This immunologic memory attributed to rapidly acquire cytotoxic fuction upon re-encounter with the pathogens (236) and consistent with another group findings that adoptively transfer of self/tumor-reactive central memory T cells mediated antitumor immunity in an established cancer model (237). Interestingly, there was a significant increase in PD-1$^+$ CD8$^+$ T cells in the group with OVA-LNP of modified mRNA whereas the PD-1$^+$ CD4$^+$ T cells increased in unmodified OVA-LNP group (Figure 4.6B).

We also evaluated the induction of OVA-specific CD4$^+$ T cell responses. As shown in Figure 4.6C, only mice immunized with unmodified OVA-LNP significantly

increased the frequencies of IL-2 and TNF-α-producing CD4$^+$ T cells. Furthermore, as shown in Figure 4.6D, both modified and unmodified OVA-LNP significantly induced higher frequencies of cytokine producing cells in OVA specific CD8$^+$ T cells. More importantly, compared with the modified OVA-LNP group, unmodified OVA-LNP induced higher percentages of granzyme B$^+$ or IFN-γ/TNFα-double producers and granzyme B/IFN-γ-double producers in CD8$^+$ T subsets (Figure 4.6E). This coordinated anti-tumor immunity induced by unmodified OVA-LNP is consistent with the delayed tumor growth and higher survival rate in tumor transplanted animals described in Figure 4.5.
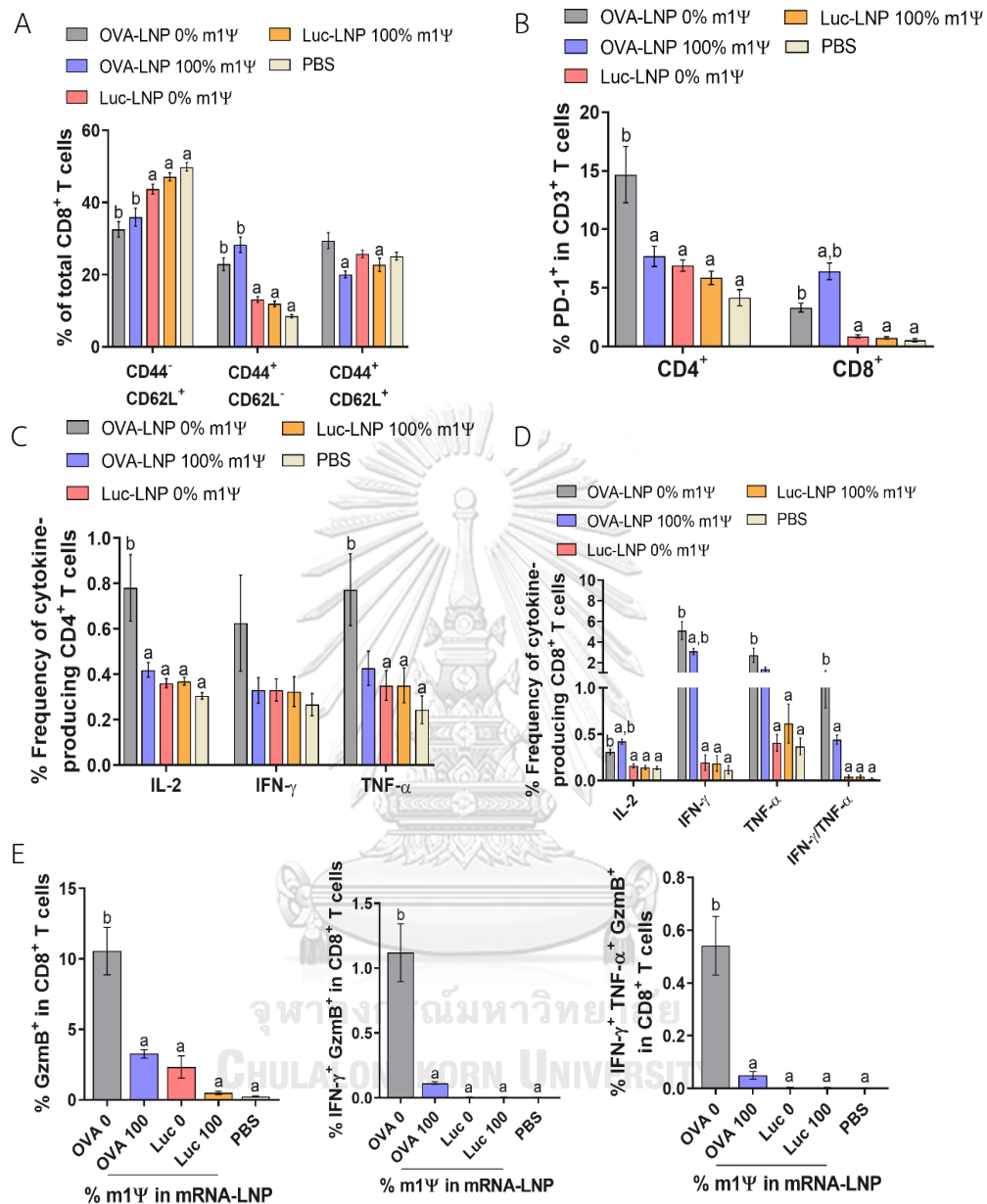
Figure 4.6 Impact of OVA-LNP on activation of splenic antigen-specific T cells in B16 tumor transplanted mice

Mice were treated as described in method 3.8.3.1.1 and the splenocytes were re-stimulated for 6 hrs with OVA$_{257-264}$ (SIINFEKL) peptide. (A) The frequencies of naïve cells (CD44$^-$CD62L$^+$), effector cells (CD44$^+$CD62L$^-$), and memory cells (CD44$^+$CD62L$^+$) in CD3$^+$CD8$^+$ T cell subsets (B) the frequencies of PD-1$^+$ CD4$^+$ and CD8$^+$ T cells and (C-D)

the frequencies of cytokines-producing CD4$^+$ and CD8$^+$ T cells are shown. (E) The OVA$_{257-264}$-specifc responses were determined and the percentages of CD8$^+$ T cells producing GzmB, IFN-γ/GzmB, or IFN-γ/TNF-α/GzmB are shown. The results are presented as the mean ± SEM of biologically independent mice (n = 7 per group). Statistical significance by one-way ANOVA with Bonferroni multiple comparisons test when $p < 0.05$ compared to the unmodified target antigen: a, or control: b.

4.2.2 IFN-I is crucial for anti-tumor response induced by unmodified mRNA vaccine.

In order to gain an insight how unmodified mRNA induces robust anti-tumor immunity, we evaluated the role of IFN-I in the therapeutic efficacy of mRNA vaccine. Mice were implanted with B16F0-OVA on day 0, followed by *i.p.* administration of anti-IFNAR1 antibody or isotype control (400 µg per mouse) on day 4 and day 8 as described in Figure 3.3. One hr after each administration of anti-IFNAR1 antibody or isotype control, mice were intramuscularly immunized with unmodified OVA-LNP. When the tumor was allowed to grow until day 42, anti-IFNAR1 antibody treatment significantly decreased the tumor growth control effect observed with the unmodified OVA-LNP in the isotype control group (Figure 4.7A). At the cellular level, anti-IFNAR1 antibody treatment decreased the expansion of splenic CD8$^+$ T cell (Figure 4.7B) and reduced antigen (OVA) specific IFN-γ-producing CD8+ T cells (Figure 4.7C), compared with the isotype control treated group. Finally, we determined the phenotypes of tumor-infiltrating immune cells on day 42. Mice receiving anti-IFNAR1 antibody showed a significant increase in PD-1 expressing tumor-infiltrated CD4$^+$ and CD8$^+$ T cells (Figure 4.7D) and a significant increase of tumor-infiltrating M2-like macrophages (CD206$^+$ F4/80$^+$), compared to the isotype control treated group (Figure 4.7E). Overall, these results strongly indicated the crucial role of IFN-I signaling in unmodified mRNA-LNP-mediated anti-tumor immunity.
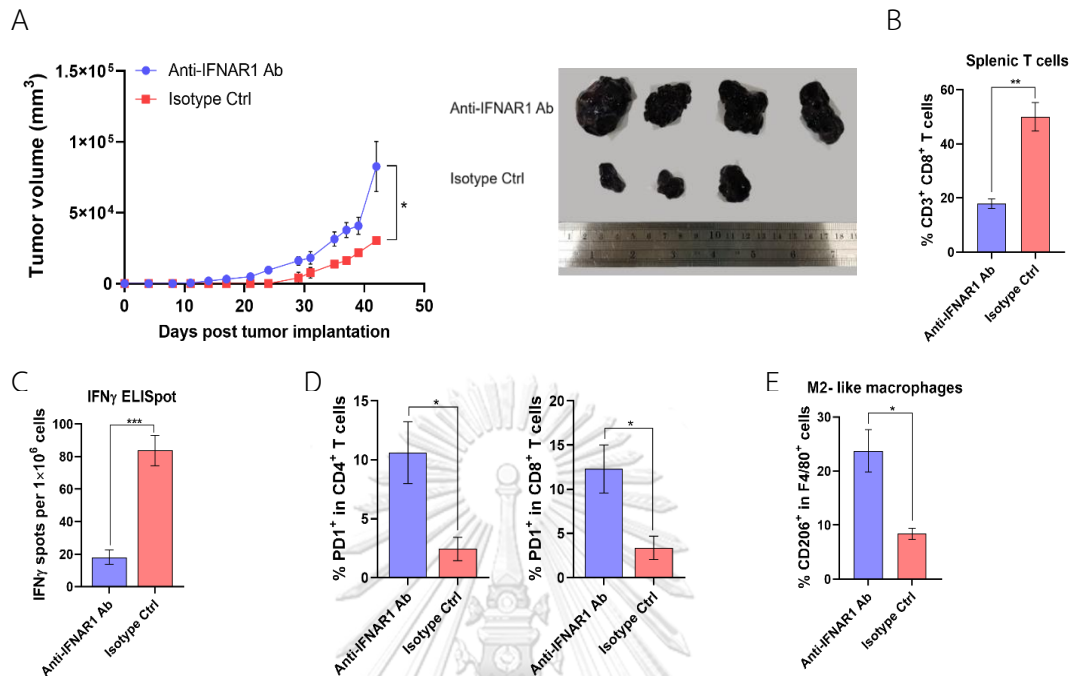
Figure 4.7 IFN-I signaling promotes antitumor response and modulates immune cell profiles in spleen.

(A) The tumor volume (left) and the representative tumor mass (right) harvested 42 days after the tumor implantation from mice treated with anti-IFNAR1 antibody or isotype control followed by immunization with unmodified OVA-LNP. (B) The frequency of splenic CD8$^+$ T cells was examined by flow cytometry. (C) ELISpot of IFN-γ producing cells among splenocytes after 48 hrs of *ex vivo* re-stimulation with OVA on day 42 after tumor implantation and mRNA vaccine treatments is shown. (D) The frequency of PD-1$^+$ cells among tumor infiltrated CD4$^+$ (left) and CD8$^+$ (right) T cells were examined by flow cytometry. (E) The frequency of tumor infiltrated CD206$^+$ macrophages was determined by flow cytometry. The results are presented as the mean ± SEM, *n* = 4 biologically independent mice per group. Statistical significance: (*) $p < 0.05$, (**) $p < 0.01$, (***) $p < 0.001$ and (****) $p < 0.0001$ by unpaired two-tailed Student's t test.

4.2.3 Unmodified OVA-LNP suppresses metastasis to lung in a melanoma model.

Next, we decided to test whether unmodified OVA-LNP induces immune response against lung metastasis in B16 melanoma model. B16F0-OVA cells were injected intraveneously to establish lung metastasis. On day 4 and 8 after tumor cell injection, mice were intramuscularly immunized with two doses of OVA-LNP (10 µg/dose) with unmodified or modified mRNA or with unrelated antigen encoding mRNA-LNP (PR8HA-LNP) or PBS. On day 18, lung metastasis were observed and the number of lung nodules were counted (Figure 4.8A-B). Strikingly, we observed that only mice immunized with unmodified OVA-LNP clearly suppressed nodule formation in the lungs while OVA-LNP with modified mRNA failed to control the lung metastasis and showed comparable numbers of lung nodules as PBS control or unrelated antigen. This result reinterated that unmodified mRNA-LNP induces robust anti-tumor immunity that includes metastasis.
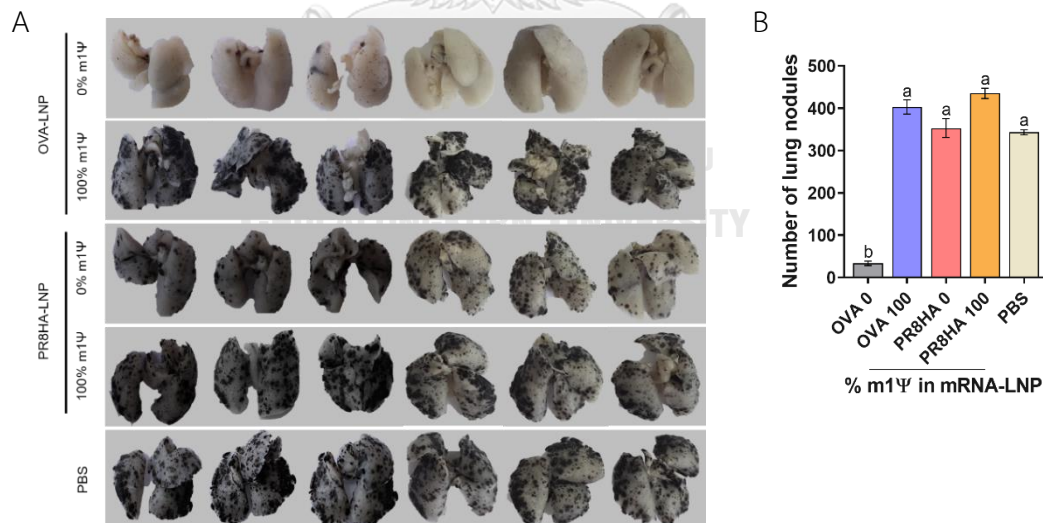
Figure 4.8 Immunization of unmodified mRNA-LNP inhibits lung metastasis of B16F0-OVA melanoma.

(A) The lungs were observed and (B) the metastatic nodules on the surface of the lungs were counted. The results are presented as the mean ± SEM of biologically independent mice (n = 6) per group. Statistical significance by one-way ANOVA with Bonferroni multiple comparisons test when $p < 0.05$ compared to the unmodified target antigen: a, or control: b.

4.2.4 Neoantigen-specific immune responses induced by unmodified mRNA control B16F10 melanoma growth.

To examine the anti-tumor efficacy of Neo-LNP in B16F10 melanoma model, mice were immunized *i.m.* with two doses of Neo-LNP (10 μg/dose) or control mCherry-LNP (10 μg/dose) with unmodified and m1Ψ substitution of 100% or PBS on day 4 and 8 after tumor implantation as described in Figure 3.2. Consistent with the robust anti-neoantigen response, tumor growth was profoundly retarded and significantly decreased in Neo-LNP vaccinated group (Figure 4.9A). One third of the Neo-LNP treated mice survived until day 35, while all mice in the control group died by day 29 (Figure 4.9B). Repeated vaccination with the unmodified Neo-LNP in B16F10 tumor-bearing mice increased splenic antigen-specific CD8$^+$ T cells that produced granzyme B (Figure 4.9C) and induced expression of PD-1 on splenic T cells, whereas this trend was not observed in m1Ψ substitution of 100% Neo-LNP (Figure 4.9D). Mice given unmodified Neo-LNP showed a significant increase in CD69$^+$ tumor-infiltrating T cells (Figure4.9E) and expression level of CD40 in cDC1 (CD11c$^+$ XCR1$^+$) (Figure 4.9F). Taken together, we confirmed that unmodified mRNA encoding tumor neoantigen formulated in LNPinduced a strong anti-tumor immune response that retarded tumor growth and partially prolonged survial of tumor bearing mice.
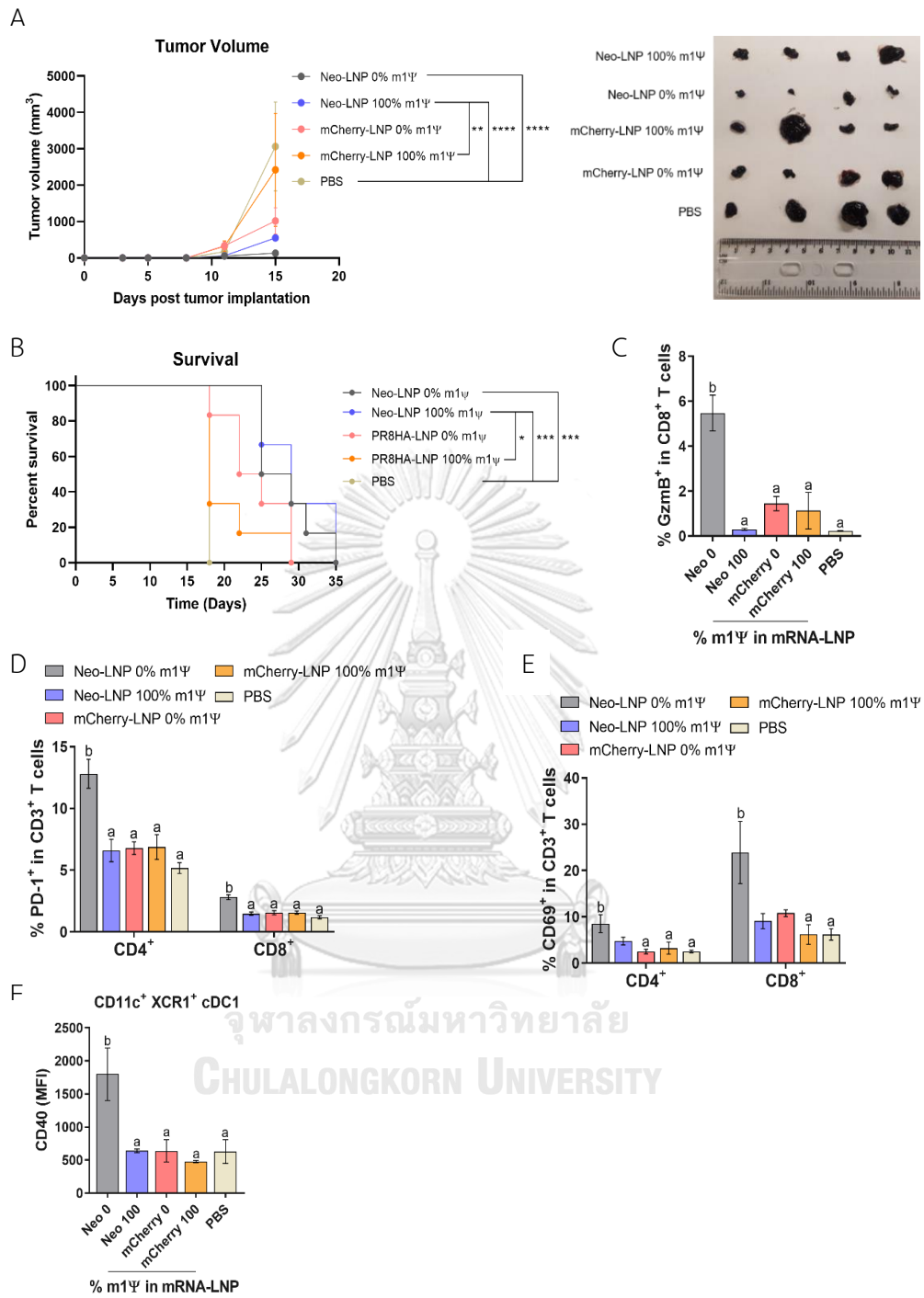
Figure 4.9 Unmodified neoantigens (Pbk-Actn4) encoding mRNA-LNP inhibits tumor growth *in vivo* and prolongs survival.

(A) Tumor volume (left) was measured (*n* = 10 per group) and the representative tumor mass (right) harvested 15 days after the tumor implantation are shown (*n* = 7

per group). (B) The percentage of survival was followed until day 35 (n = 6 per group). (C) The frequency of GzmB-producing splenic CD8$^+$ T cells on CD3$^+$CD8$^+$ T cell subsets was determined by flow cytometry. (D) Frequencies of PD-1 exhaustion marker on splenic CD4$^+$ and CD8$^+$ T cells with tumor implantation were examined. (E) The frequencies of CD69$^+$ among tumor infiltrated CD4$^+$ and CD8$^+$ T cells are shown. (F) The MFI of costimulatory molecule CD40 on tumor-infiltrating cDC1 is shown (n = 4 per group). GzmB, granzyme B. The results are presented as the mean ± SEM. Statistical significance: (*) p < 0.05, (**) p < 0.01, (***) p < 0.001 and (****) p < 0.0001 or p < 0.05 compared to the unmodified target antigen: a, or control: b by one-way ANOVA with Bonferroni multiple comparisons test. Survival curves were compared using log-rank (Mantel–Cox) test.

4.3 Synthesis of LNPs based on well-characterized lipids facilitated pDNA transfection into RAW264.7 macrophage cell line.

4.3.1   Physical properties characterization of pDNA-LNPs

As mentioned earlier, the competent vaccine largely depends on the appropriate delivery system targeting to APCs (238). The characteristic is influenced by the size and charge of particles (194). Therefore, two different formulations of LNPs were prepared by the thin-film hydration method (230). The first formula composted of DOTAP, a biodegradable cationic lipid, and DOPE neutral lipid at a 1: 1 mole ratio. The second formula contained DOTAP, DOPE and additionally included PEG2000-C18 lipid to form the complex at a 50: 49.25: 0.75 mole ratio (Table 4.1). Lipid-anchored PEG has been reported that helps in increase of circulation half-life by reducing nonspecific binding of proteins to LNPs and improve the biocompatibility of LNPs (188).

Table 4.1 Lipid mole ratio of two formulas of LNPs

Name	DOTAP	DOPE	PEG2000-C18 lipid
Formula 1; DOTAP: DOPE	50	50	0
Formula 2; DOTAP: DOPE: PEG	50	49.25	0.75

To characterize the physical properties, the size distribution and zeta potential of the pDNA-LNPs were determined at 25 °C by the dynamic light scattering system with the Zetasizer Nano ZS (Malvern, UK). The results are shown in Table 4.2 and Figure 4.10. The particle size increased as the N/P ratio decreased, and the same trend was observed in both formulas. The smallest Z-average diameter of DOTAP and DOPE or DOTAP, DOPE and PEG constituting LNPs complexed with pDNA were found at N/P ratio of 9:1 which were 188.7 ± 38.61 and 157.45 ± 0.92 nm, respectively. The largest diameter in formula one and two were 308.8 ± 22.34 and 270.25 ± 9.97, respectively. In addition, It was found that with the 0.75 mole ratio of PEG, the additional component in the LNP resulted in smaller particle size than those without. The N/P ratios of 9:1, 7:1, 5:1, 3:1, and 1:1 in both formulas possessed PDI values smaller than 0.3, which is considered a homogenous size distribution (239). The zeta potentials were positive in the pDNA-LNPs with N/P ratio of 9:1, 7:1, and 5:1 in both formulas and also 3:1 in formula one. These results indicated that the LNP composition and the amount of cationic lipid in LNPs to form complex with pDNA at different N/P ratio showed obvious effects on the physical properties.

Table 4.2 Particle size, polydispersity index and zeta potential of pDNA-LNPs

N/P ratio	Z-Average diameter (nm) ± SEM	Polydispersity Index (PDI) ± SEM	Zeta potential (mV) ± SEM
Formula 1; DOTAP: DOPE (1: 1)			
9:1	188.7 ± 38.61	0.2335 ± 0.03	36.4 ± 0.56
7:1	194.1 ± 21.21	0.2235 ± 0.02	31.4 ± 0.14
5:1	205.45 ± 18.46	0.21 ± 0.02	25 ± 1.41
3:1	264.95 ± 6.58	0.242 ± 0.09	14.44 ± 7.72
1:1	260.35 ± 64.56	0.279 ± 0.1	-10.82 ± 1.24
1:3	287.55 ± 96.80	0.3035 ± 0.1	-10.275 ± 1.73
1:5	302.95 ± 85.21	0.3125 ± 0.07	-9.88 ± 2.29
1:7	293.6 ± 56.57	0.327 ± 0.007	-9.485 ± 4.40
1:9	308.8 ± 22.34	0.415 ± 0.09	-6.39 ± 0.07
Formula 2; DOTAP: DOPE: PEG (50: 49.25: 0.75)			
9:1	157.45 ± 0.92	0.234 ± 0.01	34.1 ± 5.37
7:1	161.95 ± 18.31	0.2205 ± 0.004	19.5 ± 0.57
5:1	181.7 ± 5.8	0.2205 ± 0.006	31.2 ± 0.57
3:1	226.6 ± 25.03	0.248 ± 0.01	-5.775 ± 3.32
1:1	231.45 ± 9.12	0.2535 ± 0.02	-15.45 ± 7.71
1:3	269.95 ± 49	0.307 ± 0.01	-10.575 ± 3.85
1:5	220.55 ± 5.02	0.3175 ± 0.04	-9.345 ± 0.43
1:7	270.25 ± 9.97	0.365 ± 0.04	-11.4 ± 1.56
1:9	267.25 ± 5.02	0.36 ± 0.06	-8.06 ± 2.32
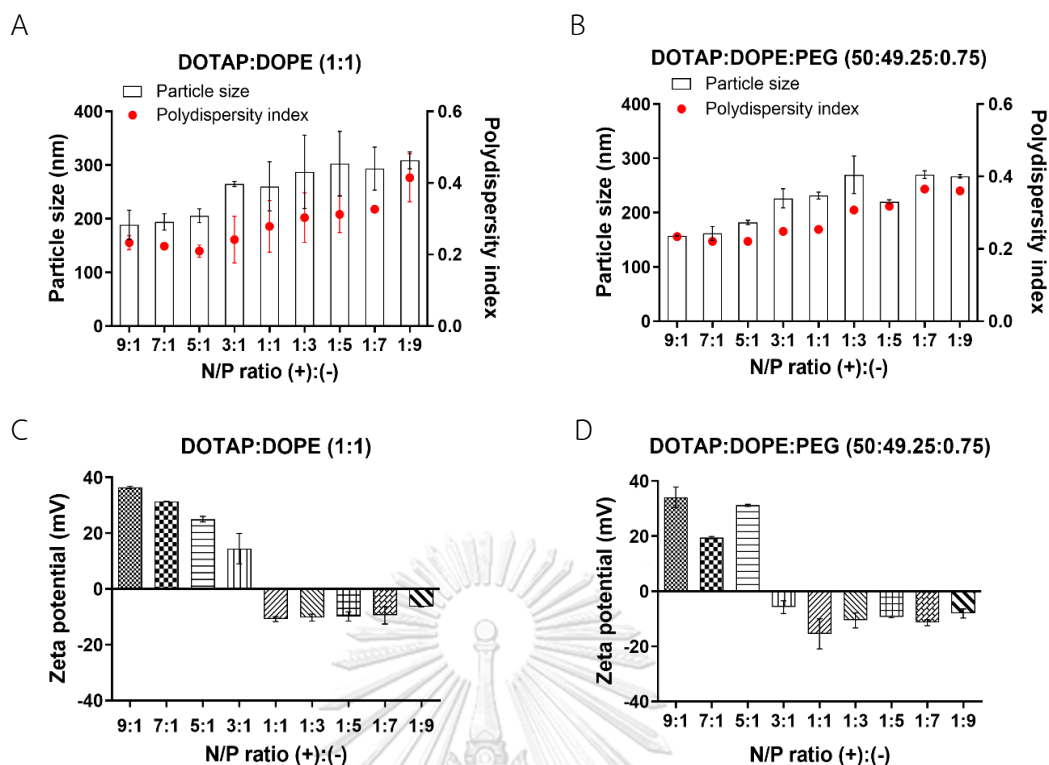
Figure 4.10 Particle size and polydispersity index (upper row) and zeta potential (lower row) values of pDNA-LNPs at different N/P ratios are shown. Particle size of formula 1; DOTAP: DOPE (1: 1) (A) and formula 2; DOTAP: DOPE: PEG (50: 49.25: 0.75) (B) upon being complexed to 1 µg of pDNA at N/P ratios of 9:1, 7:1, 5:1, 3:1, 1:1, 1:3, 1:5, 1:7, and 1:9. Zeta potential of formula 1 (C) and formula 2 (D). The results are presented as the mean ± SEM of at least duplicate samples and experiments were performed at least two times.

4.3.2 Cytotoxicity of pDNA-LNPs

Since favorable delivery system should have low cellular toxicity, the toxicity of empty cationic lipids and pDNA-LNPs towards RAW264.7 cell lines were determined using the 3-(4,5-dimethylthiazole-2-yl)-2,5-diphenyltetrazolium bromide (MTT) assay. The results were expressed as a percentage of cell viability. As shown in Figure 4.11, increasing the amount of cationic lipid (from 0 nmol to 7.407 nmol) and

complexing LNPs with 1 μg pDNA at various N/P ratios caused no significant effect on cell viability compared to non-transfected cells (control) of both formulas. These data indicated that these two cationic LNPs formulations were both safe.
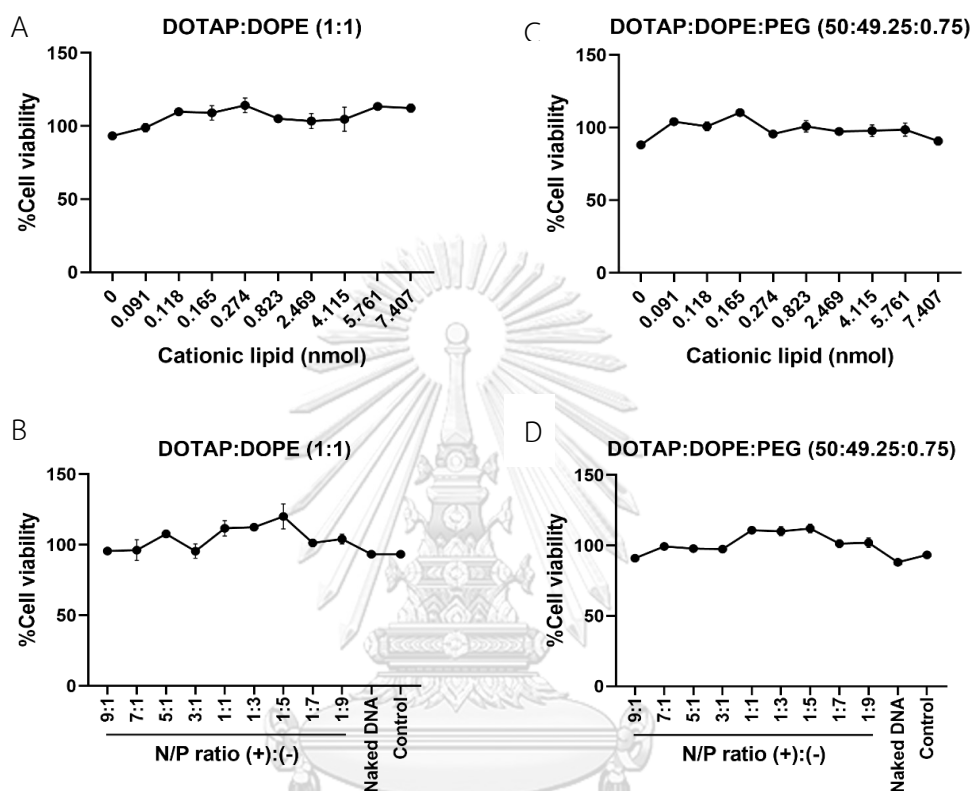
Figure 4.11 LNP formulations are non-toxic to RAW264.7 cell line.
Cell viability of RAW264.7 cell line after transfection with empty LNPs at various concentratios (upper panel) or pDNA-LNPs at different N/P ratios (lower panel) are shown. (A-B) Formulations DOTAP: DOPE (1: 1) and (C-D) DOTAP: DOPE: PEG (50: 49.25: 0.75) were complexed to 1 μg of pDNA at N/P ratios of 9:1, 7:1, 5:1, 3:1, 1:1, 1:3, 1:5, 1:7. The results are presented as the mean ± SEM of at least duplicate samples and experiments were performed at least two times.

4.3.3 Transfection and translation efficiency of pDNA-LNPs into RAW264.7 cell line

To investigate the delivery and translation efficiency of the pDNA complexed with LNPs constituting DOTAP: DOPE (1: 1 mole ratio) or DOTAP: DOPE: PEG (50: 49.25: 0.75 mole ratio) at different N/P ratios, we performed the transfection of DsRed2 red fluorescent protein encoding pDNA complexed with LNPs into RAW264.7 macrophage cell lines for 48 hrs. The results of the flow cytometry indicated that the translation of pDNA-LNPs is shown in Figure 4.12. At the N/P ratio of 3:1 in DOTAP: DOPE formula showed the most translation efficiency with significant increases in both the percentage of DsRed2-positive cells and MFI compared to non-transfected cells (control). While, DOTAP: DOPE: PEG formula at N/P ratio of 7:1, 5:1, and 1:1 showed similar translation efficiency over the control. Between the two cationic LNP formulations, there was no outstanding difference in pDNA translation efficiency.
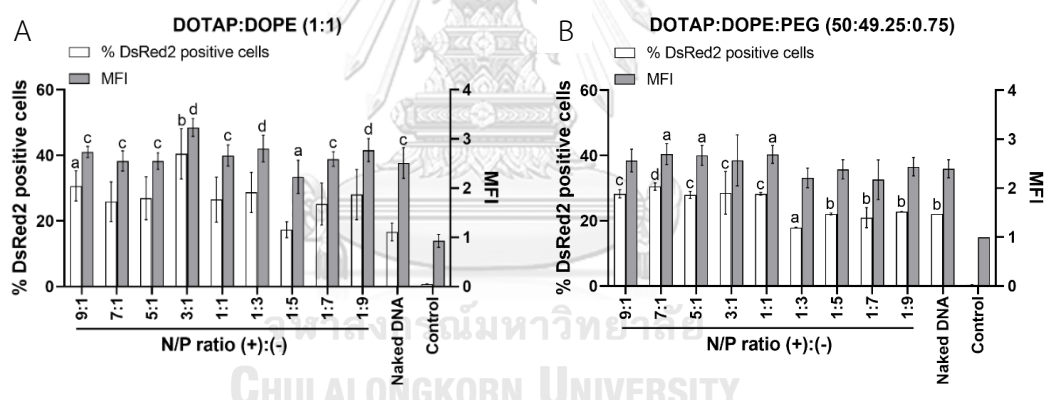
Figure 4.12 Transfection and translation efficiencies of pDNA complexed with cationic LNPs

(A) DOTAP: DOPE (1: 1) and (B) DOTAP: DOPE: PEG (50: 49.25: 0.75) with various N/P ratios (9:1, 7:1, 5:1, 3:1, 1:1, 1:3, 1:5, 1:7, 1:9) in RAW264.7 cell lines. Each bar value represents the mean ± SEM of at least duplicate samples and experiments were performed at least two times. Data are expressed as the percent of transfected cells and median fluorescence intensity (MFI) as obtained from flow cytometry analysis. (a) $p < 0.05$, (b) $p < 0.01$, (c) $p < 0.001$ and (d) $p < 0.0001$ compared with the number of non-transfected cells (control).

CHAPTER V

DISCUSSION

In the past decade, immunotherapy has been revolutionized that included several attractive cancer treatments including immune checkpoint inhibitors and adoptive cell transfer. However, the clinical outcomes were varied and could be applied to only a subgroup of patients (240). Personalized therapeutic vaccine, which works against cancer by boosting host immune response is another promising approach to trigger de novo T cell responses against tumor neoantigens with highly specific to tumors of individual patients (241).

In the first part of this study, we evaluated the translation efficiency, innate immunogenicity and APC maturation induced by different degrees of modified nucleoside in mRNA-LNP in *in vitro* and *in vivo*. For *in vitro* study, BMDCs and BMDMs were selected as target cells because they are the most important targets of mRNA vaccine and the initiation of adaptive immunity (26). This *in vitro* study used mCherry encoding mRNA which has 1,139 nucleotide sequence long and luciferase encoding mRNA which has 2,100 nucleotide sequence long (Appendix B Figure 1) as target antigens to confirm that there was no effect of antigen and sequence length on protein translation. As the nucleoside modification level increases, translation is improved in both antigens. There was a dominent secretion of IFN-I from the 0% m1Ψ substitution group and it was notable that at 40, 70 and 100% of m1Ψ substitutions showed a significant protein translation compared to untreated control. This is consistent with previous study reporting that the substitution of uridine with m1Ψ in mRNA significantly improves the translation efficiency and decreases innate immunogenicity (166).

For *in vivo* study, mRNA-LNP uptake was investigated from APCs in the secondary lymphoid organs including lymph nodes and spleens where immune cells

reside at high density and adaptive immune cells interact with antigen-MHC complexes on APCs, and then proliferate and differentiate to become effector cells (242). cDC1 are critical for antigen cross-presentation required to prime CD8^{+} T cells for optimal anti-tumor immunity and priming of CD4^{+} T cells at early stages, since cDC1 provides antigen transportation to lymph nodes for processing by cDC2 (78). CD40 signaling in cDC1 is required for tumor rejection by playing a key role in augmenting the proliferation of antigen-specific CD8^{+} T cells (78). Engagement of CD40 with its ligand induces recruitment of TNF receptor-associated factor family of proteins (TRAFs) and initiates signaling cascades that activate genes involved in cytokine production, as well as upregulation of co-stimulatory molecules such as CD80 and CD86 (243). We demonstrated that the maturation of cDC1 and cDC2 upon delivery of unmodified and 40% substitution with m1Ψ mRNA-LNP was evident compared with 100% substitution with m1Ψ mRNA-LNP. While unmodified mRNA-LNP compromises the translation efficiency of mRNA into protein antigen, its superior impact on DC maturation is beneficial for anti-tumor immunity.

Based on the result in Figure 4.3A, substitutions of 0% and 40%, but not 70% and 100% m1Ψ in mRNA-LNPs could induce serum IFN-I secretion 6 hrs after the prime and booster doses. Previous studies reported that IFN-I upregulates CD40 and CD80 expressions through an involvement of IRF-1 transcription factors (244). Binding of type I IFN-receptors activates JAK/STAT signal pathway (94) and leads to STAT1 homodimerization (103). Stat1 homodimer binds IFN-γ-activated site (GAS) motifs in the promoter regions of interferon regulatory factor-1 (IRF-1) gene and activates transcription of CD40 and CD80 genes and protein expressions (245).

Herein, we addressed the impact of different degrees of m1Ψ substitutions in mRNA on the immunogenicity. mRNAs were prepared to encode for OVA as a model antigen and somatic mutation-induced neoantigens- Pbk and Actn4 of B16F10

melanoma cells (16). Unmodified mRNA-LNP administration is associated with large amounts of systemic IFN-I 6 hrs after immunization of OVA encoding mRNA-LNP. Surprisingly, the level of IFN-I dramatically drops after the second dose of immunization which is likely the effect of unmodified mRNA. It is possible that repeated exposure to unmodified mRNA epigenetically enforces innate immune tolerance where the cells are incapable of activating certain inflammatory gene transcription (246).

The current use of mRNA vaccine for COVID-19 pandemic demonstrates the high efficacy in inducing a Th1 response in combination with humoral response by mRNA vaccine (247, 248). Indeed, besides prominent Th1-related cytokines such as IFN-γ and TNF-α and granzyme B, we also observed the increase of IL-5$^+$ CD4$^+$ T cells when unmodified mRNA-LNP was used. This balanced T helper cell response induced by unmodified mRNA may render a strong anti-tumor immune response that successfully control tumor growth. Interestingly, the increase of PD-1 expression was found on CD4$^+$ and CD8$^+$ T cells in unmodified Neo-LNP immunized group. This may be due to the robustly T cell receptor (TCR) activation.

IFN-I secretion subsequently induced following the recognition of TLR7 with unmodified mRNA causes selective induction of Th1 type immune responses (249). Possible explanations that mRNA vaccine drives Th2 differentiation are that there were secretion of IL-4 which may arise from cDC2, NK T cells, eosinophils or mast cells in the environment or a low amount of translated proteins from unmodified mRNA caused a low number of engaged TCRs, and the signal passed through the TCR may not reach the activation threshold to determine the IFN-γ gene transcription (250, 251).

For *in vivo* cytotoxic activity study, vaccination of OVA-LNP revealed a dramatically increased priming of antigen-specific T cells in the nucleoside modification regardless of the degree of m1Ψ substitution. These vaccine primed T

cells acquired full effector function and efficiently eliminated target cells with similar cytotoxicity. In our study, we did not investigate whether CD4^{+} T cells also contribute to direct tumor killing. Previous study reported the observation of a cytotoxic subset of CD4^{+} T cells (CD4 CTLs). CD4^{+} CTLs are characterized by their cytotoxic functions to secrete granzyme B and perforin and directly kill target cells. They recognize target cells via peptide-MHC II complex on APCs (252). Upon transfer of naive tumor reactive CD4^{+} T cells into lymphopenic recipients, substantial T cell expansion and differentiation were observed. Tumor regression was dependent on class II-restricted recognition of tumors by tumor-reactive CD4^{+} CTLs which developed cytotoxic activity and kill tumor (253).

In the second part of this study, we investigated the anti-tumor effects of the mRNA-LNP platform in localized and metastatic B16 melanoma models. When challenged with the highly aggressive B16 melanoma model, unmodified OVA-LNP vaccinated mice showed outstanding anti-tumor effect by extending survival time, controlling tumor growth and lung metastasis inhibition as compared to modified OVA-LNP and control treated mice. While we observed equal target cell killing activities in all mRNA-LNP regardless of the modification level in the cytotoxic assay, unmodified mRNA-LNP showed better tumor control efficacy *in vivo*. This discrepancy reflects the complex tumor microenvironment that may preclude accessibility to target tumor cells.

Better tumor control with unmodified mRNA-LNP is associated with the presence of mature tumor-infiltrating migratory cDC1. The presence of mature cDC1 in tumor may lead to more efficient antigen presentation and cross-presentation of tumor antigens and subsequent augment antigen-specific T cell immunity (254) as shown in relevant results of antigen-specific effector T cell (CD44^{+}CD62L^{-}) expansion and polyfunctional cytokine secretion after restimulated splenocytes with the OVA$_{257-264}$ (SIINFEKL) peptide. Interestingly, we found that a substantial tumor infiltrated T

cell subset (CD3$^+$) in unmodified mRNA-LNP group is CD4$^-$CD8$^-$ double negative (DN) T cells. Both TCR$\alpha\beta$ T cells and TCR$\gamma\delta$ T cells contain a small subset of DN T cells. Although the roles of these cells in tumors are still controversial, the use of DN T cells for cancer immunotherapy against blood and solid tumor were reported (255). Our results indicated that DN T cells may play a crucial role in anti-tumor immunity raised by mRNA vaccines. Therefore, characterization of the DN T cells may provide insight into the anti-tumor immunity induced by mRNA-LNP.

In the tumor microenvironment, immunosuppression and tumor evasion strategies cause an inability of the immune cells to detect and eliminate with subsequent exhaustion (40). Generally, PD-1 expression on cell surface of activated T cells is induced after TCR activation (256). Ligation of PD-1 with its ligands programmed death-ligand 1 or 2 (PD-L1 or PD-L2) induces tyrosine phosphorylation of the PD-1 cytoplasmic domain by phosphorylating kinase Lck and subsequent recruitment of cytosolic tyrosine phosphatase SHP-2 and PD-1-associated SHP-2 preferentially dephosphorylates CD28 and suppresses CD28 costimulatory signaling leading to restrained effector T cell function (43-45). In our studies, we consistently observed higher frequency of PD-1$^+$ cells in tumor infiltrating T cells when IFNAR1 was blocked. This result may imply that unmodified mRNA via IFN-I help alleviates T cell exhaustion that allows anti-tumor T cells to be fully functional. Consistent with this observation, more M2-like tumor-associated macrophages were observed when IFN-I is blocked in the mRNA/LNP vaccinated group. Taken together, we provide strong evidence that IFN-I plays an indispensable role in inducing anti-tumor response by mRNA vaccine.

The prominent therapeutic efficacy of unmodified mRNA is possibly due to activation of endosomal toll-like receptor 7/8 (TLR7/8) and subsequently causes pro-inflammatory cytokine secretion via MyD88-dependent IRF-5 phosphorylation (257). IRF-5 is critically involved in M1- macrophage polarization (258), which possesses

phagocytic capacity, and the ability to secrete reactive nitrogen and oxygen species and pro-inflammatory cytokines such as IL-6, IL-12, IL-23 and TNF-a, which in turn promote CD8$^+$ T cell and NK cell cytotoxicity. In addition, M1 macrophages secrete CXCL9, CXCL10 and CXCL15 chemokines upon STAT1 signaling, which recruit cytotoxic T lymphocytes (CTLs) to the tumor (61). Furthermore, the IRF-7 transcript was strongly induced by IFN-I. IRF-7 mediated decrease in VEGF mRNA level that inhibits lung metastasis due to the lack of tumor-angiogenesis factors (62, 244). Mice with impaired IFN-I signaling developed more lung metastases in the 4T1 mammary and lung carcinoma models, compared to wild type mice accompanied by elevated G-CSF levels in serum and enhanced CXCR2 expression on neutrophils leading to massive accumulation of neutrophils in lungs which facilitated a pre-metastatic niche formation, supporting more efficient tumor cell extravasation and proliferation (259).

Recent study identified the intrinsic adjuvant activity of the LNP itself. When used in mRNA and protein subunit vaccines, LNP exerts potent stimulatory activity against T follicular helper cell and the immune induction was superior to what induced by AddaVax formulated vaccine. Adjuvant activity of the LNP critically relies on IL-6 and its constituent ionizable lipid. Remarkably, potent immune responses from a single immunization of LNP loaded non-inflammatory nucleoside-modified mRNA was related to LNP adjuvanticity (260). Unmodified mRNA itself provides adjuvant activity through binding and activation of the innate immune sensors, mainly TLRs 3, 7, and 8 (261). In our study, we did not distinguish adjuvant activity of mRNA from LNP and the impact on anti-tumor responses may derive from LNP and/or mRNA.

In the previous study by Kranz and coworkers, a systemic immunization with three doses (40 µg/dose) of mRNA encoding OVA cleared B16-OVA lung metastasis with no tumor at 20 days after the last immunization. Their OVA mRNA construct encoded for the H-2K^b-restricted immunodominant epitope OVA $_{257-264}$ and the lipid

formulation contained DOTAP and DOPE. The mean diameter of mRNA-LNP was 200 nm (31). In our study, using two doses (10 µg/dose) of mRNA encoding whole OVA protein, we observed a similar anti-metastatic effect. Although unmodified mRNA was used in both studies, differences in the use of whole protein rather than peptide antigens and the LNP formulation and size may result in the modest differences observed. LNP used in our study is the proprietary to Acuitas Therapeutics contains a proprietary ionizable cationic lipid, cholesterol, DSPC, and a PEG-lipid with a mean diameter of 80 nm (260).

Finally, it is more relevant to real cancer settings with non-dominant antigens and tumor heterogeneity. Possibility of loss of MHC class I allele–presenting neoantigen associated with cancer immune evasion (262). Thus, vaccination with epitopes targeting both CD4 and CD8 T cells may lead to a better efficiency in antitumor response (263). In this study, Pbk-Actn4 somatic mutations of B16F10 tumor were selected and linked together as target neoantigens in mRNA-LNP vaccines. We observed less robust, but significant tumor growth retardation effect with the neoantigen vaccine compared to the OVA model. The moderate immunogenicity of neoantigens may be explained by a loss of tumor suppression gene copy number during cancer progression which enables elimination of neoantigen-expressing tumor clones (264) and exhaustion of neoantigen-specific T cells. Additional highly immunogenic neoantigens formulated in the polyepitope mRNA vaccine may help improve the anti-tumor response of mRNA vaccines using neoantigens, such as demonstrated by Kreiter *et al.* (16). Combination therapy of cancer vaccine with immune checkpoint antibodies (anti–PD-1 and anti–CTLA-4) would help in tumor regression by restoring the functionality of exhausted cells and expanding of neoantigen-specific $CD8^+$ T cell (21, 265, 266). Taken together, we provide strong evidence for the anti-tumor immune response by unmodified mRNA vaccines encoding dominant and neoantigens.

In the third part of this study, we synthesized the prototype of LNPs based on well-characterized lipids for delivery of plasmid DNA (pDNA). The size and charge of particles influenced delivery of vaccine to target APCs in lymph nodes (194, 238). We found that the smallest and the largest Z-average diameters of the pDNA complexed with LNPs constituting DOTAP: DOPE (1: 1 mole ratio) or DOTAP: DOPE: PEG (50: 49.25: 0.75 mole ratio) at different N/P ratios were within the size range for uptake by macropinocytosis (267). Moreover, as the N/P ratio decreased, the particle size increased and the same trend was observed in both formulas as shown in Figure 4.10. In addition, the decrease of N/P ratio at 1:3, 1:5, 1:7 and 1:9 in both formulas resulted in increase of PDI values bigger than 0.3, which is considered a heterogeneous size and unstable (239). This may be because the less positively charged LNPs in the ratio causes more free pDNA in the suspension which can induce electrostatic interaction of nearby LNPs to form large aggregation with the pDNA (232). It was found that while increasing PEG content in the LNP makes particle smaller and more stable (268). The positive zeta potentials were found at higher N/P ratio in both formulas. In accordance with the decrease of cationic lipid mole ratio, there were free pDNA in the suspension which caused the negative zeta potentials. Although, zeta potential generally exhibited near-neutral surface charge with increasing PEG component, it should be noted that zeta potential measurement significantly vary depending on the buffer conditions, including ionic concentration and pH (269). Both LNP formulas and pDNA-LNPs did not show significant negative effect on the RAW264.7 cell viability even at the high concentration of 7.407 nmol (the maximum concentration tested). However, the toxicity tolerance is a cell type dependent process (270). There was no significant difference in translation efficiency compared between two formulas at all N/P ratios.

In summary, the present study reveals that unmodified mRNA-LNP induces substantial IFN-I production and the maturation of DCs. In B16F0-OVA murine

melanoma model, unmodified OVA-LNP significantly reduced tumor growth and prolonged survival, compared to OVA-LNP with m1Ψ substitution. This robust anti-tumor effect correlated with the increase in intratumoral CD40$^+$ DCs and the frequency of granzyme B$^+$/IFN-γ^+/TNF-α+ polyfunctional antigen-specific CD8$^+$ T cells. Blocking type I IFN receptor completely reversed the anti-tumor immunity of unmodified mRNA-OVA reflected in a significant decrease in OVA-specific IFN-γ secreting T cells and enrichment of PD-1$^+$ tumor-infiltrating T cells. The robust anti-tumor effect of unmodified OVA-LNP was also observed in the lung metastatic tumor model. Finally, this mRNA vaccine was tested using B16F10 melanoma neoantigens (Pbk-Actn4) which resulted in delayed B16F10 tumor growth. Taken together, our findings demonstrated that an unmodified mRNA vaccine may be a better tumor vaccine strategy that induces robust antitumor immunity in IFN-I dependent manner.
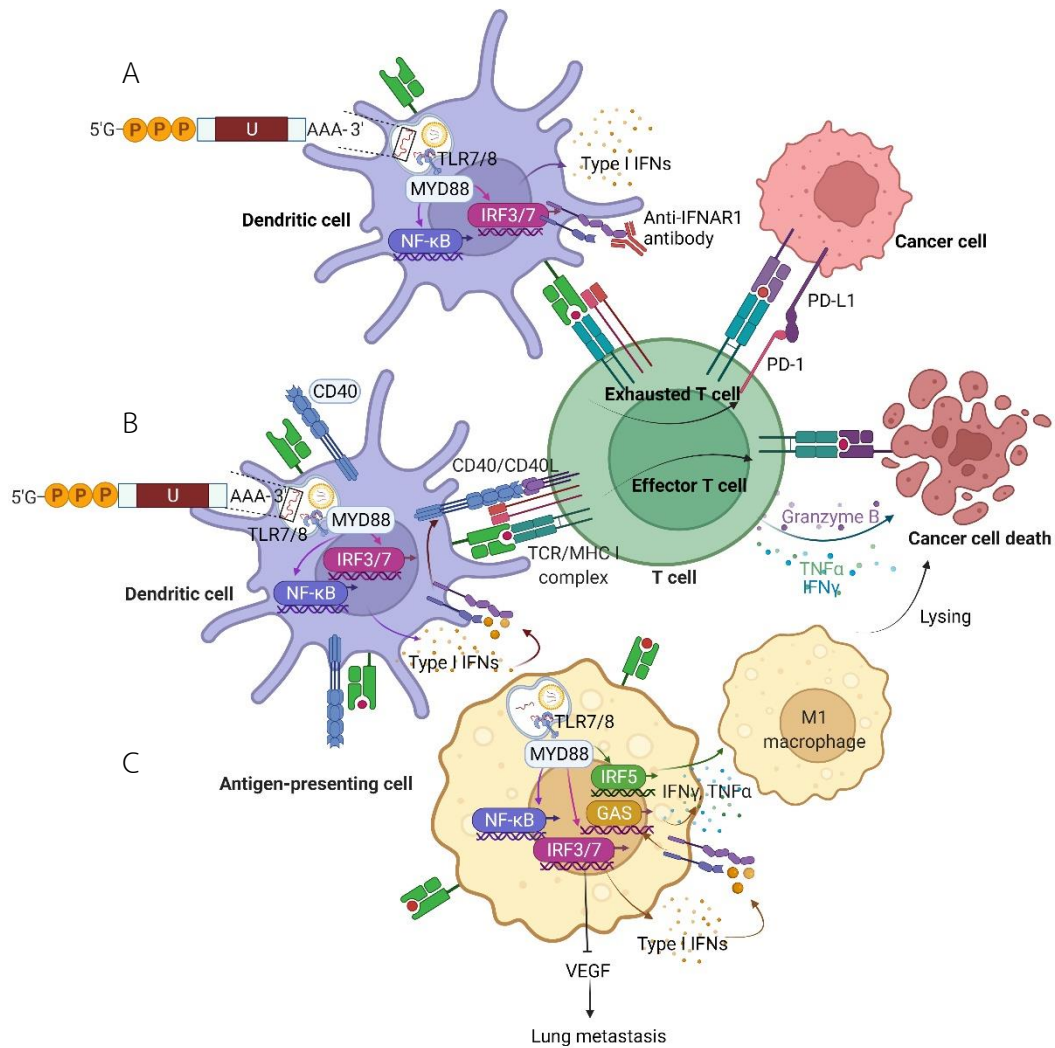
Figure 5.1 Proposed mechanism of antitumor immunity by unmodified mRNA-LNP in an IFN-I-dependent manner.

Unmodified mRNA provides adjuvant activity through recognition of uridine nucleosides by TLR-7/8 and induction of proinflammatory cytokines including IFN-I. (A) In the precense of anti-IFNAR1 antibody to block IFN-I signaling causes exhausted T cells with upregulation of PD-1 which results in uncontrolled tumor growth. (B) Intact IFN-I signaling results in the expression of CD40 which mediates effective antigen presentation and results in robust antitumor immunity by effector T cells. (C) Tumor-associated macrophage are phenotypically polarization to proinflammatory M1 macrophage by IFN-γ and TNF-α.

CHAPTER VI
CONCLUSIONS

6.1 The translation efficiency was dependent on the degree of nucleoside substitution and inversely correlated with induction of IFN-I secretion and APC maturation. The 100% m1Ψ substitution in mRNA-LNP showed the highest mRNA transfection and translation efficiencies, while unmodified mRNA-LNP induced APC maturation and IFN-I secretion.

6.2 Unmodified mRNA induced stronger Th1 response than modified mRNA.

6.3 All degrees of nucleoside substitution in OVA-LNP activated OVA-specific cytotoxic effector T cells.

6.4 Unmodified mRNA-LNP enhanced tumor-infiltrating mature migratory cDC1 and the frequency and effector function of tumor antigen-specific effector T cells.

6.5 IFN-I secretion or the downstream signaling cascades induced by unmodified mRNA-LNP resulted in a significant increase in OVA specific IFN-γ-producing T cells and decrease of the frequency of tumor-infiltrating M2-like phenotype macrophages and PD-1 expression on T cells.

6.6 Unmodified mRNA-LNP induced robust anti-tumor T cell response for controlling B16 tumor growth in both dominant OVA model antigen and non-dominant neoantigens and suppressed lung metastasis in type I IFN-dependent manner.

6.7 DOTAP: DOPE (1: 1 mole ratio) and DOTAP: DOPE: PEG (50: 49.25: 0.75 mole ratio) were safe LNPs and facilitated antigen uptake and translation in RAW264.7 cell line.

REFERENCES

1.   Sung H, Ferlay J, Siegel RL, Laversanne M, Soerjomataram I, Jemal A, et al. Global Cancer Statistics 2020: GLOBOCAN Estimates of Incidence and Mortality Worldwide for 36 Cancers in 185 Countries. CA Cancer J Clin. 2021;71(3):209-49.

2.   Gonzalez H, Hagerling C, Werb Z. Roles of the immune system in cancer: from tumor initiation to metastatic progression. Genes Dev. 2018;32(19-20):1267-84.

3.   Wang RF, Wang HY. Immune targets and neoantigens for cancer immunotherapy and precision medicine. Cell Res. 2017;27(1):11-37.

4.   Curtsinger JM, Lins DC, Mescher MF. Signal 3 determines tolerance versus full activation of naive CD8 T cells: dissociating proliferation and development of effector function. J Exp Med. 2003;197(9):1141-51.

5.   Crespo J, Sun H, Welling TH, Tian Z, Zou W. T cell anergy, exhaustion, senescence, and stemness in the tumor microenvironment. Curr Opin Immunol. 2013;25(2):214-21.

6.   Toor SM, Sasidharan Nair V, Decock J, Elkord E. Immune checkpoints in the tumor microenvironment. Semin Cancer Biol. 2020;65:1-12.

7.   Abbott M, Ustoyev Y. Cancer and the Immune System: The History and Background of Immunotherapy. Semin Oncol Nurs. 2019;35(5):150923.

8.   Ventola CL. Cancer Immunotherapy, Part 1: Current Strategies and Agents. P T. 2017;42(6):375-83.

9.   Glassman PM, Balthasar JP. Mechanistic considerations for the use of monoclonal antibodies for cancer therapy. Cancer Biol Med. 2014;11(1):20-33.

10.   Park YJ, Kuen DS, Chung Y. Future prospects of immune checkpoint blockade in cancer: from response prediction to overcoming resistance. Exp Mol Med. 2018;50(8):1-13.

11.   Bitton RJ, Guthmann MD, Gabri MR, Carnero AJ, Alonso DF, Fainboim L, et al. Cancer vaccines: an update with special focus on ganglioside antigens. Oncol Rep. 2002;9(2):267-76.

12.   Kalos M, June CH. Adoptive T cell transfer for cancer immunotherapy in the era of synthetic biology. Immunity. 2013;39(1):49-60.

13.   Arruebo M, Vilaboa N, Saez-Gutierrez B, Lambea J, Tres A, Valladares M, et al. Assessment of the evolution of cancer treatment therapies. Cancers (Basel). 2011;3(3):3279-330.

14.   Guo Y, Lei K, Tang L. Neoantigen Vaccine Delivery for Personalized Anticancer Immunotherapy. Front Immunol. 2018;9:1499.

15.   Lu YC, Robbins PF. Cancer immunotherapy targeting neoantigens. Semin Immunol. 2016;28(1):22-7.

16.   Kreiter S, Vormehr M, van de Roemer N, Diken M, Lower M, Diekmann J, et al. Mutant MHC class II epitopes drive therapeutic immune responses to cancer. Nature. 2015;520(7549):692-6.

17.   Weide B, Garbe C, Rammensee HG, Pascolo S. Plasmid DNA- and messenger RNA-based anti-cancer vaccination. Immunol Lett. 2008;115(1):33-42.

18.   De Beuckelaer A, Pollard C, Van Lint S, Roose K, Van Hoecke L, Naessens T, et al. Type I Interferons Interfere with the Capacity of mRNA Lipoplex Vaccines to Elicit Cytolytic T Cell Responses. Mol Ther. 2016;24(11):2012-20.

19.   Fiedler K, Lazzaro S, Lutz J, Rauch S, Heidenreich R. mRNA Cancer Vaccines. Recent Results Cancer Res. 2016;209:61-85.

20.   Bidram M, Zhao Y, Shebardina NG, Baldin AV, Bazhin AV, Ganjalikhany MR, et al. mRNA-Based Cancer Vaccines: A Therapeutic Strategy for the Treatment of Melanoma Patients. Vaccines (Basel). 2021;9(10).

21.   Sahin U, Oehm P, Derhovanessian E, Jabulowsky RA, Vormehr M, Gold M, et al. An RNA vaccine drives immunity in checkpoint-inhibitor-treated melanoma. Nature. 2020;585(7823):107-12.

22.   Batista Napotnik T, Polajzer T, Miklavcic D. Cell death due to electroporation - A review. Bioelectrochemistry. 2021;141:107871.

23.   Mellott AJ, Forrest ML, Detamore MS. Physical non-viral gene delivery methods for tissue engineering. Ann Biomed Eng. 2013;41(3):446-68.

24.   Mintzer MA, Simanek EE. Nonviral vectors for gene delivery. Chem Rev. 2009;109(2):259-302.

25. Li W, Szoka FC, Jr. Lipid-based nanoparticles for nucleic acid delivery. Pharm Res. 2007;24(3):438-49.

26. Reichmuth AM, Oberli MA, Jaklenec A, Langer R, Blankschtein D. mRNA vaccine delivery using lipid nanoparticles. Ther Deliv. 2016;7(5):319-34.

27. Sayour EJ, De Leon G, Pham C, Grippin A, Kemeny H, Chua J, et al. Systemic activation of antigen-presenting cells via RNA-loaded nanoparticles. Oncoimmunology. 2017;6(1):e1256527.

28. Lv H, Zhang S, Wang B, Cui S, Yan J. Toxicity of cationic lipids and cationic polymers in gene delivery. J Control Release. 2006;114(1):100-9.

29. Jain S, Kumar S, Agrawal AK, Thanki K, Banerjee UC. Enhanced transfection efficiency and reduced cytotoxicity of novel lipid-polymer hybrid nanoplexes. Mol Pharm. 2013;10(6):2416-25.

30. Macri C, Dumont C, Johnston AP, Mintern JD. Targeting dendritic cells: a promising strategy to improve vaccine effectiveness. Clin Transl Immunology. 2016;5(3):e66.

31. Kranz LM, Diken M, Haas H, Kreiter S, Loquai C, Reuter KC, et al. Systemic RNA delivery to dendritic cells exploits antiviral defence for cancer immunotherapy. Nature. 2016;534(7607):396-401.

32. Silacci M, Baenziger-Tobler N, Lembke W, Zha W, Batey S, Bertschinger J, et al. Linker length matters, fynomer-Fc fusion with an optimized linker displaying picomolar IL-17A inhibition potency. J Biol Chem. 2014;289(20):14392-8.

33. Hou X, Zaks T, Langer R, Dong Y. Lipid nanoparticles for mRNA delivery. Nat Rev Mater. 2021;6(12):1078-94.

34. Hulvat MC. Cancer Incidence and Trends. Surg Clin North Am. 2020;100(3):469-81.

35. Wang JJ, Lei KF, Han F. Tumor microenvironment: recent advances in various cancer treatments. Eur Rev Med Pharmacol Sci. 2018;22(12):3855-64.

36. Hanada KI, Yu Z, Chappell GR, Park AS, Restifo NP. An effective mouse model for adoptive cancer immunotherapy targeting neoantigens. JCI Insight. 2019;4(10).

37. Weinberg RA. How cancer arises. Sci Am. 1996;275(3):62-70.

38.   Kopfstein L, Christofori G. Metastasis: cell-autonomous mechanisms versus contributions by the tumor microenvironment. Cell Mol Life Sci. 2006;63(4):449-68.

39.   Blackadar CB. Historical review of the causes of cancer. World J Clin Oncol. 2016;7(1):54-86.

40.   Yang L, Li A, Lei Q, Zhang Y. Tumor-intrinsic signaling pathways: key roles in the regulation of the immunosuppressive tumor microenvironment. J Hematol Oncol. 2019;12(1):125.

41.   Wu AA, Drake V, Huang HS, Chiu S, Zheng L. Reprogramming the tumor microenvironment: tumor-induced immunosuppressive factors paralyze T cells. Oncoimmunology. 2015;4(7):e1016700.

42.   Croci DO, Zacarias Fluck MF, Rico MJ, Matar P, Rabinovich GA, Scharovsky OG. Dynamic cross-talk between tumor and immune cells in orchestrating the immunosuppressive network at the tumor microenvironment. Cancer Immunol Immunother. 2007;56(11):1687-700.

43.   Hui E, Cheung J, Zhu J, Su X, Taylor MJ, Wallweber HA, et al. T cell costimulatory receptor CD28 is a primary target for PD-1-mediated inhibition. Science. 2017;355(6332):1428-33.

44.   Yokosuka T, Takamatsu M, Kobayashi-Imanishi W, Hashimoto-Tane A, Azuma M, Saito T. Programmed cell death 1 forms negative costimulatory microclusters that directly inhibit T cell receptor signaling by recruiting phosphatase SHP2. J Exp Med. 2012;209(6):1201-17.

45.   Sheppard KA, Fitz LJ, Lee JM, Benander C, George JA, Wooters J, et al. PD-1 inhibits T-cell receptor induced phosphorylation of the ZAP70/CD3zeta signalosome and downstream signaling to PKCtheta. FEBS Lett. 2004;574(1-3):37-41.

46.   Parry RV, Chemnitz JM, Frauwirth KA, Lanfranco AR, Braunstein I, Kobayashi SV, et al. CTLA-4 and PD-1 receptors inhibit T-cell activation by distinct mechanisms. Mol Cell Biol. 2005;25(21):9543-53.

47.   De Beuckelaer A, Grooten J, De Koker S. Type I Interferons Modulate CD8(+) T Cell Immunity to mRNA Vaccines. Trends Mol Med. 2017;23(3):216-26.

48.   Chen DS, Mellman I. Oncology meets immunology: the cancer-immunity cycle. Immunity. 2013;39(1):1-10.

49.   Lavin Y, Mortha A, Rahman A, Merad M. Regulation of macrophage development and function in peripheral tissues. Nat Rev Immunol. 2015;15(12):731-44.

50.   Linares-Fernandez S, Lacroix C, Exposito JY, Verrier B. Tailoring mRNA Vaccine to Balance Innate/Adaptive Immune Response. Trends Mol Med. 2020;26(3):311-23.

51.   Gordon S, Pluddemann A. Tissue macrophages: heterogeneity and functions. BMC Biol. 2017;15(1):53.

52.   Movahedi K, Laoui D, Gysemans C, Baeten M, Stange G, Van den Bossche J, et al. Different tumor microenvironments contain functionally distinct subsets of macrophages derived from Ly6C(high) monocytes. Cancer Res. 2010;70(14):5728-39.

53.   Zhu Y, Herndon JM, Sojka DK, Kim KW, Knolhoff BL, Zuo C, et al. Tissue-Resident Macrophages in Pancreatic Ductal Adenocarcinoma Originate from Embryonic Hematopoiesis and Promote Tumor Progression. Immunity. 2017;47(2):323-38 e6.

54.   Bonnardel J, Guilliams M. Developmental control of macrophage function. Curr Opin Immunol. 2018;50:64-74.

55.   Chen S, Yang J, Wei Y, Wei X. Epigenetic regulation of macrophages: from homeostasis maintenance to host defense. Cell Mol Immunol. 2020;17(1):36-49.

56.   Henze AT, Mazzone M. The impact of hypoxia on tumor-associated macrophages. J Clin Invest. 2016;126(10):3672-9.

57.   Biswas SK, Mantovani A. Macrophage plasticity and interaction with lymphocyte subsets: cancer as a paradigm. Nat Immunol. 2010;11(10):889-96.

58.   Marigo I, Zilio S, Desantis G, Mlecnik B, Agnellini AHR, Ugel S, et al. T Cell Cancer Therapy Requires CD40-CD40L Activation of Tumor Necrosis Factor and Inducible Nitric-Oxide-Synthase-Producing Dendritic Cells. Cancer Cell. 2016;30(3):377-90.

59.   Mantovani A, Sozzani S, Locati M, Allavena P, Sica A. Macrophage

polarization: tumor-associated macrophages as a paradigm for polarized M2 mononuclear phagocytes. Trends Immunol. 2002;23(11):549-55.

60. Schuette V, Embgenbroich M, Ulas T, Welz M, Schulte-Schrepping J, Draffehn AM, et al. Mannose receptor induces T-cell tolerance via inhibition of CD45 and up-regulation of CTLA-4. Proc Natl Acad Sci U S A. 2016;113(38):10649-54.

61. Liu J, Geng X, Hou J, Wu G. New insights into M1/M2 macrophages: key modulators in cancer progression. Cancer Cell Int. 2021;21(1):389.

62. Lakshmi Narendra B, Eshvendar Reddy K, Shantikumar S, Ramakrishna S. Immune system: a double-edged sword in cancer. Inflamm Res. 2013;62(9):823-34.

63. Watowich SS, Liu YJ. Mechanisms regulating dendritic cell specification and development. Immunol Rev. 2010;238(1):76-92.

64. Onai N, Obata-Onai A, Schmid MA, Ohteki T, Jarrossay D, Manz MG. Identification of clonogenic common Flt3+M-CSFR+ plasmacytoid and conventional dendritic cell progenitors in mouse bone marrow. Nat Immunol. 2007;8(11):1207-16.

65. Patente TA, Pinho MP, Oliveira AA, Evangelista GCM, Bergami-Santos PC, Barbuto JAM. Human Dendritic Cells: Their Heterogeneity and Clinical Application Potential in Cancer Immunotherapy. Front Immunol. 2018;9:3176.

66. Akira S, Uematsu S, Takeuchi O. Pathogen recognition and innate immunity. Cell. 2006;124(4):783-801.

67. Vassalli G. Dendritic cell-based approaches for therapeutic immune regulation in solid-organ transplantation. J Transplant. 2013;2013:761429.

68. Banchereau J, Steinman RM. Dendritic cells and the control of immunity. Nature. 1998;392(6673):245-52.

69. DeFillipo AM, Dai J, Li Z. Heat shock-induced dendritic cell maturation is coupled by transient aggregation of ubiquitinated proteins independently of heat shock factor 1 or inducible heat shock protein 70. Mol Immunol. 2004;41(8):785-92.

70. Sauter B, Albert ML, Francisco L, Larsson M, Somersan S, Bhardwaj N. Consequences of cell death: exposure to necrotic tumor cells, but not primary

tissue cells or apoptotic cells, induces the maturation of immunostimulatory dendritic cells. J Exp Med. 2000;191(3):423-34.

71.   O'Sullivan B, Thomas R. CD40 and dendritic cell function. Crit Rev Immunol. 2003;23(1-2):83-107.

72.   Medrano RFV, Hunger A, Mendonca SA, Barbuto JAM, Strauss BE. Immunomodulatory and antitumor effects of type I interferons and their application in cancer therapy. Oncotarget. 2017;8(41):71249-84.

73.   Montoya M, Schiavoni G, Mattei F, Gresser I, Belardelli F, Borrow P, et al. Type I interferons produced by dendritic cells promote their phenotypic and functional activation. Blood. 2002;99(9):3263-71.

74.   Liu K, Victora GD, Schwickert TA, Guermonprez P, Meredith MM, Yao K, et al. In vivo analysis of dendritic cell development and homeostasis. Science. 2009;324(5925):392-7.

75.   Guilliams M, Ginhoux F, Jakubzick C, Naik SH, Onai N, Schraml BU, et al. Dendritic cells, monocytes and macrophages: a unified nomenclature based on ontogeny. Nat Rev Immunol. 2014;14(8):571-8.

76.   Schlitzer A, Ginhoux F. Organization of the mouse and human DC network. Curr Opin Immunol. 2014;26:90-9.

77.   Fuertes MB, Kacha AK, Kline J, Woo SR, Kranz DM, Murphy KM, et al. Host type I IFN signals are required for antitumor CD8+ T cell responses through CD8{alpha}+ dendritic cells. J Exp Med. 2011;208(10):2005-16.

78.   Ferris ST, Durai V, Wu R, Theisen DJ, Ward JP, Bern MD, et al. cDC1 prime and are licensed by CD4(+) T cells to induce anti-tumour immunity. Nature. 2020;584(7822):624-9.

79.   Elgueta R, Benson MJ, de Vries VC, Wasiuk A, Guo Y, Noelle RJ. Molecular mechanism and function of CD40/CD40L engagement in the immune system. Immunol Rev. 2009;229(1):152-72.

80.   Gilliet M, Cao W, Liu YJ. Plasmacytoid dendritic cells: sensing nucleic acids in viral infection and autoimmune diseases. Nat Rev Immunol. 2008;8(8):594-606.

81.   Gibson SJ, Lindh JM, Riter TR, Gleason RM, Rogers LM, Fuller AE, et al. Plasmacytoid dendritic cells produce cytokines and mature in response to the

TLR7 agonists, imiquimod and resiquimod. Cell Immunol. 2002;218(1-2):74-86.

82.   Maldonado-Lopez R, De Smedt T, Michel P, Godfroid J, Pajak B, Heirman C, et al. CD8alpha+ and CD8alpha- subclasses of dendritic cells direct the development of distinct T helper cells in vivo. J Exp Med. 1999;189(3):587-92.

83.   Kumamoto Y, Linehan M, Weinstein JS, Laidlaw BJ, Craft JE, Iwasaki A. CD301b(+) dermal dendritic cells drive T helper 2 cell-mediated immunity. Immunity. 2013;39(4):733-43.

84.   Kumar S, Jeong Y, Ashraf MU, Bae YS. Dendritic Cell-Mediated Th2 Immunity and Immune Disorders. Int J Mol Sci. 2019;20(9).

85.   Isaacs A, Lindenmann J. Virus interference. I. The interferon. Proc R Soc Lond B Biol Sci. 1957;147(927):258-67.

86.   Lukhele S, Boukhaled GM, Brooks DG. Type I interferon signaling, regulation and gene stimulation in chronic virus infection. Semin Immunol. 2019;43:101277.

87.   Chen J, Cao Y, Markelc B, Kaeppler J, Vermeer JA, Muschel RJ. Type I IFN protects cancer cells from CD8+ T cell-mediated cytotoxicity after radiation. J Clin Invest. 2019;129(10):4224-38.

88.   Platanias LC, Uddin S, Bruno E, Korkmaz M, Ahmad S, Alsayed Y, et al. CrkL and CrkII participate in the generation of the growth inhibitory effects of interferons on primary hematopoietic progenitors. Exp Hematol. 1999;27(8):1315-21.

89.   Fathers KE, Bell ES, Rajadurai CV, Cory S, Zhao H, Mourskaia A, et al. Crk adaptor proteins act as key signaling integrators for breast tumorigenesis. Breast Cancer Res. 2012;14(3):R74.

90.   Budhwani M, Mazzieri R, Dolcetti R. Plasticity of Type I Interferon-Mediated Responses in Cancer Therapy: From Anti-tumor Immunity to Resistance. Front Oncol. 2018;8:322.

91.   Zhang W, An EK, Hwang J, Jin JO. Mice Plasmacytoid Dendritic Cells Were Activated by Lipopolysaccharides Through Toll-Like Receptor 4/Myeloid Differentiation Factor 2. Front Immunol. 2021;12:727161.

92.   Ivashkiv LB, Donlin LT. Regulation of type I interferon responses. Nat Rev Immunol. 2014;14(1):36-49.

93. Nagarajan U. Induction and function of IFNbeta during viral and bacterial infection. Crit Rev Immunol. 2011;31(6):459-74.

94. Honda K, Yanai H, Takaoka A, Taniguchi T. Regulation of the type I IFN induction: a current view. Int Immunol. 2005;17(11):1367-78.

95. Yan J, Wang ZY, Yang HZ, Liu HZ, Mi S, Lv XX, et al. Timing is critical for an effective anti-metastatic immunotherapy: the decisive role of IFNgamma/STAT1-mediated activation of autophagy. PLoS One. 2011;6(9):e24705.

96. Fuertes MB, Woo SR, Burnett B, Fu YX, Gajewski TF. Type I interferon response and innate immune sensing of cancer. Trends Immunol. 2013;34(2):67-73.

97. Xin HM, Peng YZ, Yuan ZQ, Guo H. In vitro maturation and migration of immature dendritic cells after chemokine receptor 7 transfection. Can J Microbiol. 2009;55(7):859-66.

98. Krummel MF, Bartumeus F, Gerard A. T cell migration, search strategies and mechanisms. Nat Rev Immunol. 2016;16(3):193-201.

99. Roberts CA, Dickinson AK, Taams LS. The Interplay Between Monocytes/Macrophages and CD4(+) T Cell Subsets in Rheumatoid Arthritis. Front Immunol. 2015;6:571.

100. Spadaro F, Lapenta C, Donati S, Abalsamo L, Barnaba V, Belardelli F, et al. IFN-alpha enhances cross-presentation in human dendritic cells by modulating antigen survival, endocytic routing, and processing. Blood. 2012;119(6):1407-17.

101. Hervas-Stubbs S, Perez-Gracia JL, Rouzaut A, Sanmamed MF, Le Bon A, Melero I. Direct effects of type I interferons on cells of the immune system. Clin Cancer Res. 2011;17(9):2619-27.

102. Snell LM, McGaha TL, Brooks DG. Type I Interferon in Chronic Virus Infection and Cancer. Trends Immunol. 2017;38(8):542-57.

103. Delgado-Vega AM, Alarcon-Riquelme ME, Kozyrev SV. Genetic associations in type I interferon related pathways with autoimmunity. Arthritis Res Ther. 2010;12 Suppl 1:S2.

104. Vormehr M, Schrors B, Boegel S, Lower M, Tureci O, Sahin U. Mutanome Engineered RNA Immunotherapy: Towards Patient-Centered Tumor Vaccination. J

Immunol Res. 2015;2015:595363.

105.   Laidlaw BJ, Craft JE, Kaech SM. The multifaceted role of CD4(+) T cells in CD8(+) T cell memory. Nat Rev Immunol. 2016;16(2):102-11.

106.   Chang CF, Chen SL, Sung WW, Hsieh MJ, Hsu HT, Chen LH, et al. PBK/TOPK Expression Predicts Prognosis in Oral Cancer. Int J Mol Sci. 2016;17(7).

107.   Dong C, Fan W, Fang S. PBK as a Potential Biomarker Associated with Prognosis of Glioblastoma. J Mol Neurosci. 2020;70(1):56-64.

108.   Shih MC, Chen JY, Wu YC, Jan YH, Yang BM, Lu PJ, et al. TOPK/PBK promotes cell migration via modulation of the PI3K/PTEN/AKT pathway and is associated with poor prognosis in lung cancer. Oncogene. 2012;31(19):2389-400.

109.   Huang H, Lee MH, Liu K, Dong Z, Ryoo Z, Kim MO. PBK/TOPK: An Effective Drug Target with Diverse Therapeutic Potential. Cancers (Basel). 2021;13(9).

110.   Xu M, Xu S. PBK/TOPK overexpression and survival in solid tumors: A PRISMA-compliant meta-analysis. Medicine (Baltimore). 2019;98(10):e14766.

111.   Aksenova V, Turoverova L, Khotin M, Magnusson KE, Tulchinsky E, Melino G, et al. Actin-binding protein alpha-actinin 4 (ACTN4) is a transcriptional co-activator of RelA/p65 sub-unit of NF-kB. Oncotarget. 2013;4(2):362-72.

112.   Tentler D, Lomert E, Novitskaya K, Barlev NA. Role of ACTN4 in Tumorigenesis, Metastasis, and EMT. Cells. 2019;8(11).

113.   Castle JC, Kreiter S, Diekmann J, Lower M, van de Roemer N, de Graaf J, et al. Exploiting the mutanome for tumor vaccination. Cancer Res. 2012;72(5):1081-91.

114.   Kreiter S, Castle JC, Tureci O, Sahin U. Targeting the tumor mutanome for personalized vaccination therapy. Oncoimmunology. 2012;1(5):768-9.

115.   Roy PS, Saikia BJ. Cancer and cure: A critical analysis. Indian J Cancer. 2016;53(3):441-2.

116.   Hellman S, Vokes EE. Advancing current treatments for cancer. Sci Am. 1996;275(3):118-23.

117.   Hargadon KM, Johnson CE, Williams CJ. Immune checkpoint blockade therapy for cancer: An overview of FDA-approved immune checkpoint inhibitors. Int Immunopharmacol. 2018;62:29-39.

118.   Mohanty R, Chowdhury CR, Arega S, Sen P, Ganguly P, Ganguly N. CAR T cell therapy: A new era for cancer treatment (Review). Oncol Rep. 2019;42(6):2183-95.

119.   Fesnak A, Lin C, Siegel DL, Maus MV. CAR-T Cell Therapies From the Transfusion Medicine Perspective. Transfus Med Rev. 2016;30(3):139-45.

120.   Joffre O, Nolte MA, Sporri R, Reis e Sousa C. Inflammatory signals in dendritic cell activation and the induction of adaptive immunity. Immunol Rev. 2009;227(1):234-47.

121.   Long GV, Atkinson V, Cebon JS, Jameson MB, Fitzharris BM, McNeil CM, et al. Standard-dose pembrolizumab in combination with reduced-dose ipilimumab for patients with advanced melanoma (KEYNOTE-029): an open-label, phase 1b trial. Lancet Oncol. 2017;18(9):1202-10.

122.   Conlon KC, Miljkovic MD, Waldmann TA. Cytokines in the Treatment of Cancer. J Interferon Cytokine Res. 2019;39(1):6-21.

123.   Peters C, Brown S. Antibody-drug conjugates as novel anti-cancer chemotherapeutics. Biosci Rep. 2015;35(4).

124.   Chiocca EA, Rabkin SD. Oncolytic viruses and their application to cancer immunotherapy. Cancer Immunol Res. 2014;2(4):295-300.

125.   Kim EK, Ahn YO, Kim S, Kim TM, Keam B, Heo DS. Ex vivo activation and expansion of natural killer cells from patients with advanced cancer with feeder cells from healthy volunteers. Cytotherapy. 2013;15(2):231-41 e1.

126.   Saxena M, van der Burg SH, Melief CJM, Bhardwaj N. Therapeutic cancer vaccines. Nat Rev Cancer. 2021;21(6):360-78.

127.   Chamoto K, Takeshima T, Wakita D, Ohkuri T, Ashino S, Omatsu T, et al. Combination immunotherapy with radiation and CpG-based tumor vaccination for the eradication of radio- and immuno-resistant lung carcinoma cells. Cancer Sci. 2009;100(5):934-9.

128.   Organization WH. Vaccines: the powerful innovations bringing WHO's mission to life every day. 2019.

129.   Song D, Powles T, Shi L, Zhang L, Ingersoll MA, Lu YJ. Bladder cancer, a unique model to understand cancer immunity and develop immunotherapy

approaches. J Pathol. 2019;249(2):151-65.

130. Govan VA. A novel vaccine for cervical cancer: quadrivalent human papillomavirus (types 6, 11, 16 and 18) recombinant vaccine (Gardasil). Ther Clin Risk Manag. 2008;4(1):65-70.

131. Enokida T, Moreira A, Bhardwaj N. Vaccines for immunoprevention of cancer. J Clin Invest. 2021;131(9).

132. Pashayan N, Pharoah PDP. The challenge of early detection in cancer. Science. 2020;368(6491):589-90.

133. Berzofsky JA, Terabe M, Wood LV. Strategies to use immune modulators in therapeutic vaccines against cancer. Semin Oncol. 2012;39(3):348-57.

134. Lee EY, Muller WJ. Oncogenes and tumor suppressor genes. Cold Spring Harb Perspect Biol. 2010;2(10):a003236.

135. Grander D. How do mutated oncogenes and tumor suppressor genes cause cancer? Med Oncol. 1998;15(1):20-6.

136. Levine AJ, Puzio-Kuter AM. The control of the metabolic switch in cancers by oncogenes and tumor suppressor genes. Science. 2010;330(6009):1340-4.

137. Oyston P, Robinson K. The current challenges for vaccine development. J Med Microbiol. 2012;61(Pt 7):889-94.

138. Padma VV. An overview of targeted cancer therapy. Biomedicine (Taipei). 2015;5(4):19.

139. Slatko BE, Gardner AF, Ausubel FM. Overview of Next-Generation Sequencing Technologies. Curr Protoc Mol Biol. 2018;122(1):e59.

140. Li W, Zhao K, Kirberger M, Liao W, Yan Y. Next generation sequencing technologies in cancer diagnostics and therapeutics: A mini review. Cell Mol Biol (Noisy-le-grand). 2015;61(5):91-102.

141. Cheever MA, Higano CS. PROVENGE (Sipuleucel-T) in prostate cancer: the first FDA-approved therapeutic cancer vaccine. Clin Cancer Res. 2011;17(11):3520-6.

142. Rodrigues CMC, Pinto MV, Sadarangani M, Plotkin SA. Whither vaccines? J Infect. 2017;74 Suppl 1:S2-S9.

143. Li W, Joshi MD, Singhania S, Ramsey KH, Murthy AK. Peptide Vaccine:

Progress and Challenges. Vaccines (Basel). 2014;2(3):515-36.

144. Nascimento IP, Leite LC. Recombinant vaccines and the development of new vaccine strategies. Braz J Med Biol Res. 2012;45(12):1102-11.

145. Van Nuffel AM, Wilgenhof S, Thielemans K, Bonehill A. Overcoming HLA restriction in clinical trials: Immune monitoring of mRNA-loaded DC therapy. Oncoimmunology. 2012;1(8):1392-4.

146. Hobernik D, Bros M. DNA Vaccines-How Far From Clinical Use? Int J Mol Sci. 2018;19(11).

147. Edwards DK, Jasny E, Yoon H, Horscroft N, Schanen B, Geter T, et al. Adjuvant effects of a sequence-engineered mRNA vaccine: translational profiling demonstrates similar human and murine innate response. J Transl Med. 2017;15(1):1.

148. Shyu AB, Wilkinson MF, van Hoof A. Messenger RNA regulation: to translate or to degrade. EMBO J. 2008;27(3):471-81.

149. Slevin MK, Meaux S, Welch JD, Bigler R, Miliani de Marval PL, Su W, et al. Deep sequencing shows multiple oligouridylations are required for 3' to 5' degradation of histone mRNAs on polyribosomes. Mol Cell. 2014;53(6):1020-30.

150. Verbeke R, Lentacker I, De Smedt SC, Dewitte H. The dawn of mRNA vaccines: The COVID-19 case. J Control Release. 2021;333:511-20.

151. Dolgin E. The tangled history of mRNA vaccines. Nature. 2021;597(7876):318-24.

152. Wolff JA, Malone RW, Williams P, Chong W, Acsadi G, Jani A, et al. Direct gene transfer into mouse muscle in vivo. Science. 1990;247(4949 Pt 1):1465-8.

153. Pardi N, Hogan MJ, Porter FW, Weissman D. mRNA vaccines - a new era in vaccinology. Nat Rev Drug Discov. 2018;17(4):261-79.

154. Stuart LM. In Gratitude for mRNA Vaccines. N Engl J Med. 2021;385(15):1436-8.

155. Schlake T, Thess A, Fotin-Mleczek M, Kallen KJ. Developing mRNA-vaccine technologies. RNA Biol. 2012;9(11):1319-30.

156. Kumar P, Sweeney TR, Skabkin MA, Skabkina OV, Hellen CU, Pestova TV. Inhibition of translation by IFIT family members is determined by their ability to

interact selectively with the 5'-terminal regions of cap0-, cap1- and 5'ppp- mRNAs. Nucleic Acids Res. 2014;42(5):3228-45.

157. Vaidyanathan S, Azizian KT, Haque A, Henderson JM, Hendel A, Shore S, et al. Uridine Depletion and Chemical Modification Increase Cas9 mRNA Activity and Reduce Immunogenicity without HPLC Purification. Mol Ther Nucleic Acids. 2018;12:530-42.

158. Strong TV, Hampton TA, Louro I, Bilbao G, Conry RM, Curiel DT. Incorporation of beta-globin untranslated regions into a Sindbis virus vector for augmentation of heterologous mRNA expression. Gene Ther. 1997;4(6):624-7.

159. Hanson G, Coller J. Codon optimality, bias and usage in translation and mRNA decay. Nat Rev Mol Cell Biol. 2018;19(1):20-30.

160. Thess A, Grund S, Mui BL, Hope MJ, Baumhof P, Fotin-Mleczek M, et al. Sequence-engineered mRNA Without Chemical Nucleoside Modifications Enables an Effective Protein Therapy in Large Animals. Mol Ther. 2015;23(9):1456-64.

161. Kozak M. At least six nucleotides preceding the AUG initiator codon enhance translation in mammalian cells. J Mol Biol. 1987;196(4):947-50.

162. Martins R, Queiroz JA, Sousa F. Ribonucleic acid purification. J Chromatogr A. 2014;1355:1-14.

163. Baiersdorfer M, Boros G, Muramatsu H, Mahiny A, Vlatkovic I, Sahin U, et al. A Facile Method for the Removal of dsRNA Contaminant from In Vitro-Transcribed mRNA. Mol Ther Nucleic Acids. 2019;15:26-35.

164. Kariko K, Muramatsu H, Ludwig J, Weissman D. Generating the optimal mRNA for therapy: HPLC purification eliminates immune activation and improves translation of nucleoside-modified, protein-encoding mRNA. Nucleic Acids Res. 2011;39(21):e142.

165. Vlatkovic I. Non-Immunotherapy Application of LNP-mRNA: Maximizing Efficacy and Safety. Biomedicines. 2021;9(5).

166. Kariko K, Muramatsu H, Welsh FA, Ludwig J, Kato H, Akira S, et al. Incorporation of pseudouridine into mRNA yields superior nonimmunogenic vector with increased translational capacity and biological stability. Mol Ther. 2008;16(11):1833-40.

167.   Anderson BR, Muramatsu H, Nallagatla SR, Bevilacqua PC, Sansing LH, Weissman D, et al. Incorporation of pseudouridine into mRNA enhances translation by diminishing PKR activation. Nucleic Acids Res. 2010;38(17):5884-92.

168.   Dammes N, Peer D. Paving the Road for RNA Therapeutics. Trends Pharmacol Sci. 2020;41(10):755-75.

169.   Ogris M, Brunner S, Schuller S, Kircheis R, Wagner E. PEGylated DNA/transferrin-PEI complexes: reduced interaction with blood components, extended circulation in blood and potential for systemic gene delivery. Gene Ther. 1999;6(4):595-605.

170.   Xu S, Yang K, Li R, Zhang L. mRNA Vaccine Era-Mechanisms, Drug Platform and Clinical Prospection. Int J Mol Sci. 2020;21(18).

171.   Kowalski PS, Rudra A, Miao L, Anderson DG. Delivering the Messenger: Advances in Technologies for Therapeutic mRNA Delivery. Mol Ther. 2019;27(4):710-28.

172.   Miao L, Zhang Y, Huang L. mRNA vaccine for cancer immunotherapy. Mol Cancer. 2021;20(1):41.

173.   Bessis N, GarciaCozar FJ, Boissier MC. Immune responses to gene therapy vectors: influence on vector function and effector mechanisms. Gene Ther. 2004;11 Suppl 1:S10-7.

174.   Baum C, Kustikova O, Modlich U, Li Z, Fehse B. Mutagenesis and oncogenesis by chromosomal insertion of gene transfer vectors. Hum Gene Ther. 2006;17(3):253-63.

175.   Waehler R, Russell SJ, Curiel DT. Engineering targeted viral vectors for gene therapy. Nat Rev Genet. 2007;8(8):573-87.

176.   Thomas CE, Ehrhardt A, Kay MA. Progress and problems with the use of viral vectors for gene therapy. Nat Rev Genet. 2003;4(5):346-58.

177.   Kauffman KJ, Webber MJ, Anderson DG. Materials for non-viral intracellular delivery of messenger RNA therapeutics. J Control Release. 2016;240:227-34.

178.   Guan S, Rosenecker J. Nanotechnologies in delivery of mRNA therapeutics using nonviral vector-based delivery systems. Gene Ther. 2017;24(3):133-43.

179.   Carrasco MJ, Alishetty S, Alameh MG, Said H, Wright L, Paige M, et al.

Ionization and structural properties of mRNA lipid nanoparticles influence expression in intramuscular and intravascular administration. Commun Biol. 2021;4(1):956.

180. Ye T, Li F, Ma G, Wei W. Enhancing therapeutic performance of personalized cancer vaccine via delivery vectors. Adv Drug Deliv Rev. 2021;177:113927.

181. Freyn AW, Ramos da Silva J, Rosado VC, Bliss CM, Pine M, Mui BL, et al. A Multi-Targeting, Nucleoside-Modified mRNA Influenza Virus Vaccine Provides Broad Protection in Mice. Mol Ther. 2020;28(7):1569-84.

182. Aldosari BN, Alfagih IM, Almurshedi AS. Lipid Nanoparticles as Delivery Systems for RNA-Based Vaccines. Pharmaceutics. 2021;13(2).

183. Granados-Riveron JT, Aquino-Jarquin G. Engineering of the current nucleoside-modified mRNA-LNP vaccines against SARS-CoV-2. Biomed Pharmacother. 2021;142:111953.

184. Balazs DA, Godbey W. Liposomes for use in gene delivery. J Drug Deliv. 2011;2011:326497.

185. Koltover I, Salditt T, Radler JO, Safinya CR. An inverted hexagonal phase of cationic liposome-DNA complexes related to DNA release and delivery. Science. 1998;281(5373):78-81.

186. Soenen SJ, Brisson AR, De Cuyper M. Addressing the problem of cationic lipid-mediated toxicity: the magnetoliposome model. Biomaterials. 2009;30(22):3691-701.

187. Filion MC, Phillips NC. Toxicity and immunomodulatory activity of liposomal vectors formulated with cationic lipids toward immune effector cells. Biochim Biophys Acta. 1997;1329(2):345-56.

188. Owens DE, 3rd, Peppas NA. Opsonization, biodistribution, and pharmacokinetics of polymeric nanoparticles. Int J Pharm. 2006;307(1):93-102.

189. Yu B, Wang X, Zhou C, Teng L, Ren W, Yang Z, et al. Insight into mechanisms of cellular uptake of lipid nanoparticles and intracellular release of small RNAs. Pharm Res. 2014;31(10):2685-95.

190. Yamada Y, Sato Y, Nakamura T, Harashima H. Evolution of drug delivery

system from viewpoint of controlled intracellular trafficking and selective tissue targeting toward future nanomedicine. J Control Release. 2020;327:533-45.

191.   Nakamura T, Harashima H. Dawn of lipid nanoparticles in lymph node targeting: Potential in cancer immunotherapy. Adv Drug Deliv Rev. 2020;167:78-88.

192.   Schudel A, Francis DM, Thomas SN. Material design for lymph node drug delivery. Nat Rev Mater. 2019;4(6):415-28.

193.   Kreiter S, Selmi A, Diken M, Koslowski M, Britten CM, Huber C, et al. Intranodal vaccination with naked antigen-encoding RNA elicits potent prophylactic and therapeutic antitumoral immunity. Cancer Res. 2010;70(22):9031-40.

194.   Nakamura T, Kawai M, Sato Y, Maeki M, Tokeshi M, Harashima H. The Effect of Size and Charge of Lipid Nanoparticles Prepared by Microfluidic Mixing on Their Lymph Node Transitivity and Distribution. Mol Pharm. 2020;17(3):944-53.

195.   Supersaxo A, Hein WR, Steffen H. Effect of molecular weight on the lymphatic absorption of water-soluble compounds following subcutaneous administration. Pharm Res. 1990;7(2):167-9.

196.   Oberli MA, Reichmuth AM, Dorkin JR, Mitchell MJ, Fenton OS, Jaklenec A, et al. Lipid Nanoparticle Assisted mRNA Delivery for Potent Cancer Immunotherapy. Nano Lett. 2017;17(3):1326-35.

197.   Wang Y, Zhang L, Xu Z, Miao L, Huang L. mRNA Vaccine with Antigen-Specific Checkpoint Blockade Induces an Enhanced Immune Response against Established Melanoma. Mol Ther. 2018;26(2):420-34.

198.   Verbeke R, Lentacker I, De Smedt SC, Dewitte H. Three decades of messenger RNA vaccine development. Nano Today. 2019;28:100766.

199.   Manolova V, Flace A, Bauer M, Schwarz K, Saudan P, Bachmann MF. Nanoparticles target distinct dendritic cell populations according to their size. Eur J Immunol. 2008;38(5):1404-13.

200.   Akinc A, Maier MA, Manoharan M, Fitzgerald K, Jayaraman M, Barros S, et al. The Onpattro story and the clinical translation of nanomedicines containing nucleic acid-based drugs. Nat Nanotechnol. 2019;14(12):1084-7.

201.   Polack FP, Thomas SJ, Kitchin N, Absalon J, Gurtman A, Lockhart S, et al.

Safety and Efficacy of the BNT162b2 mRNA Covid-19 Vaccine. N Engl J Med. 2020;383(27):2603-15.

202.   Anderson EJ, Rouphael NG, Widge AT, Jackson LA, Roberts PC, Makhene M, et al. Safety and Immunogenicity of SARS-CoV-2 mRNA-1273 Vaccine in Older Adults. N Engl J Med. 2020;383(25):2427-38.

203.   Broos K, Van der Jeught K, Puttemans J, Goyvaerts C, Heirman C, Dewitte H, et al. Particle-mediated Intravenous Delivery of Antigen mRNA Results in Strong Antigen-specific T-cell Responses Despite the Induction of Type I Interferon. Mol Ther Nucleic Acids. 2016;5(6):e326.

204.   Kowalczyk A, Doener F, Zanzinger K, Noth J, Baumhof P, Fotin-Mleczek M, et al. Self-adjuvanted mRNA vaccines induce local innate immune responses that lead to a potent and boostable adaptive immunity. Vaccine. 2016;34(33):3882-93.

205.   Pardi N, Tuyishime S, Muramatsu H, Kariko K, Mui BL, Tam YK, et al. Expression kinetics of nucleoside-modified mRNA delivered in lipid nanoparticles to mice by various routes. J Control Release. 2015;217:345-51.

206.   Zuckerman JN. The importance of injecting vaccines into muscle. Different patients need different needle sizes. BMJ. 2000;321(7271):1237-8.

207.   Lu F, Hogenesch H. Kinetics of the inflammatory response following intramuscular injection of aluminum adjuvant. Vaccine. 2013;31(37):3979-86.

208.   Awate S, Babiuk LA, Mutwiri G. Mechanisms of action of adjuvants. Front Immunol. 2013;4:114.

209.   Pfaar O, Cazan D, Klimek L, Larenas-Linnemann D, Calderon MA. Adjuvants for immunotherapy. Curr Opin Allergy Clin Immunol. 2012;12(6):648-57.

210.   Mesa C, Fernandez LE. Challenges facing adjuvants for cancer immunotherapy. Immunol Cell Biol. 2004;82(6):644-50.

211.   Vermaelen K. Vaccine Strategies to Improve Anti-cancer Cellular Immune Responses. Front Immunol. 2019;10:8.

212.   Lo JA, Fisher DE. The melanoma revolution: from UV carcinogenesis to a new era in therapeutics. Science. 2014;346(6212):945-9.

213.   Liu Y, Sheikh MS. Melanoma: Molecular Pathogenesis and Therapeutic Management. Mol Cell Pharmacol. 2014;6(3):228.

214. Bray F, Ferlay J, Soerjomataram I, Siegel RL, Torre LA, Jemal A. Global cancer statistics 2018: GLOBOCAN estimates of incidence and mortality worldwide for 36 cancers in 185 countries. CA Cancer J Clin. 2018;68(6):394-424.

215. Naik PP. Role of Biomarkers in the Integrated Management of Melanoma. Dis Markers. 2021;2021:6238317.

216. Garnett M, Bottomley W. Mutations of the BRAF gene in human cancer. Nature. 2002;417:949-54.

217. Sosman JA, Kim KB, Schuchter L, Gonzalez R, Pavlick AC, Weber JS, et al. Survival in BRAF V600-mutant advanced melanoma treated with vemurafenib. N Engl J Med. 2012;366(8):707-14.

218. Eroglu Z, Ribas A. Combination therapy with BRAF and MEK inhibitors for melanoma: latest evidence and place in therapy. Ther Adv Med Oncol. 2016;8(1):48-56.

219. Overwijk WW, Restifo NP. B16 as a mouse model for human melanoma. Curr Protoc Immunol. 2001;Chapter 20:Unit 20 1.

220. Tsukamoto K, Jackson IJ, Urabe K, Montague PM, Hearing VJ. A second tyrosinase-related protein, TRP-2, is a melanogenic enzyme termed DOPAchrome tautomerase. EMBO J. 1992;11(2):519-26.

221. Schumacher TN, Schreiber RD. Neoantigens in cancer immunotherapy. Science. 2015;348(6230):69-74.

222. Arya S, Lin Q, Zhou N, Gao X, Huang JD. Strong Immune Responses Induced by Direct Local Injections of Modified mRNA-Lipid Nanocomplexes. Mol Ther Nucleic Acids. 2020;19:1098-109.

223. McGrath JC, Drummond GB, McLachlan EM, Kilkenny C, Wainwright CL. Guidelines for reporting experiments involving animals: the ARRIVE guidelines. Br J Pharmacol. 2010;160(7):1573-6.

224. Palaga T, Buranaruk C, Rengpipat S, Fauq AH, Golde TE, Kaufmann SH, et al. Notch signaling is activated by TLR stimulation and regulates macrophage functions. Eur J Immunol. 2008;38(1):174-83.

225. Jin D, Sprent J. GM-CSF Culture Revisited: Preparation of Bulk Populations of Highly Pure Dendritic Cells from Mouse Bone Marrow. J Immunol.

2018;201(10):3129-39.

226.   Fujimura T, Nakagawa S, Ohtani T, Ito Y, Aiba S. Inhibitory effect of the polyinosinic-polycytidylic acid/cationic liposome on the progression of murine B16F10 melanoma. Eur J Immunol. 2006;36(12):3371-80.

227.   Durward M, Harms J, Splitter G. Antigen specific killing assay using CFSE labeled target cells. J Vis Exp. 2010(45).

228.   Sheehan KC, Lai KS, Dunn GP, Bruce AT, Diamond MS, Heutel JD, et al. Blocking monoclonal antibodies specific for mouse IFN-alpha/beta receptor subunit 1 (IFNAR-1) from mice immunized by in vivo hydrodynamic transfection. J Interferon Cytokine Res. 2006;26(11):804-19.

229.   Ben-Yehuda H, Matcovitch-Natan O, Kertser A, Spinrad A, Prinz M, Amit I, et al. Maternal Type-I interferon signaling adversely affects the microglia and the behavior of the offspring accompanied by increased sensitivity to stress. Mol Psychiatry. 2020;25(5):1050-67.

230.   Zhang H. Thin-Film Hydration Followed by Extrusion Method for Liposome Preparation. Methods Mol Biol. 2017;1522:17-22.

231.   Patil YP, Jadhav S. Novel methods for liposome preparation. Chem Phys Lipids. 2014;177:8-18.

232.   Metwally AA, Pourzand C, Blagbrough IS. Efficient Gene Silencing by Self-Assembled Complexes of siRNA and Symmetrical Fatty Acid Amides of Spermine. Pharmaceutics. 2011;3(2):125-40.

233.   Whitt M, Buonocore L, Rose JK. Liposome-mediated transfection. Curr Protoc Immunol. 2001;Chapter 10:Unit 10 6.

234.   Wherry EJ, Blattman JN, Murali-Krishna K, van der Most R, Ahmed R. Viral persistence alters CD8 T-cell immunodominance and tissue distribution and results in distinct stages of functional impairment. J Virol. 2003;77(8):4911-27.

235.   Wherry EJ, Teichgraber V, Becker TC, Masopust D, Kaech SM, Antia R, et al. Lineage relationship and protective immunity of memory CD8 T cell subsets. Nat Immunol. 2003;4(3):225-34.

236.   Barber DL, Wherry EJ, Ahmed R. Cutting edge: rapid in vivo killing by memory CD8 T cells. J Immunol. 2003;171(1):27-31.

237. Klebanoff CA, Gattinoni L, Torabi-Parizi P, Kerstann K, Cardones AR, Finkelstein SE, et al. Central memory self/tumor-reactive CD8+ T cells confer superior antitumor immunity compared with effector memory T cells. Proc Natl Acad Sci U S A. 2005;102(27):9571-6.

238. Gasteiger G, Ataide M, Kastenmuller W. Lymph node - an organ for T-cell activation and pathogen defense. Immunol Rev. 2016;271(1):200-20.

239. Dragicevic-Curic N, Scheglmann D, Albrecht V, Fahr A. Temoporfin-loaded invasomes: development, characterization and in vitro skin penetration studies. J Control Release. 2008;127(1):59-69.

240. Zhu S, Zhang T, Zheng L, Liu H, Song W, Liu D, et al. Combination strategies to maximize the benefits of cancer immunotherapy. J Hematol Oncol. 2021;14(1):156.

241. Blass E, Ott PA. Advances in the development of personalized neoantigen-based therapeutic cancer vaccines. Nat Rev Clin Oncol. 2021;18(4):215-29.

242. Ruddle NH, Akirav EM. Secondary lymphoid organs: responding to genetic and environmental cues in ontogeny and the immune response. J Immunol. 2009;183(4):2205-12.

243. Ma DY, Clark EA. The role of CD40 and CD154/CD40L in dendritic cells. Semin Immunol. 2009;21(5):265-72.

244. Bauvois B, Nguyen J, Tang R, Billard C, Kolb JP. Types I and II interferons upregulate the costimulatory CD80 molecule in monocytes via interferon regulatory factor-1. Biochem Pharmacol. 2009;78(5):514-22.

245. Paun A, Pitha PM. The IRF family, revisited. Biochimie. 2007;89(6-7):744-53.

246. Divangahi M, Aaby P, Khader SA, Barreiro LB, Bekkering S, Chavakis T, et al. Trained immunity, tolerance, priming and differentiation: distinct immunological processes. Nat Immunol. 2021;22(1):2-6.

247. Jeyanathan M, Afkhami S, Smaill F, Miller MS, Lichty BD, Xing Z. Immunological considerations for COVID-19 vaccine strategies. Nat Rev Immunol. 2020;20(10):615-32.

248. Bettini E, Locci M. SARS-CoV-2 mRNA Vaccines: Immunological Mechanism and Beyond. Vaccines (Basel). 2021;9(2).

249.   Swiecki M, Colonna M. Type I interferons: diversity of sources, production pathways and effects on immune responses. Curr Opin Virol. 2011;1(6):463-75.

250.   Constant SL, Bottomly K. Induction of Th1 and Th2 CD4+ T cell responses: the alternative approaches. Annu Rev Immunol. 1997;15:297-322.

251.   Rogers PR, Croft M. Peptide dose, affinity, and time of differentiation can contribute to the Th1/Th2 cytokine balance. J Immunol. 1999;163(3):1205-13.

252.   Takeuchi A, Saito T. CD4 CTL, a Cytotoxic Subset of CD4(+) T Cells, Their Differentiation and Function. Front Immunol. 2017;8:194.

253.   Quezada SA, Simpson TR, Peggs KS, Merghoub T, Vider J, Fan X, et al. Tumor-reactive CD4(+) T cells develop cytotoxic activity and eradicate large established melanoma after transfer into lymphopenic hosts. J Exp Med. 2010;207(3):637-50.

254.   Liang Y, Hannan R, Fu YX. Type I IFN Activating Type I Dendritic Cells for Antitumor Immunity. Clin Cancer Res. 2021;27(14):3818-24.

255.   Wu Z, Zheng Y, Sheng J, Han Y, Yang Y, Pan H, et al. CD3(+)CD4(-)CD8(-) (Double-Negative) T Cells in Inflammation, Immune Disorders and Cancer. Front Immunol. 2022;13:816005.

256.   Meng X, Liu X, Guo X, Jiang S, Chen T, Hu Z, et al. FBXO38 mediates PD-1 ubiquitination and regulates anti-tumour immunity of T cells. Nature. 2018;564(7734):130-5.

257.   Schoenemeyer A, Barnes BJ, Mancl ME, Latz E, Goutagny N, Pitha PM, et al. The interferon regulatory factor, IRF5, is a central mediator of toll-like receptor 7 signaling. J Biol Chem. 2005;280(17):17005-12.

258.   Chistiakov DA, Myasoedova VA, Revin VV, Orekhov AN, Bobryshev YV. The impact of interferon-regulatory factors to macrophage differentiation and polarization into M1 and M2. Immunobiology. 2018;223(1):101-11.

259.   Wu CF, Andzinski L, Kasnitz N, Kroger A, Klawonn F, Lienenklaus S, et al. The lack of type I interferon induces neutrophil-mediated pre-metastatic niche formation in the mouse lung. Int J Cancer. 2015;137(4):837-47.

260.   Alameh MG, Tombacz I, Bettini E, Lederer K, Sittplangkoon C, Wilmore JR, et al. Lipid nanoparticles enhance the efficacy of mRNA and protein subunit

vaccines by inducing robust T follicular helper cell and humoral responses. Immunity. 2021;54(12):2877-92 e7.

261. Dalpke A, Helm M. RNA mediated Toll-like receptor stimulation in health and disease. RNA Biol. 2012;9(6):828-42.

262. Tran E, Robbins PF, Lu YC, Prickett TD, Gartner JJ, Jia L, et al. T-Cell Transfer Therapy Targeting Mutant KRAS in Cancer. N Engl J Med. 2016;375(23):2255-62.

263. Alspach E, Lussier DM, Miceli AP, Kizhvatov I, DuPage M, Luoma AM, et al. MHC-II neoantigens shape tumour immunity and response to immunotherapy. Nature. 2019;574(7780):696-701.

264. Takeda K, Nakayama M, Hayakawa Y, Kojima Y, Ikeda H, Imai N, et al. IFN-gamma is required for cytotoxic T cell-dependent cancer genome immunoediting. Nat Commun. 2017;8:14607.

265. Ali OA, Lewin SA, Dranoff G, Mooney DJ. Vaccines Combined with Immune Checkpoint Antibodies Promote Cytotoxic T-cell Activity and Tumor Eradication. Cancer Immunol Res. 2016;4(2):95-100.

266. Li S, Simoni Y, Zhuang S, Gabel A, Ma S, Chee J, et al. Characterization of neoantigen-specific T cells in cancer resistant to immune checkpoint therapies. Proc Natl Acad Sci U S A. 2021;118(30).

267. Danaei M, Dehghankhold M, Ataei S, Hasanzadeh Davarani F, Javanmard R, Dokhani A, et al. Impact of Particle Size and Polydispersity Index on the Clinical Applications of Lipidic Nanocarrier Systems. Pharmaceutics. 2018;10(2).

268. Ryals RC, Patel S, Acosta C, McKinney M, Pennesi ME, Sahay G. The effects of PEGylation on LNP based mRNA delivery to the eye. PLoS One. 2020;15(10):e0241006.

269. Suk JS, Xu Q, Kim N, Hanes J, Ensign LM. PEGylation as a strategy for improving nanoparticle-based drug and gene delivery. Adv Drug Deliv Rev. 2016;99(Pt A):28-51.

270. Sohaebuddin SK, Thevenot PT, Baker D, Eaton JW, Tang L. Nanomaterial cytotoxicity is composition, size, and cell type dependent. Part Fibre Toxicol. 2010;7:22.

APPENDIX

APPENDIX A

LIST OF PREPARING REAGENTS

1) DMEM complete media (100 ml)

DMEM	87	ml
FBS	10	ml
1 M HEPES free acid	1	ml
100 mM sodium pyruvate	1	ml
100x Penicillin/Streptomycin G	1	ml

2) BMDM media (100 ml)

L929 culture supernatant	20	ml
DMEM complete media	75	ml
Horse serum	5	ml

3) Freezing media for BMDM cryopreservation

3.1) Freezing media A (10 ml)

FBS	2	ml
DMEM	8	ml

3.2) Freezing media B (10 ml)

FBS	2	ml
DMSO	2	ml
DMEM	6	ml

Mix A and B at 1:1 ratio

4) BMDC media (100 ml)

RPMI-1640	84.9	ml

FBS	10	ml
1 M HEPES	1	ml
100 mM sodium pyruvate	1	ml
100x Penicillin/Streptomycin G	1	ml
100x GlutaMAX	1	ml
100x MEM Non-Essential Amino Acid	1	ml
1000x 2-Mercaptoethanol	0.1	ml

Add GM-CSF 20 ng/ml and IL-4 10 ng/ml or 5 ng/ml

5) B16F0-OVA media (100 ml)

RPMI-1640	84.5	ml
FBS	10	ml
1 M HEPES	1	ml
100 mM sodium pyruvate	1	ml
100x Penicillin/Streptomycin G	1	ml
100x GlutaMAX	1	ml
100x MEM Non-Essential Amino Acid	1	ml
1000x 2-Mercaptoethanol	0.1	ml
G418 (stock concentration 100 mg/ml)	0.4	ml

6) Freezing media for B16F0-OVA cryopreservation (10 ml)

B16F0-OVA media	9	ml
DMSO	1	ml

7) B16F10-Luc2 media (100 ml)

DMEM	88.9	ml
FBS	10	ml

100x Penicillin/Streptomycin G	1	ml
Blasticidin (stock concentration 10 mg/ml)	0.1	ml

8) Freezing media for B16F10-Luc2 cryopreservation (10 ml)

B16F10-Luc2 media	9.5	ml
DMSO	0.5	ml

9) Freezing media for RAW264.7 cell line (10 ml)

DMEM complete media	9	ml
DMSO	1	ml

10) 1x PBS, pH 7.4 (1000 ml)

NaCl	8	g
KCl	0.2	g
Na_2HPO_4	3.63	g
KH_2PO_4	0.24	g
DDW	1000	ml

Adjust pH to 7.4 with HCl or NaOH and autoclave sterilize at 121°C for 15 minutes

11) MTT solution, working at 5 mg/ml (40 ml)

MTT	200	mg
Sterile 1x PBS	40	ml

Vortex until dissolve and filter sterilize solution through 0.2 μm filter

12) 1.5 M Tris-HCl, pH 8.8 (1,000 ml)

Trisma base	181.71	g

DDW	1000	ml

Adjust pH to 8.8 with HCl

13) 1 M Tris-HCl, pH 6.8 (1,000 ml)

Trisma base	121.14	g
DDW	1000	ml

Adjust pH to 6.8 with HCl

14) SDS-polyacrylamide gel

    12.1)   8% polyacrylamide gel (8 ml)

DDW	4.236	ml
40% Acrylamide and Bis-acrylamide solution	1.6	ml
1.5 M Tris-HCl, pH 8.8	2	ml
10% SDS	80	µl
10% APS	80	µl
TEMED	4	µl

    12.2)   15% polyacrylamide gel (2 ml)

DDW	1.204	ml
40% Acrylamide and Bis-acrylamide solution	0.25	ml
1 M Tris-HCl pH 6.8	0.504	ml
10% SDS	20	µl
10% APS	20	µl
TEMED	2	µl

15) 5x Running buffer (1,000 ml)

Trisma base	15.1	g
Glycine	94	g
SDS	5	g
DDW	1000	ml

16) Transfer buffer (1,000 ml)

Trisma base	5.08	g
Glycine	2.9	g
SDS	0.37	g
Absolute methanol	200	ml
DDW	800	ml

17) 6x Gel loading buffer (10 ml)

0.5 M Tris-HCl pH 6.8	7	ml
SDS	1	g
Glycerol	3	ml
Bromophenol blue	0.001	g
β-mercaptoethanol	0.5	ml

18) ECL substrate of HRP

18.1)   Coumaric acid solution

Coumaric acid	90	mM
DMSO	10	ml

Store at -20°C.

18.2)   Luminol solution

Luminol	250	mM

	DMSO	10	ml

Store at -20°C.

18.3) Solution A

100 mM Tris-HCl, pH 8.5	2.5	ml
Coumaric acid solution	11	µl
Luminol solution	25	µl

18.4) Solution B

100 mM Tris-HCl, pH 8.5	2.5	ml
H_2O_2	1.5	ml

19) Film developer and fixer

Each was diluted with tap water at 1:5

20) Coating buffer, pH 9.5 (1,000 ml)

$NaHCO_3$	8.4	g
Na_2CO_3	3.56	g
DDW	1000	ml

Adjust pH to 9.5 and filter sterilize solution through 0.2 µm filter

21) Blocking buffer (10% FBS in 1x PBS) (100 ml)

FBS	10	ml
1x PBS	90	ml

22) TMB buffer, pH 4.0 (1,000 ml)

Tri-potassium citrate monohydrated	66.5	mg

Citric acid	39.38	g
DDW	1000	ml

Adjust pH to 4.0 with HCl

23) TMB substrate

3,3',5,5'-tetramethylbensidine	2.5	mg
DMSO	250	µl

Freshly prepare before use

24) TMB substrate solution

TMB buffer	10	ml
TMB substrate	250	µl
30% H_2O_2	2.5	µl

25) 2N H_2SO_4 stop solution (500 ml)

Absolute H_2SO_4	27	ml
DDW	473	ml

26) 1N H_2SO_4 stop solution (500 ml)

Absolute H_2SO_4	13.5	ml
DDW	486.5	ml

27) PBS-T (1,000 ml)

Tween-20	0.5	ml
1x PBS	1000	ml

28) FACS staining buffer (2% FBS in 1x PBS) (100 ml)

FBS	2	ml
1x PBS	98	ml

29) Red blood cell lysis buffer (50 ml)

NH_4Cl	0.415	g
0.5 M EDTA	10	µl
$NaHCO_3$	0.05	g
DDW	50	ml

Filter sterilization through 0.2 µm filter and store at 4℃

30) Fekete's solution (1,000 ml)

| 100% ethanol	700	ml
DDW	228	ml
37% Formaldehyde solution	32	ml
Glacial acetic acid	40	ml

Store at room temperature

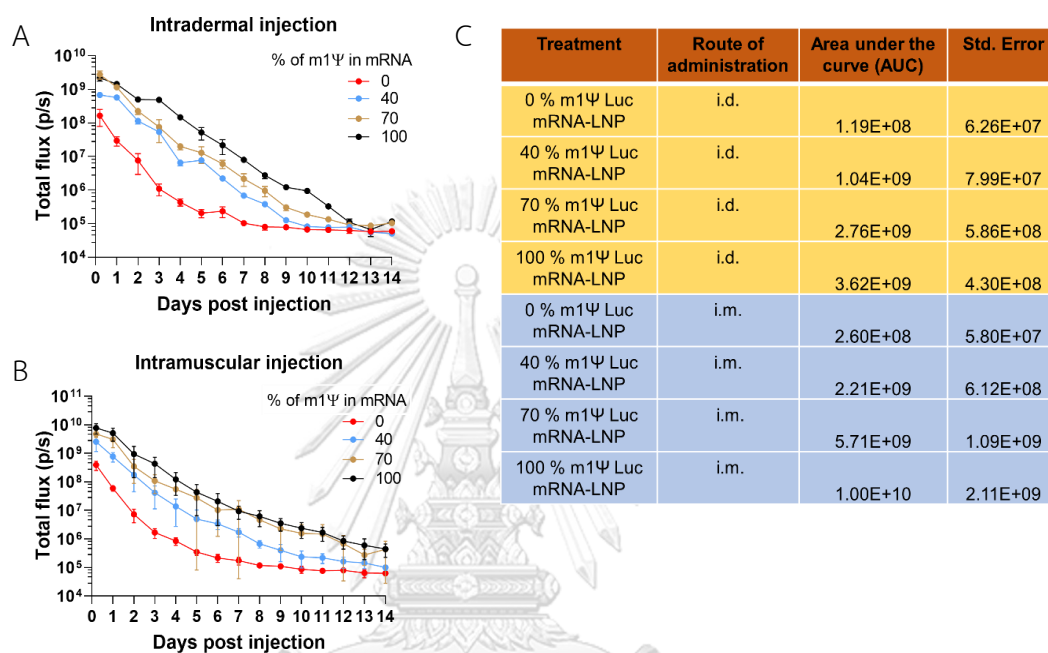# APPENDIX B

SUPPLEMENT
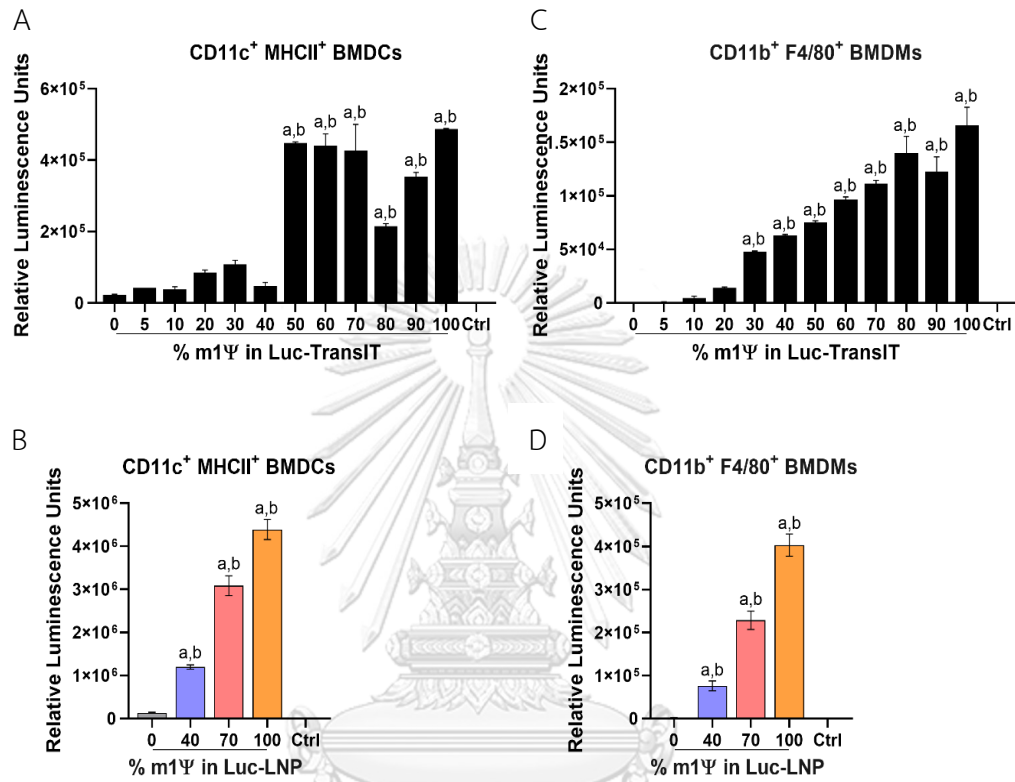
Supplement Figure 1 Efficiency of TransIT and LNP for *in vitro* luciferase mRNA transfection

Firefly luciferase expression following transfection of (A-B) BMDCs and (C-D) BMDMs with luciferase-encoding mRNA modified with different % of m1Ψ (0.1 µg) using TransIT reagent (upper row) or LNP (lower row). The control were untranfected cells. The results are presented as the mean ± SEM of at least duplicate samples and experiments were performed at least two times. Statistical significance by one-way ANOVA with Bonferroni multiple comparisons test were indicated when $p < 0.05$ compared to the unmodified target antigen: a, or control: b.
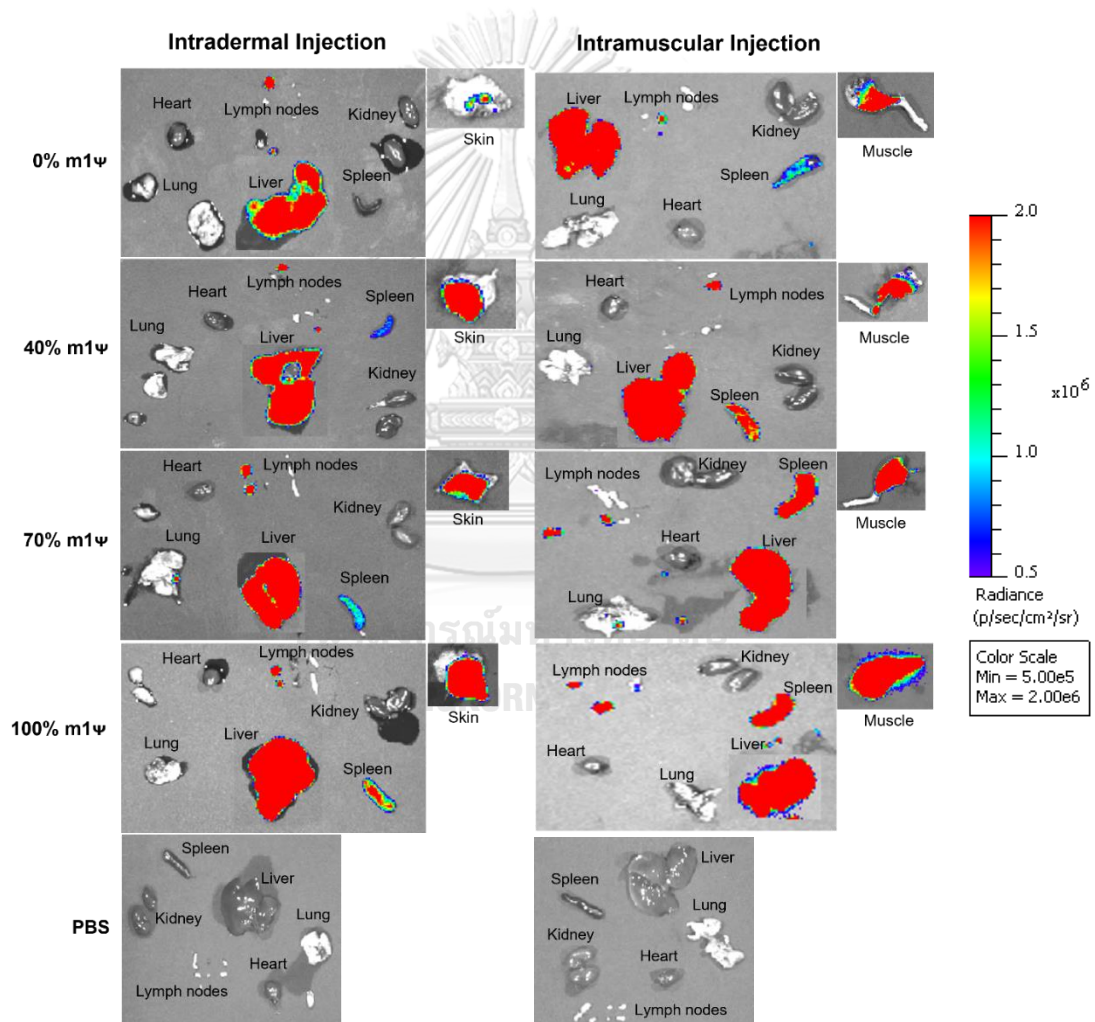

Supplement Figure 2 *Ex vivo* bioluminescence imaging of mRNA-LNP in mice

IVIS images of organs excised from C57BL/6 mice after 4 hrs injected by intradermal and intramuscular routes with 5.0 µg of luciferase encoding mRNA-LNP with different percentages of m1Ψ. The scale of luminescence is indicated.

Treatment	Route of administration	Area under the curve (AUC)	Std. Error
0 % m1Ψ Luc mRNA-LNP	i.d.	1.19E+08	6.26E+07
40 % m1Ψ Luc mRNA-LNP	i.d.	1.04E+09	7.99E+07
70 % m1Ψ Luc mRNA-LNP	i.d.	2.76E+09	5.86E+08
100 % m1Ψ Luc mRNA-LNP	i.d.	3.62E+09	4.30E+08
0 % m1Ψ Luc mRNA-LNP	i.m.	2.60E+08	5.80E+07
40 % m1Ψ Luc mRNA-LNP	i.m.	2.21E+09	6.12E+08
70 % m1Ψ Luc mRNA-LNP	i.m.	5.71E+09	1.09E+09
100 % m1Ψ Luc mRNA-LNP	i.m.	1.00E+10	2.11E+09

**Supplement Figure 3** Translational kinetics of mRNA-LNP *in vivo*

Quantification of the bioluminescence signal was measured in C57BL/6 mice injected with 5.0 µg of luciferase encoding mRNA-LNP with different percentages of m1Ψ via (A) *i.d.* and (B) *i.m.* routes. The bioluminescence intensity was evaluated from 4 hrs until 14 days post injection. Error bars represent the SEM. (C) The area under the activity time curve shows the total amount of protein produced from luciferase encoding mRNA-LNP over time from 4 hrs to 14 days post injection (*n* = 3 per group).
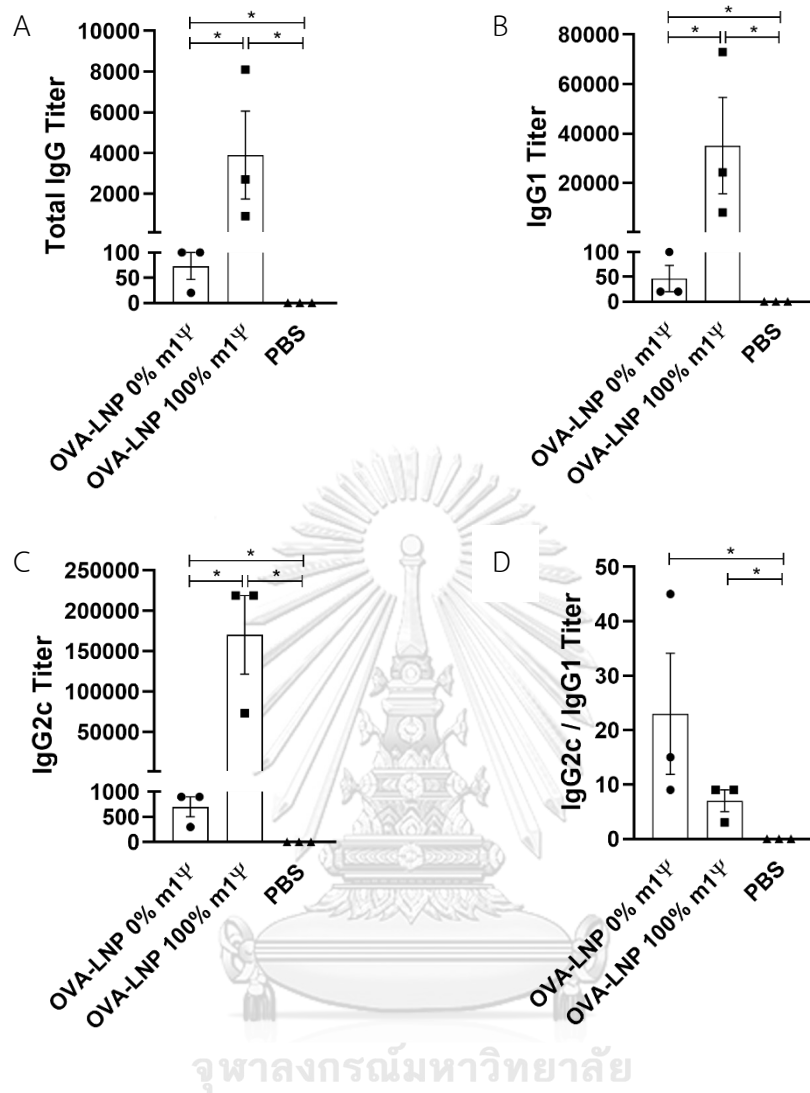
Supplement Figure 4 Serological responses in mice immunized with ovalbumin encoding mRNA-LNP with 0 or 100% of m1Ψ

Two weeks after the last immunization, blood was collected for measuring ovalbumin specific (A) total IgG, (B) IgG1, and (C) IgG2c. (D) The ratio of IgG2c to IgG1 was shown. Data represents the mean ± SEM. The significance of differences between groups was determined by a student's t-test. (*) $p < 0.05$
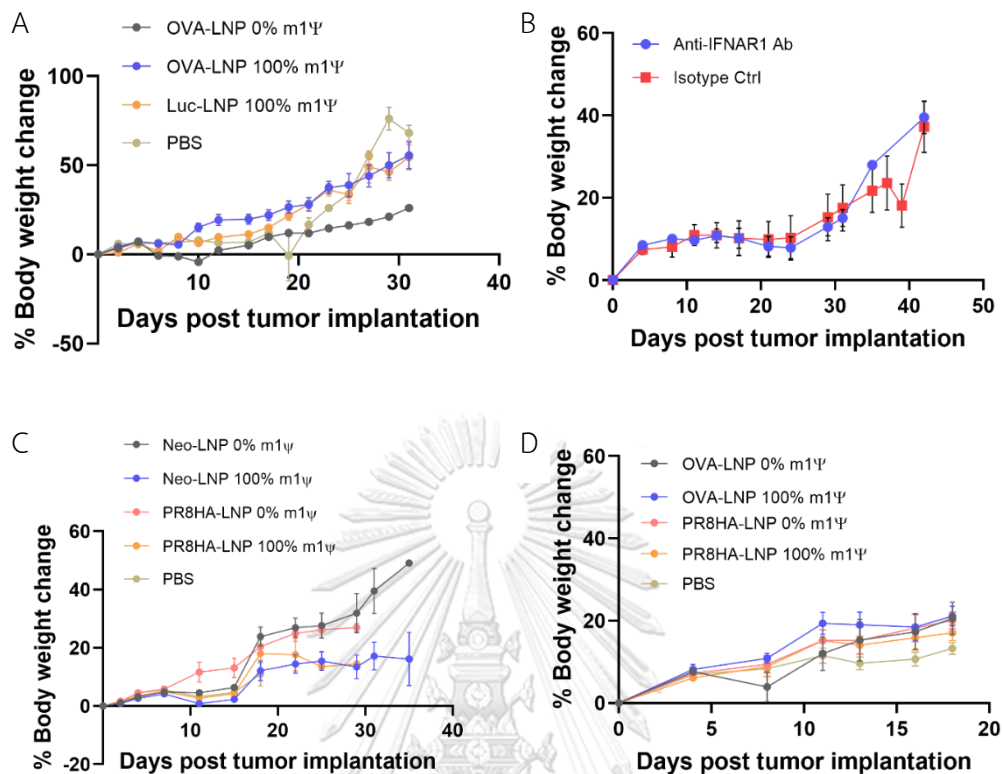
Supplement Figure 5 Immunization of mRNA-LNP in tumor-bearing mice does not dramatically cause body weight loss.

(A) Percent of body weight changes of B16F0-OVA tumor-bearing mice which received OVA mRNA-LNPs is shown. (B) Percent of body weight changes of B16F0-OVA tumor-bearing mice which were immunized with OVA mRNA-LNPs in the absence or presence of type I IFN neutralizing antibody is shown. (C) Percent of body weight changes of mice implanted with B16F0-OVA tumor for lung metastasis and OVA mRNA-LNPs is shown. (D) Percent of body weight changes of B16F10-Luc2 tumor-bearing mice which was immunized with Neo mRNA-LNPs is shown. Each dot are represented as the mean ± SEM, n = 4-9 biologically independent mice per group.

VITA

NAME   Chutamath Sittplangkoon

DATE OF BIRTH   31 May 1994

PLACE OF BIRTH   Bangkok, Thailand

INSTITUTIONS ATTENDED   Major in Biology, Department of Zoology, Faculty of
                        Science, Kasetsart University

HOME ADDRESS   105 Moo2 Taykoa, Samkhok, Pathum Thani, 12160,
                        Thailand